Nonlinear and Adaptive Control Algorithms for Electrohydraulic Active Suspension Systems

by

Amhmed MOHAMED AL AELA

MANUSCRIPT-BASED THESIS PRESENTED TO ÉCOLE DE TECHNOLOGIE SUPÉRIEURE IN PARTIAL FULFILLMENT FOR THE DEGREE OF DOCTOR OF PHILOSOPHY
Ph. D.

MONTREAL, AUGUST 05, 2021

ÉCOLE DE TECHNOLOGIE SUPÉRIEURE
UNIVERSITÉ DU QUÉBEC

BOARD OF EXAMINERS (THESIS PH.D.)

THIS THESIS HAS BEEN EVALUATED

BY THE FOLLOWING BOARD OF EXAMINERS

Mr. Jean-Pierre Kenné, Thesis Supervisor
Department of Mechanical Engineering, École de technologie supérieure

Mrs. Honorine Angue Mintsa, Thesis Co-supervisor
Department of Electro-Mechanical Engineering, École Polytechniqe de Masuku

Mr. Tony Wong, President of the Board of Examiners
Department of Automotive Production Engineering, École de technologie supérieure

Mr. Anh Dung Ngo, Member of the jury
Department of Mechanical Engineering, École de technologie supérieure

Mr. Francis A. Okou, External Evaluator
Department of Electrical and Computer Engineering, Royal Military College of Canada
Kingston, Canada

THIS THESIS WAS PRENSENTED AND DEFENDED

IN THE PRESENCE OF A BOARD OF EXAMINERS AND PUBLIC ON

AT ÉCOLE DE TECHNOLOGIE SUPÉRIEURE

ACKNOWLEDGMENT

The resulting work in this thesis is done in several years at the Laboratory of Integrated Production Technologies, Department of Mechanical Engineering, École de Technologie supérieure (ÉTS), Université du Québec in Montreal. During the several years, I have intensively learned to improve my education in mechatronic engineering. Thus, this work was dedicated to the development of control law strategies for electrohydraulic active suspension systems.

I would like to thank the supervisor: Professor Jean-Pierre KENNE, for allowing me to carry out the research and helping me in some way to accomplish the research in this thesis. I would also like to thank the co-supervisor, Professor Honorine Angue-Mintsa, to advise me to achieve the best way to finish this work. I might not have enough time to pay attention to my family. So, I would like to give special thanks to my spouse Hanan Khalifa and my children: Mohamed, Sufian, Tareg, Abdullah, Khalifa, and Sarah, for their tremendous support in giving their time through this journey.

I want to thank the Libyan ministry of higher education for funding my study in the École de Technologie Supérieure ÉTS. Moreover, I want to thank the Canadian Bureau for International Education (CBIE) for taking responsibility to organize my study. Finally, I would like to thank École de Technologie Supérieure (ÉTS) for supporting and providing me with excellent working conditions.

ALGORITHMES DE COMMANDE NON LINÉAIRE ET ADAPTATIVE POUR LES SYSTÈMES ELECTRO-HYDRAULIQUES DE SUSPENSION ACTIVE

Amhmed MOHAMED AL AELA

RESUME

Cette thèse propose de nouvelles stratégies de commande pour les systèmes de suspension active dans le domaine automobile. Les systèmes de modélisation de la suspension active électrohydraulique des voitures sont caractérisés par plusieurs phénomènes, tels que la dynamique non linéaire, les incertitudes paramétriques et les non-linéarités incertaines. Par conséquent, des lois de commande ont été développées dans cette thèse pour une suspension active électrohydraulique de quart de voiture SISO, une suspension active électrohydraulique de quart de voiture restreinte SISO et une suspension active électrohydraulique filtrée pour voiture complète MIMO.

La première stratégie de commande de cette thèse se concentre sur le confort des passagers pour un système de suspension active représentant le quarte de voiture. Le système dynamique de la suspension active de quart de voiture est connu par l'incertitude du modèle non apparié. Par conséquent, l'entrée de commande ne peut pas complètement annuler les incertitudes du système. Ainsi, un système de commande backstepping a été appliqué pour résoudre ce problème. Cependant, la régression du système de commande backstepping est fastidieuse et difficile à déterminer. Ainsi, le système de réseau neuronal à fonction de base radiale a été appliqué pour représenter des fonctions compliquées. Par conséquent, un système de commande backstepping adaptative du réseau neuronal a été développé pour la rétroaction semi-stricte SISO d'un système de suspension active électrohydraulique d'un quart de voiture.

La deuxième stratégie de commande proposée aborde le compromis entre le confort des passagers, la tenue de route, les limites de débattement de la suspension et les oscillations de débattement de la suspension pour une suspension active électrohydraulique quart de voiture. Même si la première stratégie de commande indiquait une compensation de position de masse suspendue élevée, elle présentait les pires oscillations de tenue de route et de course de suspension. Par conséquent, nous avons conçu un nouveau système de modèle pour aborder explicitement la tenue de route, qui a été appelée un système de pneu d'atterrissage dynamique. Nous avons également considéré des limites de course de suspension non symétriques au lieu de celles de la plupart des études précédentes. En conséquence, un filtre de commande non linéaire a été développé pour suivre les restrictions de suspension. Ainsi, la deuxième stratégie de commande proposée était le filtre de commande non linéaire combiné avec le système de commande adaptative des réseaux de neurones, qui peut parfaitement gérer les restrictions de suspension, les non-linéarités dynamiques et les incertitudes du système.

La troisième stratégie de commande a été développée pour les systèmes de suspension active des voitures complètes. Bien que la deuxième stratégie de commande ait démontré avec succès l'efficacité de la commande, elle a été conçue pour une suspension active d'un quart de voiture. De plus, la plupart des études précédentes sur les systèmes de commande de suspension active des voitures complètes ne portaient pas clairement sur la tenue de route et la robustesse des commandes. Par conséquent, le troisième système de commande a été développé pour le système de suspension active électrohydraulique MIMO non linéaire de voiture complète en présence à la fois d'une perturbation de la route raide et de perturbations aérodynamiques externes. Le troisième système de commande se compose du système de backstepping adaptative des réseaux neuronaux et de quatre filtres de commande non linéaires. Un système de dynamique zéro a également été appliqué pour garantir la stabilité du système.

Les résultats de la simulation montrent que les systèmes de commande proposés atteignent avec succès les objectifs de commande. La première stratégie de commande peut offrir un excellent confort de conduite pour une suspension active en quart de voiture. La deuxième loi de commande proposée permet de gérer puissamment le compromis entre confort des passagers, tenue de route et débattement de la suspension pour une suspension active en quart de voiture. Enfin, la troisième stratégie de commande peut atteindre les performances optimales de suspension en améliorant le confort des passagers, en maintenant la tenue de route, en évitant d'atteindre les limites de débattement de la suspension, en réduisant les oscillations de débattement de la suspension et en surmontant les non-linéarités dynamiques et les incertitudes du système pour une suspension active de voiture complète.

Mots clés: Systèmes de suspension active, système de commande backstepping, réseaux de neurones, commande adaptatives, systèmes électrohydraulique, systèmes à dynamique zéro

NONLINEAR AND ADAPTIVE CONTROL ALGORITHMS FOR ELECTROHYDRAULIC ACTIVE SUSPENSION SYSTEMS

Amhmed MOHAMED AL AELA

ABSTRACT

This thesis proposes novel control strategies for automobile active suspension systems. The car electrohydraulic active suspension modeling systems were characterized by several phenomena, such as nonlinear dynamics, parametric uncertainties, and uncertain nonlinearities. Therefore, the control laws were developed in this thesis for a SISO quarter car electrohydraulic active suspension, a SISO restricted quarter car electrohydraulic active suspension, and MIMO full car filtered electrohydraulic active suspension.

The first control strategy in this thesis focuses on passenger comfort for a quarter car active suspension system. The dynamic system of the quarter car active suspension is known by unmatched model uncertainty. Hence, the control input cannot altogether cancel out the system uncertainties. Thus, a backstepping control system was applied to solve this issue. However, the regression of the backstepping control system is tedious and challenging to determine. So, the Radial basis function neural network system was applied to represent complicated functions. Consequently, an adaptive neural network backstepping control system was developed for SISO semi-strict feedback of a quarter car electrohydraulic active suspension system.

The second proposed control strategy addresses the compromise between passenger comfort, road holding, suspension travel limits, and suspension travel oscillations for a quarter car electrohydraulic active suspension. Even though the first control strategy indicated high sprung mass position compensation, it had the worst road holding and suspension travel oscillations. Therefore, we have designed a new model system to explicitly address road holding, which was called a dynamic landing tire system. We have also considered nonsymmetric suspension travel limits instead of that in most previous studies. Accordingly, a nonlinear control filter was developed to track the suspension restrictions. Thus, the second proposed control strategy was the combined nonlinear control filter with the adaptive neural networks control system, which can perfectly deal with the suspension restrictions, dynamic nonlinearities, and system uncertainties.

The third control strategy was developed for full car active suspension systems. Although the second control strategy was successfully demonstrated the control effectiveness, it was designed for a quarter car active suspension. Moreover, most previous studies for full car active suspension control systems were not clearly addressed road holding and control robustness. Therefore, the second control system was evolved for the MIMO nonlinear of full car electrohydraulic active suspension system in the presence of both a stiff road perturbation and external aerodynamic disturbances. The third control system consists of the adaptive neural networks backstepping control system and four nonlinear control filters. A zero dynamics system was also applied to guarantee system stability.

The simulation results show that the proposed control systems are successfully achieved the control objectives as follows. Firstly, the first control strategy can provide an excellent ride comfort for a quarter car active suspension. Secondly, the second proposed control law can powerfully manage the compromise between passenger comfort, road holding, and suspension travel for a quarter car active suspension. Finally, the third control strategy can achieve the optimal suspension performance of improving passenger comfort, maintaining road holding, avoiding reaching suspension travel limits, reducing suspension travel oscillations, and overcoming dynamic nonlinearities and system uncertainties for full car active suspension.

Keywords: Active suspension, backstepping control system, neural networks, adaptive control systems, electrohydraulic systems, zero dynamics systems

TABLE OF CONTENTS

Page

LIST OF TABLES

Page

LIST OF FIGURES

Page

LIST OF ABREVIATIONS

ANNC	Adaptive neural networks control system
EHSS	Electrohydraulic servovalve system
MIMO	Multiple Input Multiple Output
NAC	Novel adaptive control system
PID	Proportional Integral differential control law
LQR	Linear quadratic regulator
RANNC	Robust adaptive neural network control system
RBFNN	Radial basis function neural networks
SISO	Single Input Single Output

LIST OF SYMBOLS

$\mathbf{A_a}$	Reference aerodynamic area, $\boldsymbol{m^2}$
A_p	Actuator piston area, m^2
A_v	Spool valve projected area, m^2
b_j	Gaussian function width for RBFNN
C_d	Low discharge coefficient, -
C_D	Mean aerodynamic drag coefficient
C_h	A reduced positive factor for the operational hydraulic pressure
C_{tp}	Coefficient of leakage, $m^5/(Ns)$
c_i	A positive constant
$\boldsymbol{c_i}$	A positive definite matrix
C_f	Lateral friction coefficient
$\acute{C}_L$	Modified lift force coefficient
C_{ns_i}	The nonlinear damper coefficient, Ns/m
C_R	Mean rolling moment coefficient
C_p	Mean pitching moment coefficient
C_{sf}	Parameter for static friction
C_s	Suspension viscous coefficient, Ns/m
C_t	Tire viscous coefficient, Ns/m
C_v	An amplified positive factor for the opening spool servovalve area
$\mathrm{f_i}$	Unknown function i
$\hat{\mathrm{f}}_\mathrm{i}$	An approximate smooth function i
F_{a_i}	A crosswinds aerodynamic reaction force acting on the unsprung mass i, N
F_{c0}	Coulomb friction coefficient
F_{ns_i}	The nonlinear spring force, N
F_{s0}	Static friction coefficient
g	Gravitational acceleration, m/s^2
$\mathrm{g_i}$	Unknown modeling function i

$h_i(\zeta)$	Hidden Gaussian functions of the radial basis function neural networks
I_θ	Pitching moment of inertia, $k\text{g}\,m^2$
I_ω	Rolling moment of inertia, $k\text{g}\,m^2$
$K_{u\,min}$	Lower bound control signal gain, m^2/V
$K_{u\,max}$	Upper bound of control signal gain, m^2/V
K_s	Suspension spring stiffness, N/m
K_t	Tire spring stiffness, N/m
l	Number of RFBNN nodes
l_f	A car length from front wheels to the centre of gravity, m
l_r	A car length from a rear wheel to the centre of gravity, m
m	Number of variables in the compact set
$m_{1,2,3,4}$	Positive constants
m_s	Quarter car sprung mass, Kg
m_u	Unsprung mass (wheel), Kg
M_s	Car sprung mass, Kg
n	State-space order system
$n_{1,2}$	Positive constants
P	A positive definite matrix
P_L	Operational hydraulic pressure, N/m^2
P_s	Pressure supply, N/m^2
q	Hight of car center gravity, m
R_h	Road holding factor, (-)
ST	Suspension travel, m
ST_D	Minimum allowable of suspension travel “contraction”, m
ST_E	Maximum allowable of suspension travel “expansion”, m.
$tr(*)$	Trace of square (*) matrix
U_a	Mean wind velocity, m/s
V_t	Hydraulic actuator volume, m^3
W_i	An unknown weight vector for RBFNN

w_l	A car width from left wheels to the centre of gravity, m
w_r	A car width from right wheels to the centre of gravity, m
W_{us}	Suspension weight, N
X_L	The landing tire position, m
X_u	Unsprung mass position, m
X_s	Sprung mass position, m
$\dot{X}_s$	Sprung mass velocity, m/s
$\ddot{X}_s$	Sprung mass acceleration, m/s^2
$\dot{X}_u$	Unsprung mass velocity, m/s
$\ddot{X}_u$	Unsprung mass acceleration, m/s^2
$\check{X}_u$	Unsprung mass position nonlinear control filter output, m
Z	The virtual control coordinate
$\mathbf{Z}$	The virtual control vector
δ	Steering angle, rad
δ_0	Positive constant of a nonlinear control filter
σ	Parameter for viscous friction
τ_v	Servovalve time constant, s
β_e	Effective bulk modulus, N/m^2
ρ	Hydraulic oil density, kg/m^3
$\mathcal{H}_i(\zeta)$	A basis function vector of the radial basis function neural networks
κ_{st}	Positive constant
κ_{Rh}	Positive constant
κ_w	Positive constant
$\psi(*)$	Fourth order nonlinear function
$\phi(*)$	Fourth order nonlinear function
$\Phi(u)$	The control input vector
$\varphi_{i,j}$	Centers of the receptive field in RBFNN
$\boldsymbol{\mathcal{M}}$	Equivalent mass matrix
ρ	Hydraulic oil density, kg/m^3

ρ_a	Air density
ε_N	Positive designed error of RBFNN
$\propto$	A virtual control function
$\boldsymbol{\zeta}$	RBFNN compact set parameters

INTRODUCTION

Electrohydraulic servosystems (EHSS) are essential elements in several engineering fields, such as industrial machines, aerospace flight control actuators, automobiles, and robotics. The main advantages of EHSS are to deliver fast, accurate response and simple construction. Besides, EHSS is a high power-to-weight ratio compared with mechanical and electrical systems. Furthermore, EHSS has a long life because of lubricating itself. One of the EHSS applications is vehicle electrohydraulic active suspension systems.

The suspension system is a mechanical vibration system. The primary purposes of the vehicle active suspension systems are to isolate the car cabin from road perturbations and to provide vehicle handling (stability) at different operation conditions. The automobile suspension system is also used as a bridge between chassis and wheels to maintain the wheels in the proper steer and perpendicular direction to the road surface. The vehicle suspension can also react to (acceleration, braking, cornering) forces and resist rolling. Typically, the suspension system consists of a sprung weight, unsprung weights, springs, dampers, and mechanisms. The vehicle suspension systems can be classified into three categories: a passive suspension, a semi-active suspension, and an active suspension. First, the passive suspension is designed to provide a specific range of adjustment between ride comfort and road holding because it does not contain a feedback control system. Therefore, the passive suspension has a limited compromise between ride comfort and road holding. Second, the semi-active suspension system has a controllable damper, which contains a feedback control system. The semi-active suspension system provides a better quality of performance compared to the passive suspension system. However, the force range is limited because the damper force constraints velocity. Finally, the active suspension system can respond the vertical road disturbance by using its EHSS system. The active suspension system is a wider range of force, no force-velocity constraint, and better performance. However, the active suspension is high power consumption and has many inherent nonlinearities and uncertainties in dynamic systems.

Several researchers have been developed linear control laws for quarter car active suspension systems. For example, a proportional integral derivative control law (PID) is widely applied in engineering applications, which can eliminate all present, previous, and forecast errors. Furthermore, the PID parameters can be tuned using several tuning methods such as Ziegler-Nichols, Cohen, and others. Hence, many investigators have designed the PID controller to reduce the sprung mass acceleration of active suspension systems. On the other hand, several researchers have developed a Linear Quadratic Regulator control system (LQR) to minimize the sprung mass vertical acceleration and obtain better passenger comfort for quarter car active suspension systems. Even though linear controllers had some improvement in control performances, they had degraded because of the dynamic system nonlinearities and uncertainties. Hence, other control strategies such as nonlinear control systems can be applied to overcome the system's nonlinearities and uncertainties.

0.1 Problematic research

In order to overcome the dynamic nonlinearities and uncertainties of active suspension systems, many researchers have developed nonlinear control strategies for quarter car active suspension systems such as sliding mode control system, backstepping control law. Although nonlinear control systems have the ability to overcome dynamic nonlinearities, they may not be able to deal with system uncertainties. Consequently, adaptive control systems can immediately update the parameters of a system. Therefore, hybrid control systems of adaptive nonlinear control systems were designed based on Lyapunov candidate functions for active suspension systems. There are several adaptive control systems such as discontinuous projection, fuzzy, Neural networks. Besides, many articles proved that adaptive neural networks could have better control performance than other conventional adaptive control systems.

Although most researchers have proven improvements in their control performances to obtain better passenger comfort, they did not clearly address road holding and suspension travel limits. In most previous studies, the road holding modeling system was a conditional formula

that may not obviously help to design the control law. Therefore, a novel modeling system was created in this research and called a dynamic landing tire system. The dynamic landing tire system contains a dynamic landing position and road holding ratio state variables. On the other hand, non-symmetrical suspension deflections were also considered in this thesis to realize the operation conditions: a suspension contraction limit and a suspension expansion limit. Even though the control law provides excellent sprung mass position compensation, as shown in Chapter 2, there are many suspension travel oscillations. Thus, a nonlinear control filter was developed in this research to address ride comfort, road holding, and suspension travel limits. The nonlinear control filter can also decrease the suspension travel oscillations by selecting a proper gain filter bandwidth. Hence, the nonlinear control filter can combine with the adaptive neural networks backstepping control system to provide better passenger comfort, maintain road holding, avoid reaching suspension travel limits, reduce suspension travel oscillations, and cope with the dynamic nonlinearities and uncertainties.

Even though the hybrid control system of adaptive neural networks backstepping control system coupled with a nonlinear control filter can address the suspension restrictions, the control law was designed for a SISO quarter car electrohydraulic active suspension. In order to develop a control system for full car electrohydraulic active suspension, several researchers have developed many control laws. However, the road holding could not study at stiff road perturbations. Plus, external aerodynamics disturbances were not addressed in that studies. Therefore, the authors have developed robust adaptive neural networks backstepping for multi-input-multi-output (MIMO) filtered full car electrohydraulic active suspension in the presence of both stiff road perturbation and external aerodynamic disturbances. The novelty of the study in Chapter 4 are to introduce the dynamic landing system, non-symmetric suspension travel limits, and external aerodynamic disturbances for full car electrohydraulic active suspension. Zero dynamics were also guaranteed.

0.2 Objectives and contributions

The main objectives of this thesis are to develop nonlinear control laws for car active suspension systems based on enhancing passenger comfort, maintaining road holding,

avoiding reaching suspension travel, reducing suspension travel oscillations, and overcoming the dynamic nonlinearities and uncertainties. The specific objectives of this study are:

1. To determinate a control law to minimize a sprung mass acceleration for a nonlinear and uncertain mathematical model of a quarter car active suspension.
2. To create a mathematical modeling system to evaluate a required tire landing displacement and road holding ratio, which called a dynamic landing tire system.
3. To design a nonlinear control filter to represent the input desired control signal.
4. To investigate a control law for a restricted quarter car active suspension using the previously established model.
5. To develop a control law for MIMO full car active suspension system in the presence of both external aerodynamic disturbances and stiff road perturbations.

The first chapter is a comprehensive literature review. It includes physical descriptions of significant suspension classifications and active suspension control survey. The physical descriptions consist of introduction, vehicle positive suspension systems, semi-active suspension systems, and active suspension systems. In this chapter, previous works of active suspension control systems are also mentioned according to the model complexity and control strategies. Finally, the research methodology and contributions are also announced as general and specific objectives and three research contributions.

In the second chapter, an adaptive neural networks backstepping control system (ANNC) is developed for the SISO nonlinear modeling system of a quarter car active suspension. This chapter presents five sections of introduction, the notation and problem statement, the control law design, the simulation study, and conclusions.

In the third chapter, there are five sections, including introduction, problem statement, control design, simulation comparative study, and conclusion. We have created a new mathematical modeling system for a dynamic landing tire, and non-symmetrical suspension travel limits are also considered in the problem statement section. In the control design section, a nonlinear control was developed to address the suspension restrictions.

In the fourth chapter, robust adaptive neural networks backstepping control MIMO system is investigated for MIMO nonlinear modeling of full car filtered electrohydraulic active suspension systems. There are also five sections in this chapter, as well as chapters 2 and 3. In the control design section, the control stability and zero dynamics system were guaranteed.

Finally, the conclusion summarizes the three contributions that are in chapters 2, 3 and 4. The recommendation describes the future works.

CHAPTER 1

LITERATURE REVIEW

This chapter is organized to search the previous researches that are related to the work in this thesis. This chapter has been written as an introduction, vehicle passive suspension systems, semi-active suspension systems, active suspension systems, active suspension control strategies, and contributions with research methodology.

1.1 Introduction

The vehicle suspension is a substantial device in the car structure, reducing transferred vertical road energies to the vehicle body (sprung mass) to provide passenger comfort. Thus, the car suspension is connected between the sprung mass and axles of the wheels. There are several suspension classifications: passive suspension, semi-active suspension, and active suspension. In general, the car passive suspension system consists of a sprung mass, unsprung masses, springs, and dampers. The semi-active suspension structure is a similar passive suspension structure except for controllable dampers. The active suspension has a sprung mass, unsprung masses, springs, dampers, and actuators. In addition, the researchers have classified the vehicle suspension system into three other categories according to the degrees of freedom feature complicity such as full suspension, half suspension, and quatre suspension (Baumal et al., 1998; Alleyne et Hedrick, 1995; Malcolm et al., 2002; Yamashita et al., 1994). The full car suspension system is seven degrees of the freedom vibration system. The half-car suspension modeling system was existed to evaluate four degrees of the freedom vibration system. Finally, the quarter car suspension system was existed to evaluate two degrees of the freedom vibration system.

1.2 Vehicle passive suspension systems

Vehicle suspension systems followed relatively closely the evolution of the vehicle industry. In the 17th century, the first metal springs were developed for transportation technology (Guglielmino et al., 2008). Nowadays, the passive suspension system is an essential system in the conventional vehicle structure. In passive suspension, springs and dampers are supported between the vehicle body (sprung mass) and the axles of the wheels (unsprung masses). So, the springs absorb vertical road energies; and the dampers dissipate them to minimize sprung mass accelerations to provide passenger comfort. Passive suspension is an open-loop control system, which does not have a feedback control signal.

Plenty of researches have modeled several mathematical passive suspension systems. In Figure 1.1, simple mathematical modeling of two degrees freedom for a quarter car passive suspension system was applied to study the suspension performance (Kim, 1996; Hrovat, 1997; Satoh, 1990; Thomson, 1970).

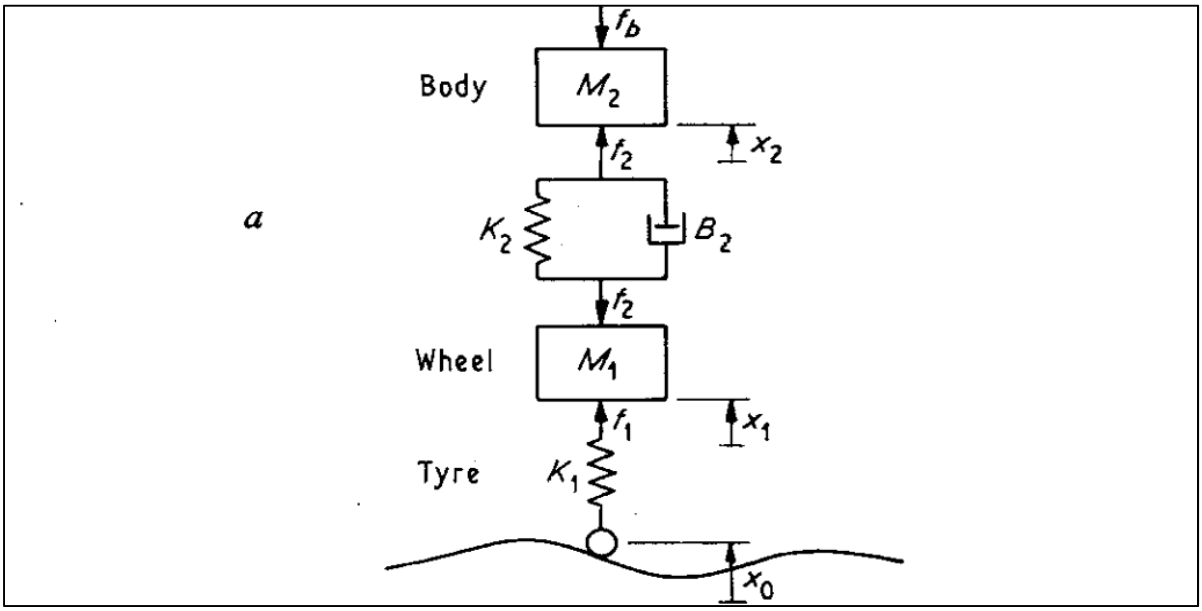

Figure 1.1 Quarter car passive suspension (Thomson, 1970)

Let the state variables be a sprung mass position X_2, unsprung mass position X_1, and the vertical road position X_0. The passive suspension components are a spring stiffness (K_2), damping coefficient (B_2), and tire stiffness (K_1). The suspension spring and damper are connected between the wheel mass and the vehicle body (Alkhatib, 2004). The quarter car passive suspension can be represented.

$$m_2\ddot{X}_2 = -K_2(X_2 - X_1) - B_2\left(\dot{X}_2 - \dot{X}_1\right) \tag{1.1}$$

$$m_u\,\ddot{X}_u = K_2(X_2 - X_1) + B_2\left(\dot{X}_2 - \dot{X}_1\right) - K_1(X_1 - X_0) \tag{1.2}$$

The passive suspension system is an open-loop control system. Hence, Figure 1.3 shows an equivalent block diagram of the quarter car passive suspension, which sketched in Figure 1.1 (Thomson, 1970).

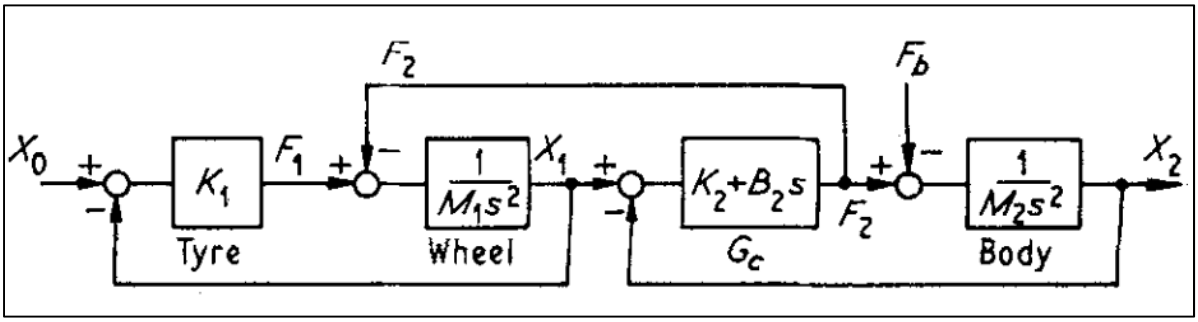

Figure 1.2 Quarter car Passive suspension block diagram (Thomson, 1970)

The block diagram passive suspension in Figure 1.2 may be considered as two stages of the mechanical filter. Hence, Passive suspension is worked as a low-pass filter, which significantly attenuated the medium and high road frequency perturbations. In (Rajamani, 2012), the linear elements of the passive suspension can be solved to obtain several transfer functions, which represent a sprung mass acceleration $H_A(s)$, a sprung mass position $H_p(s)$, suspension travel $H_{SD}(s)$, and tire deflection $H_{td}(s)$. The passive suspension modeling system in equations (1.1) and (1.2) can be written as follows.

$$\dot{x} = Ax + L\dot{x}_0 \tag{1.3}$$

where $A = \begin{bmatrix} 0 & 1 & 0 & -1 \\ -\frac{K_2}{m_2} & -\frac{B_2}{m_2} & 0 & \frac{B_2}{m_2} \\ 0 & 0 & 0 & 1 \\ \frac{K_2}{m_1} & \frac{B_2}{m_1} & -\frac{K_1}{m_1} & 0 \end{bmatrix}$, $L = \begin{bmatrix} 0 \\ 0 \\ -1 \\ 0 \end{bmatrix}$, $x = \begin{bmatrix} x_s - x_u \\ \dot{x}_s \\ x_u - x_r \\ \dot{x}_u \end{bmatrix}$

In order to analyze passenger comfort, the acceleration transfer function $H_A(s)$ can be evaulated as follows.

$$H_A(s) = \frac{\ddot{x}_2(s)}{\dot{x}_0(s)}$$

$$= \frac{K_1 S(B_2 S + K_2)}{m_1 m_2 S^4 + B_2(m_2 + m_1)S^3 + \big((K_2 + K_1)m_2 + K_2 m_1\big)S^2 + K_1 B_2 S + K_2 K_1} \tag{1.4}$$

The rattle space transfer function $H_{SD}(s)$ is also an important factor as follows.

$$H_{SD}(s) = \frac{x_2(s) - x_1(s)}{x_0(s)}$$

$$= \frac{-m_2 K_1 S^2}{m_1 m_2 S^4 + B_2(m_2 + m_1)S^3 + \big((K_2 + K_1)m_2 + K_2 m_1\big)S^2 + K_1 B_2 S + K_2 K_1} \tag{1.5}$$

The transmissibility ratio $H_p(s)$ is defined the sprung mass isolation.

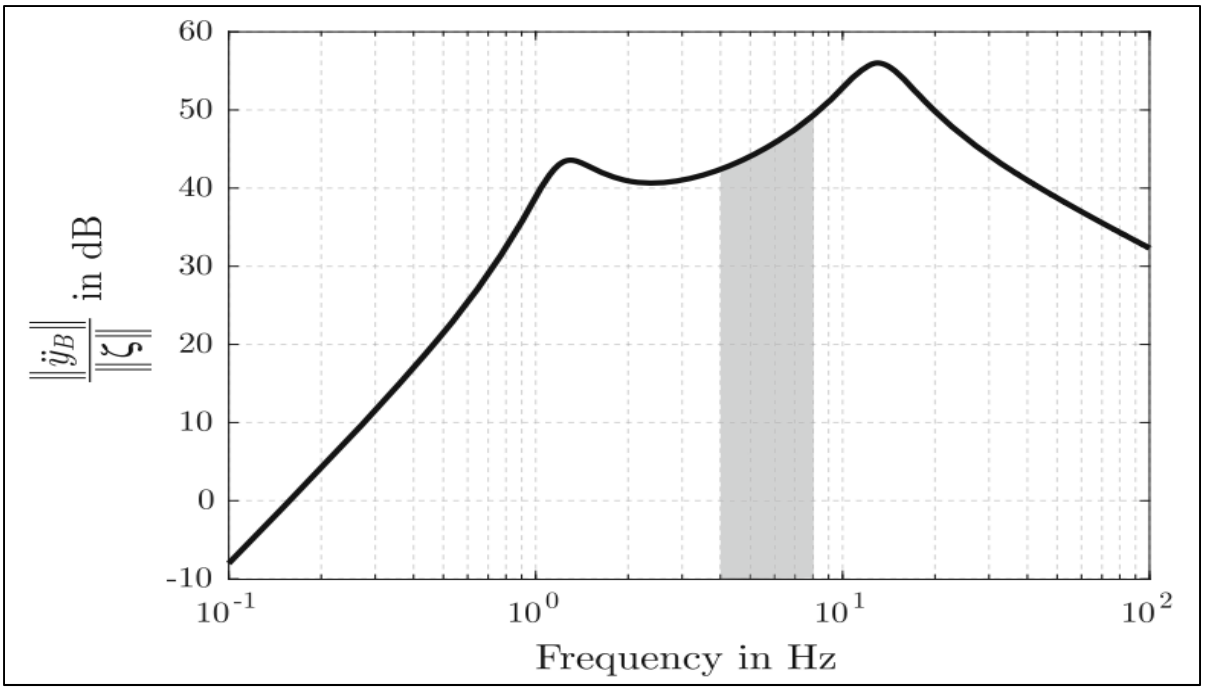

Figure 1.3 The human sensitivity in the range 4–8 Hz (Lugner, 2019)

$$H_p(s) = \frac{x_2(s)}{x_0(s)}$$

$$= \frac{K_1(B_2S + K_2)}{m_1m_2S^4 + B_2(m_2 + m_1)S^3 + \big((K_2 + K_1)m_2 + K_2m_1\big)S^2 + K_1B_2S + K_2K_1} \tag{1.6}$$

The transfer function of tire deflection $H_{td}(s)$ can be represensted

$$H_{td}(s) = \frac{x_u(s) - x_r(s)}{x_r(s)}$$

$$= \frac{-m_1m_2S^3 - B_2(m_2 + m_1)S^2 - K_2(m_2 + m_1)S}{m_1m_2S^4 + B_2(m_2 + m_1)S^3 + \big((K_2 + K_1)m_2 + K_2m_1\big)S^2 + K_1B_2S + K_2K_1} \tag{1.7}$$

In general, the frequency response function of the sprung mass acceleration $H_A(s)$ can show the typical two peaks near the eigenfrequencies in the presence of a harmonic road perturbation, as shown in Figure 1.3.

The sensitive human frequency is about 3-8 Hz (Tuan et al., 2001). Therefore, the suspension design must avoid eigenfrequencies in that the human sensitivity range. On the other hand, the passive suspension system has conflicting performances between passenger comfort and road holding. In Figure 1.4, there is a tradeoff between ride comfort and road holding. The soft suspension travel of passive suspension provides a high level of ride comfort and low vehicle stability; otherwise, hard suspension travel makes an excellent road holding while lots of road excitations transfer to the vehicle body (Savitski et al., 2017).

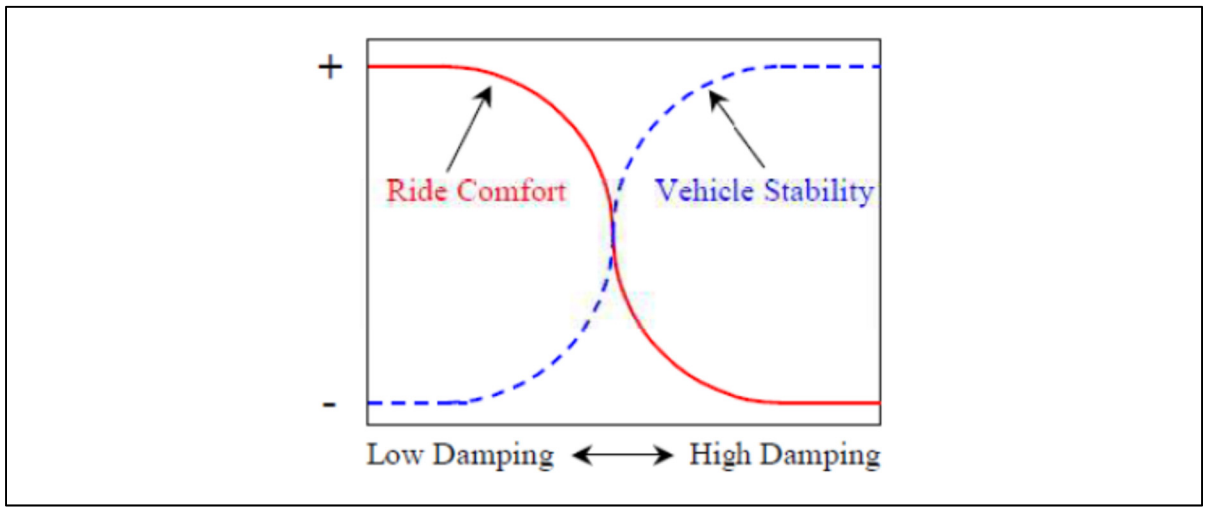

Figure 1.4 Compromise between ride comfort and vehicle stability for passive suspension system (Desai et Kale, 2016)

In addition, there is also a tradeoff between ride comfort and suspension travel, as shown in Figure 1.5. The dimensionless root mean square (RMS) of the sprung mass acceleration was plotted versus the suspension travel. The RMS vertical sprung mass acceleration decreases by increasing both damping ratio and tire deflection. Otherwise, the RMS vertical acceleration is increased.

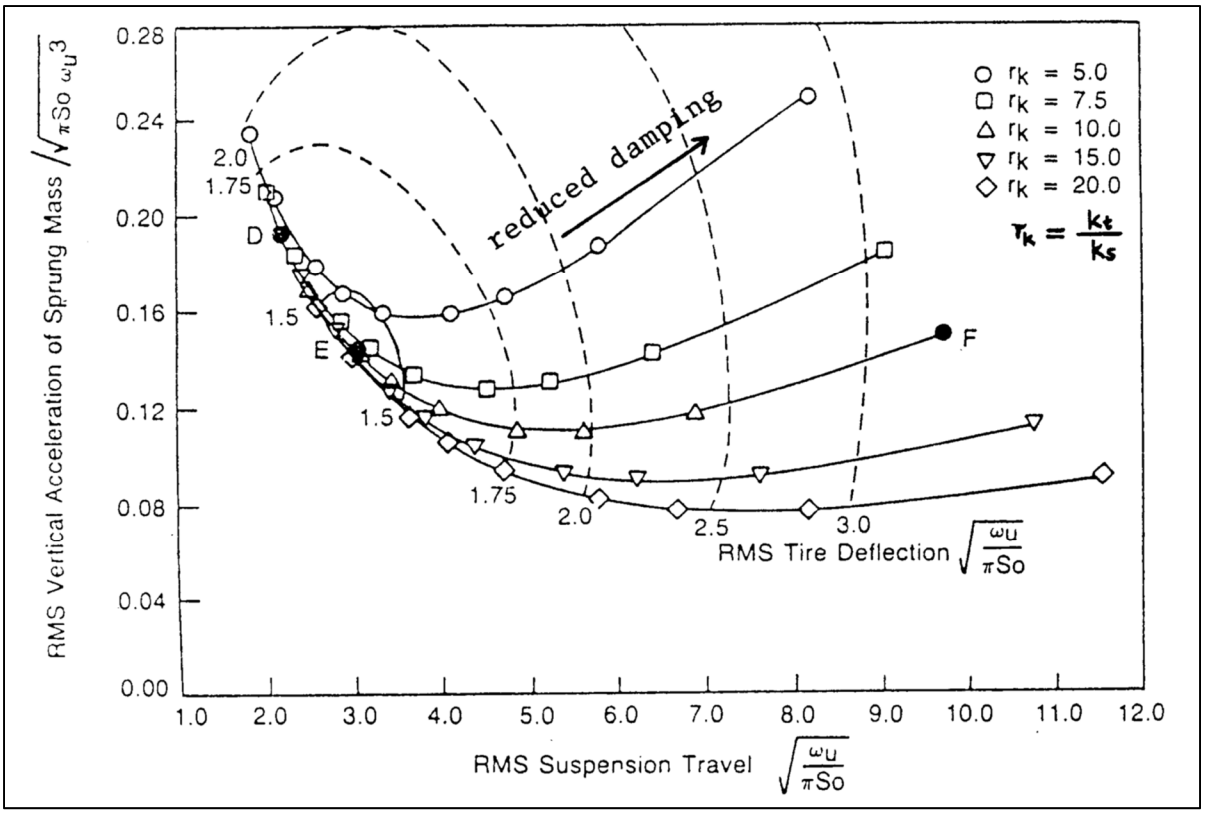

Figure 1.5 Dimensionless relationship between several suspension outputs (Yue, 1987)

In conclusion, there are several compromise suspension performance functions in quarter car passive suspension systems. For instance, there are a tradeoff between passenger comfort and vehicle stability, a tradeoff between passenger comfort and suspension travel, and a tradeoff between passenger comfort and tire deflection. The full car passive suspension system is briefly introduced in the following topic.

The full automobile passive suspension system is essential in conventional vehicles. It is connected between the vehicle chassis and the four unsprung masses (wheels). Therefore, the full car passive suspension has seven degrees of freedom vibration system, which are sprung mass directions (heave, angular roll, and angular pitch) and four unsprung mass directions.

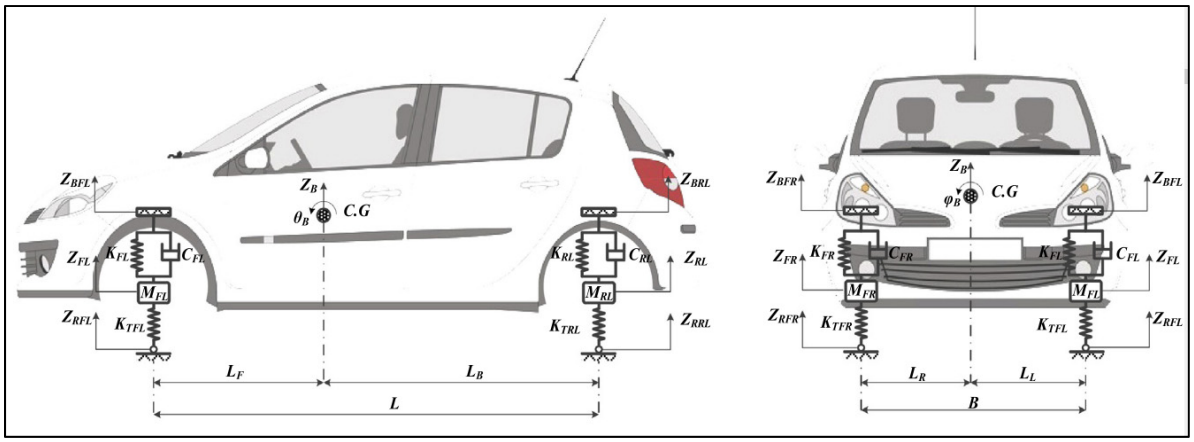

Figure 1.6 Full car passive suspension (Abdelkareem, 2018)

The principle work of the full passive suspension system is to absorb road energies into springs and dissipate them into the dampers to provide passenger comfort. The second primary purposes of the full car passive suspension system are to keep car stability (road holding) during the braking, steering, and maneuverability. The road holding quality provides the safety driving, especially during braking, cornering, and swerving. The road excitations may generate from the unevenness of a road, the wind, rotating unbalance of the wheel, a defect in the tire, and suddenly barking.

1.3 Semi-active suspension systems

A semi-active suspension system is as similar to a passive suspension system except for the damper, controlled by feedback control system. External electrical power is required to adjust the damping level and to operate the controller and sensors. The semi-active suspension system provides a better quality of performance compared with the passive suspension system. Figure 1.7 shows a sketch of the main components of the semi-active suspension system. The main ideas of the semi-active suspension are to adjust the coefficient of the suspension damper between soft and hard. The semi-active suspension damper can provide asymmetric damping force in compression or extension. Semi-active suspension systems are basically classified into orifice variable-based semi-active suspension and Magnetorheological fluid-based semi-active suspension (Tseng et Hedrick, 1994).

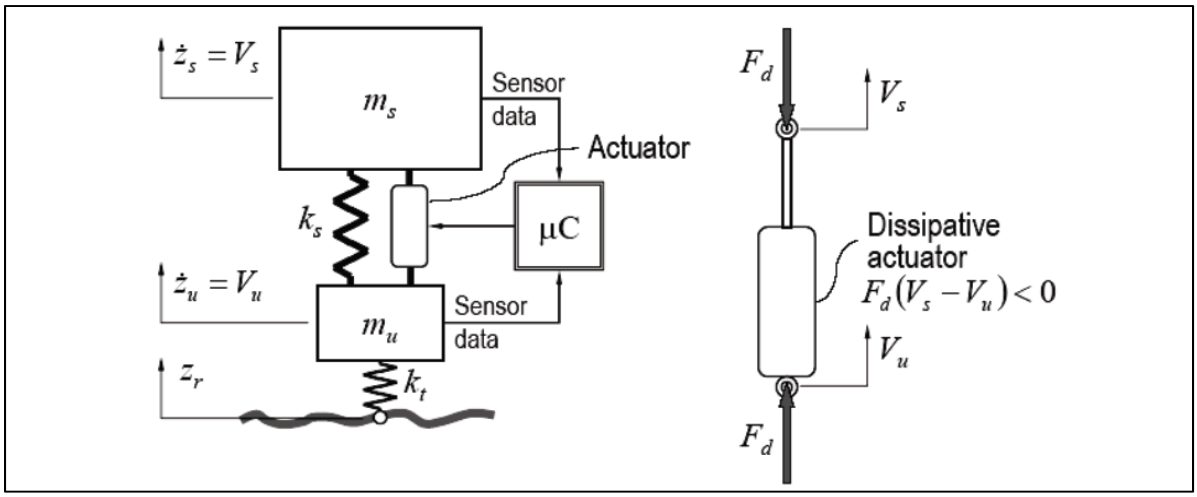

Figure 1.7 Semi-active Suspension physical model (Fijalkowski, 2011)

The orifice variable damping system is a semi-active suspension system such as a skyhook controller. In 1974, Karnopp et al. gave the name for this logic, called skyhook (Guglielmino et al., 2008). The skyhook controller permits the damping coefficient to vary between high and low damping levels to improve passenger comfort. The ideal skyhook control is an on-off control system as follows.

$$F_d = F_{\text{skyhook}} = \begin{cases} c_{sky}\dot{Z}_u & (\dot{Z}_s - \dot{Z}_u)\dot{Z}_s > 0 \\ 0 & (\dot{Z}_s - \dot{Z}_u)\dot{Z}_s \leq 0 \end{cases} \tag{1.8}$$

where $\dot{Z}_s$ is the absolute sprung mass velocity, and $\dot{Z}_u$ is the absolute velocity of the sprung mass. The skyhook damper can reduce body vertical acceleration to approximately one and half of that in passive suspension at low frequencies (Satoh et al., 1990).

The other class of semi-active suspension is Magneto-Rheological (MR) Damper. The MR dampers are used Magneto-rheological fluids to obtain controllable fluids in semi-active dampers. The rheological properties are rapidly varied fluid viscosity by applying a magnetic field. There are several rheological fluids in this technique, such as magneto-rheological fluids

(MRF), nano-magneto-rheological fluids (NMRF), and magneto-rheological elastomers (MRE) (Fijalkowski, 2011).

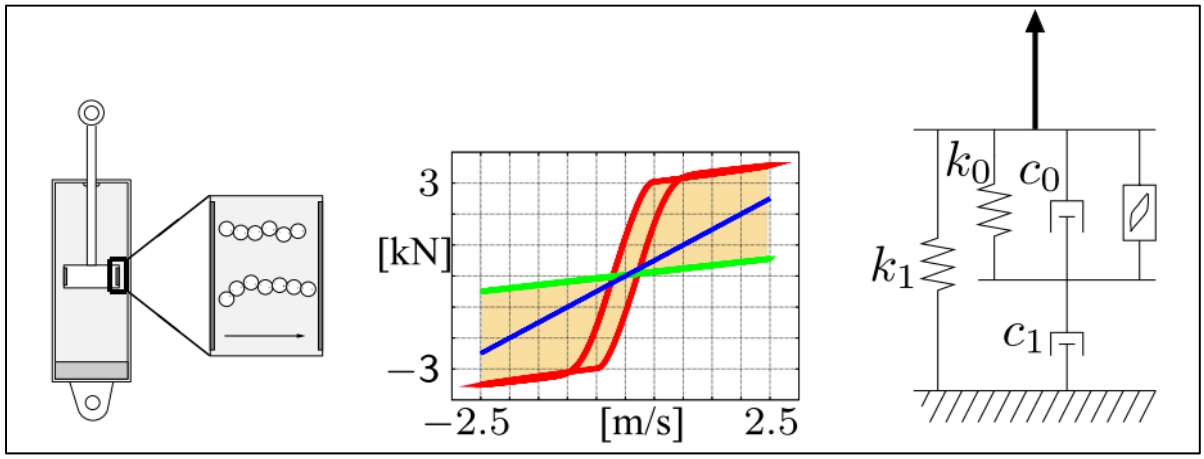

Figure 1.8 Controllable electrorheological fluids (ERF) shock absorber (Rettig et Stryk, 2005)

In Figure 1.8, the ERF variable viscous force is generated between two electrodes, as shown in the middle and left sketches.

The disadvantages of the variable damper systems are difficult to implement a high force at low velocities and a low force at high velocities in real-time.

1.4 Active suspension systems

Active suspension systems are a huge research area for more than six decades. In 1956, the earlier attempt to reduce a vehicle's body deflection was a using Packard torsion bar suspension with both an electric motor and an air suspension (Thomson, 1970). The active suspension system can precisely respond the vertical road disturbances. Therefore, the active suspension can prevent the transmission of vertical road energy to the vehicle's body on rough and bumpy roads. In addition, the active suspension is also suitable for leveling flat a vehicle's body during accelerating, braking, and cornering. The hydraulic actuators can rapidly respond

under a control system based on control law design to compensate the sprung mass position more than 70% of that in passive suspension (Kim et Ro, 1998). There are three active suspension models applied to evaluate control law performance: a quarter, half, and full car active suspension systems. Several actuator types can be used in active suspension systems, such as a hydraulic actuator, an electric actuator, and a pneumatic actuator. The main task of the active suspension actuator is to disperse energy from the sprung mass. The best control design can perfectly manage the compromise between vehicle ride comfort to road handling. Therefore, there is an actuator for each wheel in the full car active suspension. The full car active suspension is similar to passive suspension, which has seven degrees of freedom. Therefore, the sprung mass moves into three directions (bouncing, rolling, pitching) and four vertical directions of the wheels. Several sensors are used to measure sprung mass accelerations, positions. The basic configuration of the hydraulic active suspension is in Figure 1.9.

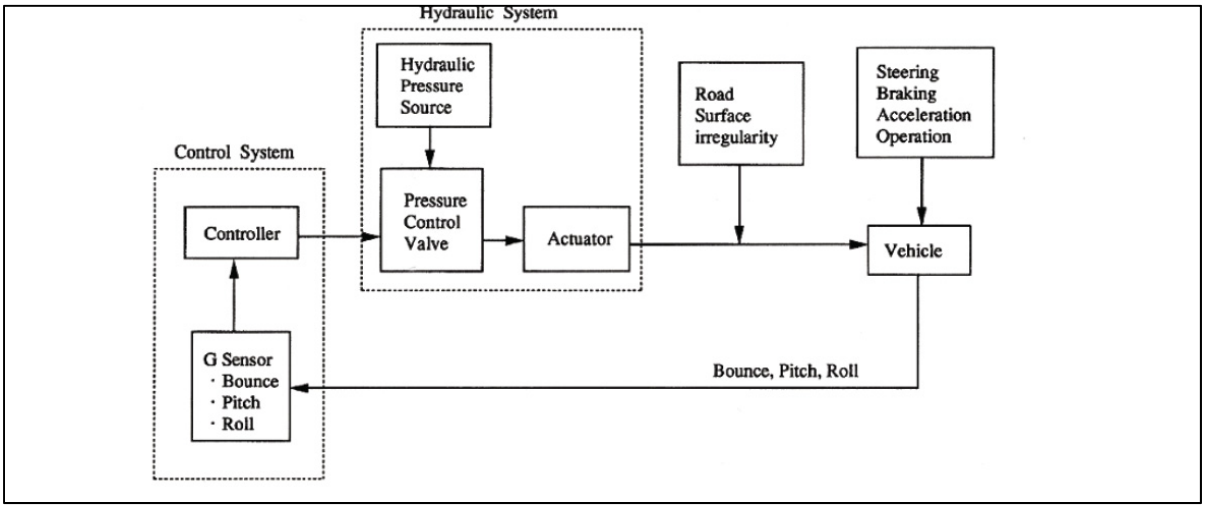

Figure 1.9 Hydraulic and control systems for active suspension (Jurgen, 1999)

The operational hydraulic pressure is monitored by several sensors to suppress changes in sprung mass positions and reduce road vibration effects (Jurgen, 1999). In Figure 1.10, there is a general full car active suspension layout. Therefore, the principal and accessory components of the electrohydraulic active suspension system are four primary actuators,

control unit, multivalve unit, accumulators, several sensors, the main hydraulic pump, the oil cooler, reservoir oil tank, and others.

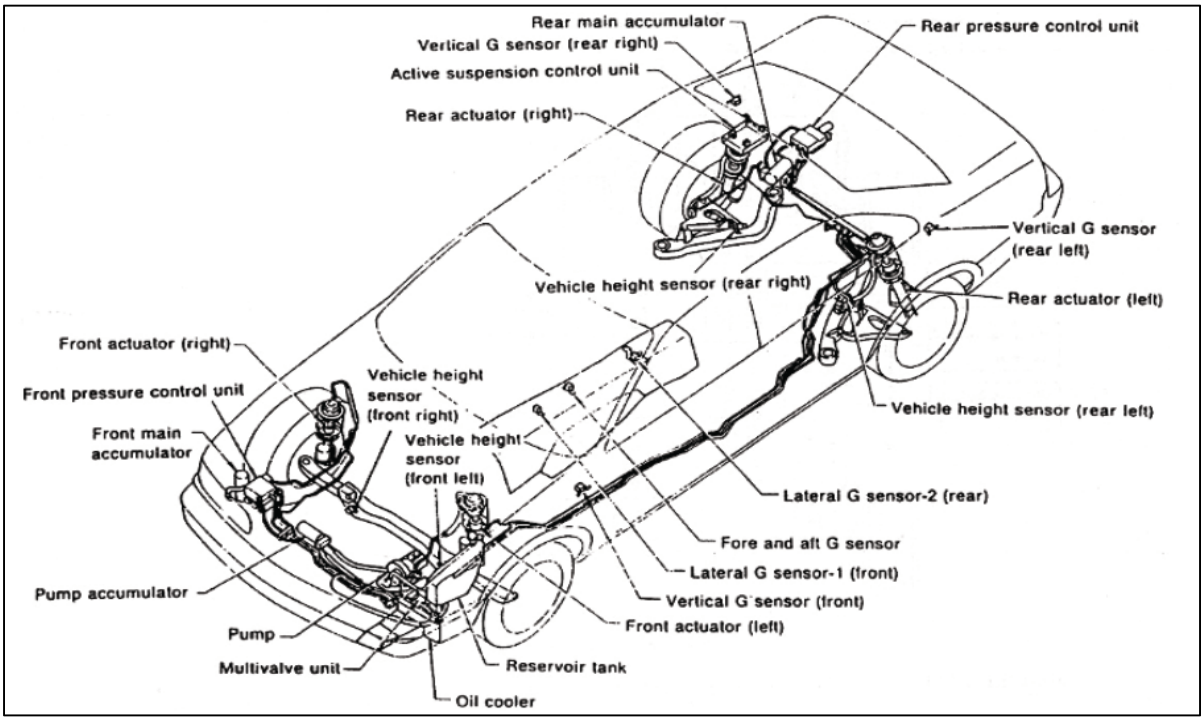

Figure 1.10 Main components of a full car electrohydraulic active suspension (Jurgen, 1999)

Figure 1.10 shows a full car active suspension, which consists of springs, dampers, tires, and electrohydraulic servovalve systems (EHSS). The electrohydraulic servovalve system (EHSS) is characterized by being fast, accurate, simple construction, high power to weight ratio, long life, low maintenance cost, and powerful responses. Figure 1.11 shows that a schematic diagram of the EHSS for a quarter car active suspension system consists of oil a pump, a pump accumulator, a multivalve unit, the main accumulator, a pressure control unit, an actuator, several sensors, and a control system (Jurgen, 1999). The oil pump supplies the necessary oil power supply.

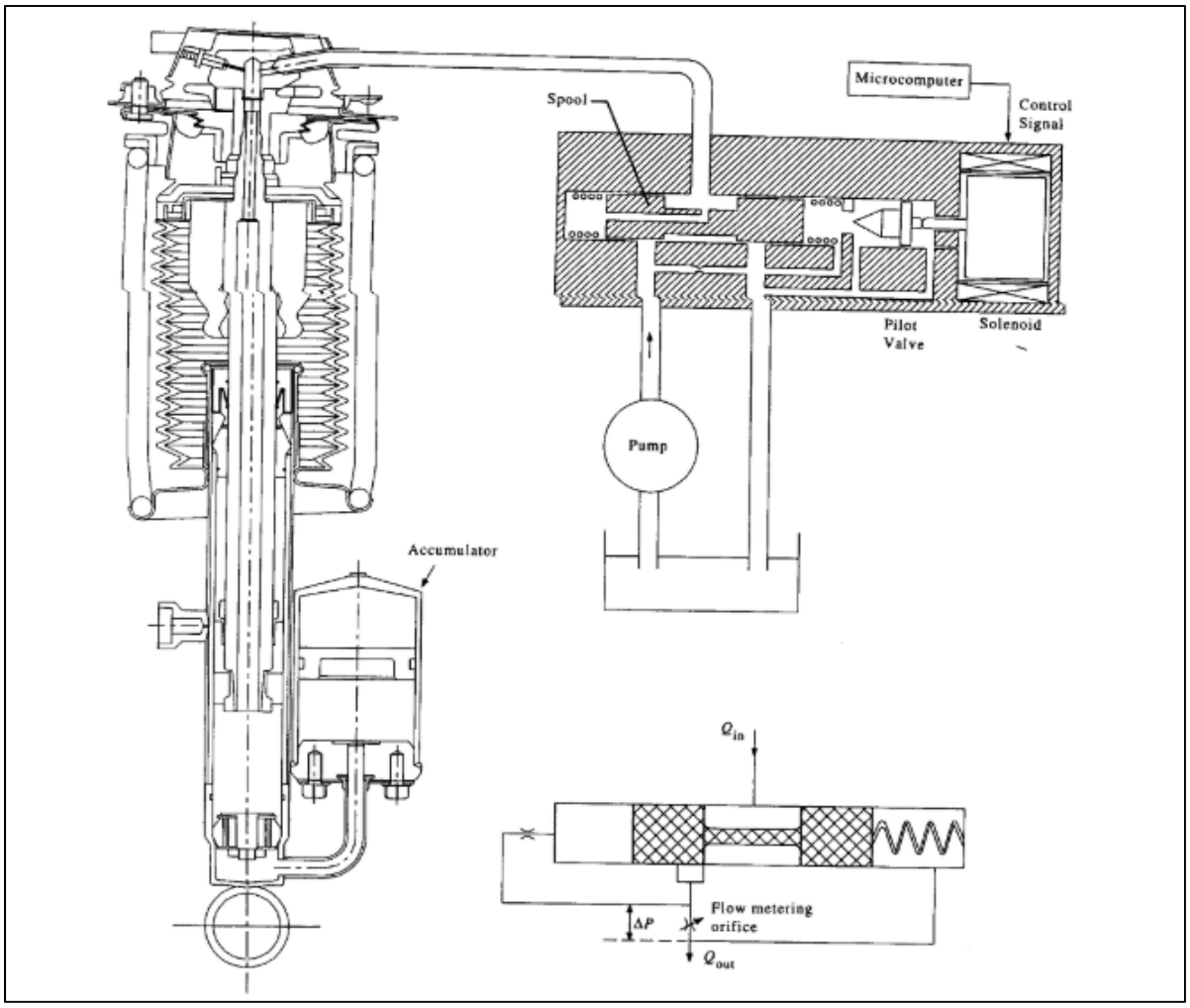

Figure 1.11 Schematic diagram of Nissan Infinity Q45a Electrohydraulic Pressure Control System (Hrovat, 1997)

The purpose of the pump accumulator is to remove the pulsating action of the oil pump from the oil pressure supply. The multivalve unit is necessary to control the hydraulic pressure supply to the actuators. The main accumulator remains the oil pressure constant, which compensates the required amount of the oil mass flow rate due to various oil domains to the actuators. The pressure control unit controls the operational hydraulic pressure for actuators according to signals received from the control unit. Actuators are constructed from the hydraulic power cylinder, a sub-accumulator, damping valves, and other accessories. In order

to absorb and damp the road high frequency, the actuator must have both the sub-accumulator and damping valve.

The quarter car active suspension system is a simple model, as shown in Figure 1.12. The main components of the quarter car active suspension are a sprung mass (m_s), an unsprung mass (m_u), a spring (k_s), a damper (b_s), an actuator (F_a), and a tire stiffness (k_t).

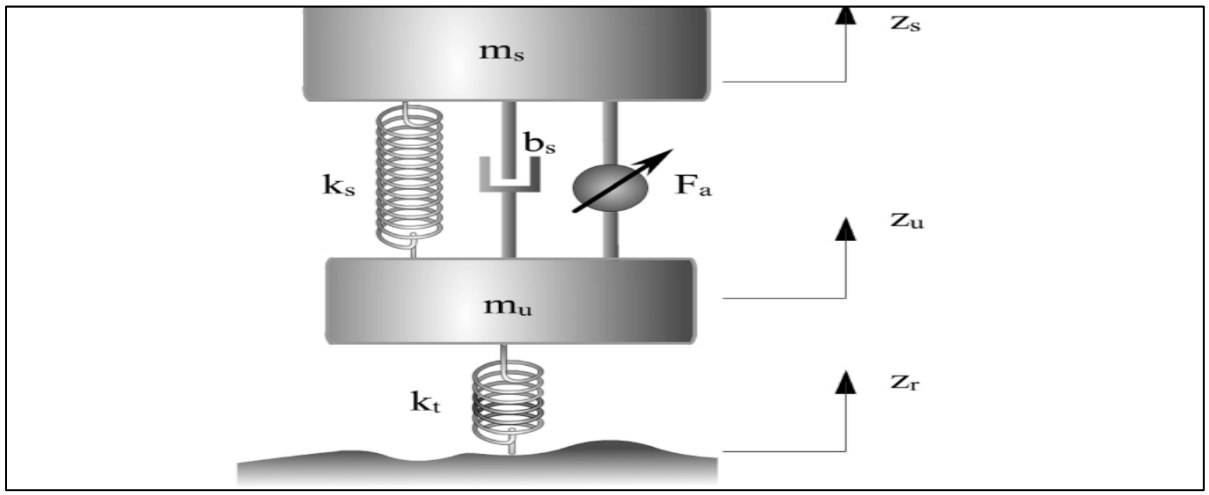

Figure 1.12 Simple sketch of a quarter car active suspension (Rajamani, 2012)

Figure 1.13 shows the suspension performance for active, semi-active, and passive suspension systems.

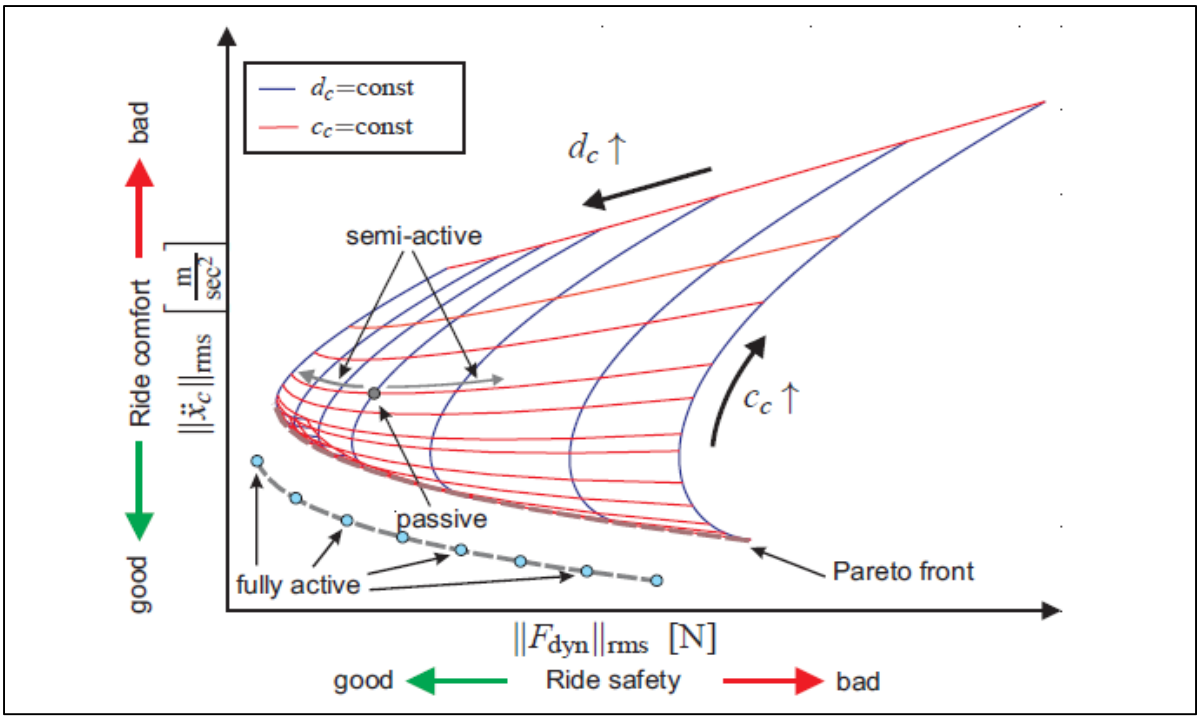

Figure 1.13 The tradeoff between ride comfort and ride safety (Koch, 2011)

Accordingly, the minimized root mean square of sprung mass acceleration $\|x_c\|_{rms}$ provides better passenger comfort. Low damping d_c and low stiffness c_c can make the suspension travel soft. Consequently, the suspension provides better passenger comfort. However, the suspension travel oscillations may reach their limits. On the other hand, the root mean square of the dynamic tire force $\|F_{dyn}\|_{rms}$ must be also minimized to obtain a good road holding. Thus, the tires must remain in contact with the road surface to ensure the bounded F_{dyn}. In semi-active suspension, the damper can be adjusted to improve passenger comfort or road holding better than passive suspension. Finally, the fully active suspension provides the best compromise between road holding and ride comfort. However, the fully active suspension needs high external power.

1.5 Suspension performance functions

It can conclude that the vehicle active suspension design must consider several functions of performance. In (Gillespie, 1992), the suspension performance has six functions and describes as follows.

Passenger Comfort: the sensitive human frequency is about 3-8 Hz (Tuan et al., 2001). Therefore, the sprung mass acceleration must be reduced to the human's comfort. However, ride improvements always degrade performance in the other modes.

Suspension travel limits: suspension travel is a suspension stroke on an unregular road. In bad road conditions, Passenger comfort needs to increase in suspension travel and oscillations. Thus, suspension travel may reach and hit the limit stop. As a result, the active suspension may be damaged if the control law is not a tradeoff between passenger comfort and suspension travel limits.

Road holding: Road holding is an important parameter, which can maintain road tire conductivity. Therefore, Road holding can improve brake, acceleration, and cornering. On the other hand, there is also a compromise between passenger comfort and road holding.

Roll Control: roll control in cornering can be reduced using an anti-rolling bar and actuator force to prevent body roll. Several parameters monitor the roll control, such as vehicle speed, steer angle, steer rate, and lateral acceleration.

Dive Control: during braking, the vehicle dive (forward pitch) can increase by increasing the braking rate.

Squat Control: during longitudinal acceleration, the vehicle squat (rearward pitch) can increase by increasing the longitudinal acceleration rate.

1.6 Active suspension control strategies

Many studies in car active suspension systems to improve suspension performance (ride comfort, ride safety). In that studies, there were several control strategies applied for the active suspension systems, such as linear control systems, nonlinear control systems, adaptive control systems, adaptive neural network control systems, and robust adaptive neural network control MIMO systems.

There were many works that used linear control systems as follows. Thomson has early designed a feedback compensator for a quarter car active suspension (Thomson, 1970). a compensation H_o was added into the feedback path, as shown in Figure 1.14. A single transfer function ($G_c(s) = K_2 + B_2S$) was applied to control the overall transmission ($T_0 = X_2/X_0$), the secondary ($T_n = -X_2/F_b$), and the axle response ($T_1 = X_1/F_0$).

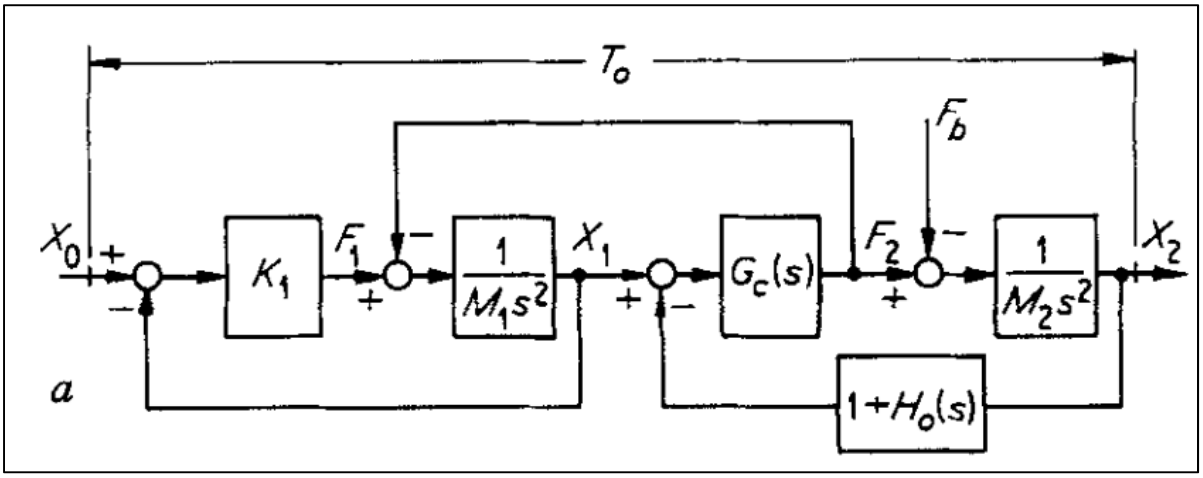

Figure 1.14 A block diagram of a quarter car active suspension of a feedback system (Thomson, 1970)

Although the results showed an improvement in ride comfort, there were large tire dynamic deflections. In later decades, several studies were developed a linear quadratic regulator (LQR) for quarter car active suspension systems (Shirdel et al., 2010; Pratheepa, 2010; Hassan, 1986;

Yue, 1987). The Linear Quadratic Regulator is a well-known control method that determines optimally controlled feedback gains to ensure the closed-loop stable and high-performance design of a system. the LQR was designed based on minimizing the linear quadratic cost function. The results exhibited that LQR provided better compensation than the passive suspension; however, the tire deflection was worse than passive suspension. The electrohydraulic of the servosystem was also not addressed.

Although the electrohydraulic servosystems provide accurate tracking positions, the EHSS has highly nonlinear dynamics and mostly model uncertainties due to parametric uncertainties and uncertain nonlinearities (Sallah, 2015). Therefore, several studies were developed to cope with undesired phenomena. In (Alleyne et Lui, 2000), a Lyapunov-based force control approach was investigated for a hydraulic cylinder servovalve system; the modeling uncertainties were addressed using a gradient parameter estimation scheme. In that study, the results showed a good control performance. A robust adaptive control was applied for an electrohydraulic servovalve system (Yao et al., 1998). Thus, simulation results showed that the designed control system yielded a better tracking performance and a high robust parameter adaption. A discontinuous projection-based adaptive sliding mode control was developed to handle various parameter uncertainties and uncertain nonlinearities for a hydraulic actuator (Duraiswamy et Chiu, 2003). Although the study results showed good control performance, the servovalve dynamic system was not addressed. In conclusion, EHSS can be used in the active suspension systems. In order to address the electrohydraulic active suspension system, A proportional integral derivative control system PID was used for quarter car active suspension systems to reduce the sprung mass acceleration (Abd El-Nasser et al., 2015; Abdalla et al., 2015; Hanafi, 2010; Karam et al., 2008; Mouleeswaran, 2012a). The PID control theory works to eliminate or minimize the error deviation in the system that is a difference between the desired reference point and measured process value, by adjusting a plant variable to a new control value. There were improvements in ride comfort to that in passive suspension. However, the PID needs to tuning parameters to provide better performance. Therefore, many researchers have investigated nonlinear control strategies to cope with nonlinearity and uncertainties in the active suspension systems.

A sliding mode control system (SMC) was applied for active suspension systems in many studies (Alleyne et Hedrick, 1995; Kim et Ro, 1998). Sliding mode control is a particular case of feedback linearization and also calls a variable structure control. The SMC theory alters a nonlinear dynamic system by using a discontinuous control signal to make sliding on a cross-section of the system (Slotine, 1991). Even though the SMC indicated high control performance, there is some chattering in control signals. Other researchers have investigated a backstepping control system for active suspension systems (Hu et Liu, 2008; Lin et Kanellakopoulos, 1997). In general, active suspension modeling systems have multiple dynamics (Mechanical, hydraulic, electrical) systems and mismatched uncertainties (Liu, 2013). Therefore, the backstepping control approach was a good choice to control active suspension systems. Backstepping design is recursively serious of steps. The steps start back from the control input with the lower dimension subsystem scalar equation. Each step results in the next step design, which is separated by a large number of integrations. The final step is designed for true control input, which exists by the final Lyapunov function. The final Lyapunov function consists of summing the Lyapunov functions of the other stages. The results of the previous works showed that there was progress in control performance. However, there was a noise in the control signal because of nonlinearities in modeling certain functions. The major problem with this approach is to determine regression matrices of nonlinear and uncertain modeling systems. In order to overcome the nonlinearities and uncertainties of active suspension systems, adaptive nonlinear control systems must be designed.

The nonadaptive controller remains fixed parameters as long as applying the system. So, the nonadaptive controller is designed depending on its structure and design on a priori information. On the other hand, the controller that based on a posterior information (changes in parameters) is called an adaptive controller (De Queiroz et al., 2000). Therefore, plenty of investigators have developed adaptive control systems for active suspension systems. An adaptive sliding mode control system was developed to compensate for an active suspension system (Alleyne et Hedrick, 1995). A comparative study between active and passive suspensions was presented in that article. An adaptive multi-surface sliding control system was developed for a non-autonomous quarter car active suspension; the results showed a better

improvement in a sprung mass position compensation than passive suspension (Chen et Huang, 2005). An adaptive backstepping control scheme was investigated for a quarter car active suspension (Sun et al., 2014); a discontinuous projection was adaptively applied for the quarter car active suspension system. However, the electrohydraulic servovalve system of the active suspension was not addressed in that study. A hybrid controller of an H_∞ with adaptive control systems was investigated to address a quarter automobile electrohydraulic active suspension system (Fukao et al., 1999). Although the results showed improvements in control performance, the suspension parameters were partially known. A hybrid controller of a higher order sliding mode control system coupled with a particle swarm optimization approach was investigated for a quarter car active suspension (Qin et al., 2017); the sprung mass position compensation was better improved compared to passive suspension and other controllers. Most previous studies were adaptively applied discontinuous projection methods. However, adaptive neural networks control systems can compensate for the sprung mass position and overcome a dynamic system's nonlinearities and uncertainties. An adaptive neural networks control system was investigated for a quarter car active suspension (Huang et al., 2015). The results showed that vehicle body position was highly compensated compared to passive suspension. Even though the previous works showed improvements in suspension performance, the dynamic tire liftoff was not precisely addressed.

Several articles were developed for a full vehicle active suspension. D Saifiaa et al. have developed a Takagi-Sugeno fuzzy for a full car active suspension (Liu et Li, 2013); there was improved control performance compared with passive suspension. A dynamic neural network-based feedback linearization control system was designed for active full car suspension using PSO (Pedro et al., 2018). The results showed improving control performance versus passive suspension and PID control systems. However, a high control chattering was generated in the control signal. An H_∞ static output feedback control system was investigated to improve passenger comfort under suspension constraints of full car active suspension (Haiping et al., 2013). In addition, many articles were recently published to develop different control strategies for full car active suspension systems. A fault-tolerant-control scheme based on an extended state observer was applied for full car active suspension (Gang, 2020). A terminal sliding mode

controller and fractional order terminal sliding mode controller were designed for an active suspension system (Yuvapriya et al., 2020). An active disturbance rejection and fuzzy sliding mode control systems were developed to improve the ride comfort of full car suspension systems (Wang et al., 2021). A hybrid interval type-2 fuzzy logic controller was investigated for full vehicle active suspension (Yatak et Sahin, 2021). A distributed state estimation architecture was designed for an active suspension system (Yin et al., 2021). Even though the previous studies were shown improvements in control performance, both the external aerodynamic disturbances and a high-frequency bumpy road design were not addressed for full car active suspension systems. The effect of the sudden air turbulence may rock the vehicle. In order to design an excellent control system for full car active suspension, the modeling system must be precise.

1.7 Contributions

The main contribution of this study is to develop new control law strategies based on electrohydraulic active suspension systems. In this thesis, we contribute two published articles and submit another one as follows.

1.7.1 Contribution 1

An adaptive neural network backstepping control system (ANNC) was designed for a quarter car active suspension system. The mathematical modeling system is an unmatched model uncertainty because the modeling system consists of several modeling systems, and the control signal does not appear in all state-space equations. Hence, the backstepping control system has the ability to deal with unmatched model systems. Furthermore, the adaptive neural network can approximate the unknown smooth functions of the semi-strict feedback quarter car active suspension systems. This work was published in SAGE journal of vibration and control on November 30, 2020.

1.7.2 Contribution 2

Although Contribution 1 obtained high sprung mass position compensation, the ANNC provides the worst road holding and highest suspension travel oscillations than in passive suspension. Thus, the authors have created a dynamic landing tire modeling system and unsymmetrical suspension travel limits to address road holding and suspension travel limits. Therefore, a nonlinear control filter was established for ride comfort, road holding, and suspension travel limits. The nonlinear control filter contains three regions: a dead zone, a dynamic landing tire nonlinear function, and a suspension deflection nonlinear function. The novel adaptive control strategy was the ANNC coupled with the nonlinear control system. Therefore, the adaptive control system can provide passenger comfort, maintain road holding, reduce suspension travel oscillations, prevent hitting suspension travel limits, and overcome nonlinearities and uncertainties. This article was published in MDPI journal of machines on July 8, 2020.

1.7.3 Contribution 3

In Contribution 2, the novel adaptive control system made better-improving passenger comfort, maintaining road holding, and avoiding reaching suspension travel limits. However, the control law in Contribution 2 was for a SISO quarter car electrohydraulic active suspension system. Thus, the authors have redeveloped the control law that was investigated in the contribution 2 for full car active suspension systems. The external aerodynamic disturbances and stiff road perturbations were taken into consideration in Contribution 3. Therefore, a robust adaptive neural networks control system (RANNC) was investigated for MIMO nonlinear filtered electrohydraulic active suspension. The RANNC is a hybrid control system and consists of an adaptive neural network backstepping control system coupled with four nonlinear control systems. This work was submitted to journal of vehicle system dynamics in May 2021.

1.8 Conclusion

In this chapter, the literature review has briefly surveyed several related topics to this research. The topics in this chapter are an introduction, vehicle passive suspension systems, semi-active suspension systems, active suspension systems, Suspension performance functions, active suspension control strategies, and conclusion.

CHAPTER 2

ADAPTIVE NEURAL NETWORK AND NONLINEAR ELECTROHYDRAULIC ACTIVE SUSPESION CONTROL SYSTEM

Amhmed Mohamed Al Aela[a], Jean-Pierre Kenne[b], Honorine Angue Mintsa[c]

[a, b] Department of Mechanical Engineering, École de technologie supérieure,
1100, Notre Dame Street West, Montreal Quebec, Canada, H3C 1K3
[c] Department of Mechanical Engineering, Ecole polytechnique de Masuku (EPM), Masuku, Franceville, Haut-Ogooué, Gabon

Paper published in *Journal of Vibration and Control*, November 2020
https://journals.sagepub.com/doi/abs/10.1177/1077546320975979

Abstract

In this paper, an Adaptive Neural Network Control system (ANNC) is proposed for a quarter-car electrohydraulic active suspension system coping with dynamic nonlinearities and uncertainties. The proposed control system is primarily designed to stabilize a sprung mass position of the quarter-car electrohydraulic active suspension. Linear controllers such as the Proportional Integral Differential controller (PID) have limited control performances. The limited control performances are caused by dynamic phenomena such as nonlinearity, parametric uncertainties, and stiff external disturbances. To overcome these dynamic phenomena, we propose a combined adaptive radial basis function neural network (RBFNN) with a backstepping control system for a quarter-car active suspension system. This set-up can handle the unmatched model uncertainty of the system, while the adaptive neural network can take care of its unknown smoothing functions. In general, RBFNN can represent a complicated

function, and therefore, semi-strict-feedback dynamic systems are considered to simplify the ANNC design. Simulation results are indicated to illustrate ANNC effectiveness.

Keywords: Active suspension, radial basis function neural networks, backstepping control system, adaptive control.

2.1 Introduction

Electrohydraulic servo systems (EHSS) are powerful systems used to deliver fast, accurate, and excellent power responses (Zheng and Yao, 2019). These systems have a higher power-to-weight ratio than mechanical and electrical systems. Engineering applications that use EHSS include industrial machines, aerospace flight control actuators, automobiles, and robotics. In this study, we focus primarily on a quarter-car electrohydraulic active suspension system. This system is a mechanical vibration that provides a compromise between passenger comfort and road holding by using an electrohydraulic actuator. However, electrohydraulic active suspension systems present several undesirable characteristics, such as nonlinear dynamics, parametric uncertainties, and external perturbations.

Although EHSS has several benefits in engineering applications, EHSS is known as a highly nonlinear dynamics system and largely modeled uncertainties of parametric uncertainties and uncertain nonlinearities (Sallah et al., 2015). In (Alleyne and Liu, 2000), a Lyapunov-based control was developed to compensate friction for an electrohydraulic servosystem. In that study, the results showed improvements in control performance. A feedback linearization-based position control was applied for EHSS (Mintsa et al., 2011). In that study, the controller was built based on the Lyapunov-Like approach. The results showed improved control performance compared with the classical PID controller. An indirect adaptive backstepping control was investigated for an electro-hydraulic servovalve system (Kaddissi et al., 2011); the results showed the proposed control system could compensate the noise signal compared with nonadaptive backstepping.

The active suspension system is one of the engineering applications, which use EHSS. For example, in (Ahmed et al.,2015), the PID controller was developed for a quarter car active suspension model system. The results showed improvement in control performance, which reduced transmitting road energy to the sprung mass. However, all parameters are known. In (Tandel et al.,2014), the PID controller was implemented for quarter vehicle active suspension. In that study, parametric uncertainties were manually considered; there was an improvement in control performance to that in passive suspension. Even though linear control systems provide improvements in control performance, they cannot overcome the system's nonlinearities and uncertainties.

Many researchers have developed control strategies to compensate for some of the nonlinearities and uncertainties inherent in electrohydraulic active suspension systems. For example, a restrictive backstepping controller was designed for a strict-feedback active suspension (Karlsson et al., 2001). In (Kim, 1996), an indirect adaptive controller was applied for a quarter car active suspension. A multi-objective control system was investigated for a quarter-car active suspension (Sun et al.,2014). Although the preceding works showed control performance improvements, their control strategies were not addressed the electrohydraulic servosystem. In (Lin and Kanellakopoulos, 1997), a backstepping control law was investigated for a quarter-car active suspension; zero dynamics system was considered in the control design. However, all model parameters were known in that study. In (Alleyne and Hedrick, 1995), a sliding mode control was developed for a quarter car active suspension system. In that study, an adaptive scheme was determined to update the electrohydraulic parameters; the results showed an improvement in control performance to that in passive suspension. However, all suspension parameters were known. A hybrid controller was used to address a parametric uncertainty of an active suspension hydraulic cylinder (Fukao et al.,1999). In that study, the hybrid control system consisted of a H_∞ approach and an adaptive control system. However, the suspension parameters were partially known. A higher-order sliding mode control system coupled with a particle swarm optimization approach was developed for active suspension (Qin et al., 2017). In that study, the results showed better improvements in control performance.

Although parametric uncertainties were estimated by using discontinuous projection methods in previous control strategies, adaptive intelligent control systems have since been applied to deal with the nonlinearities and uncertainties of active suspension systems; such systems include neural networks and fuzzy control systems. A new hybrid control system approach that combines a sliding mode and fuzzy control systems has been developed to reduce control signal chattering for a quarter-car electrohydraulic active suspension (Shaer et al., 2016). Adaptive neural networks exceed traditional adaptive control techniques by making provisions for self-learning (Liu, 2013). In (Yao et al., 2019), an adaptive rise control of hydraulic systems with multilayer neural networks was developed; the results showed good control compensation despite of both matched and mismatched model uncertainties. Adaptive neural networks have been developed for unknown nonlinear dynamics of a quarter-car active suspension; however, the electrohydraulic servo system was not modeled to design the adaptive control system (Huang et al., 2015). In conclusion, many control laws have been designed to cope with dynamic nonlinearities and parametric uncertainties of electrohydraulic active suspension systems. Furthermore, control laws with adaptive neural networks have better transient response compared with conventional control laws. Although several researchers have developed adaptive multilayer neural networks for electrohydraulic control systems, the radial basis function neural networks are preferred by researchers for several reasons:

1- The radial basis function neural networks have good generalization ability and simple network compared to that in the multilayer feed-forward network (Liu, 2018).
2- The radial basis function neural networks are much faster training compared to the multilayer neural networks (Du and Swamy, 2014).
3- The radial basis function neural networks have a single intermediate hidden layer; hence, the adaptive radial basis function neural networks can be simply designed.

In this study, the adaptive neural network control (ANNC) system is designed to overcome undesired phenomena to work efficiently and survive long durations in real conditions. Hence, all parameters in the modeling system are assumed to be unknown; three unknown functions are existed to lump all dynamic nonlinearities and model uncertainties. Furthermore, an unknown coefficient of the control signal is chosen to be known bounds. Therefore, we develop

the ANNC system to cope with these phenomena. The ANNC consists of a backstepping control law coupled with adaptive neural networks. The dynamic mathematical system of a quarter-car active suspension has an unmatched model uncertainty, which means the control signal does not appear in all state-space equations. Hence, the control input cannot completely cancel out the uncertainties from the system, which is where a backstepping control system comes in with possible solutions (Krstic et al.,1995). However, the primary difficulty with backstepping control design lies in determining a regression matrix that requires that the mathematical model of unknown functions should be in linear form. Consequently, the mathematical modeling of the quarter-car active suspension system can be a semi-strict-feedback dynamic system, which determines to lump all model uncertainties into three unknown smooth functions. Thus, a linear radial basis function neural network (RBFNN) is chosen to compensate for unknown smooth functions adaptively. The benefits brought about by the ANNC consist in cancelling out any unmatched active suspension model uncertainty, in addition to adaptively compensating for unknown smooth functions of the semi-strict feedback system. This study's main contribution is to overcome the dynamic nonlinearities and model uncertainties due to the parametric uncertainties, a road excitation and a sprung mass external disturbance in the modeling system.

This paper is organized as follows: Section 2.2 describes the notation and problem statement. The problem statement provides a brief physical description of a quarter-car active suspension, as well as the mathematical modeling of the system. This modeling consists of two parts, namely, a semi-strict-feedback active suspension and radial basis function neural networks. In section 2.3, the control law design is introduced. Also, the stability control law design is guaranteed. A designed example illustrating the proposed control effectiveness is discussed in section 2.4. The simulation study is analyzed in the time and in the frequency domains. In section 2.5, conclusions and future work are discussed.

2.2 Notation and problem statement

The main components of the quarter-car active suspension are a sprung mass and an unsprung mass dynamic system, as shown in Figure 1. There are several components between the two masses, such as a spring, a damper, an electrohydraulic servovalve system, and other accessories. A tire is in between the unsprung mass and the road surface. The active suspension system has the ability to respond to vertical changes in the sprung mass position.

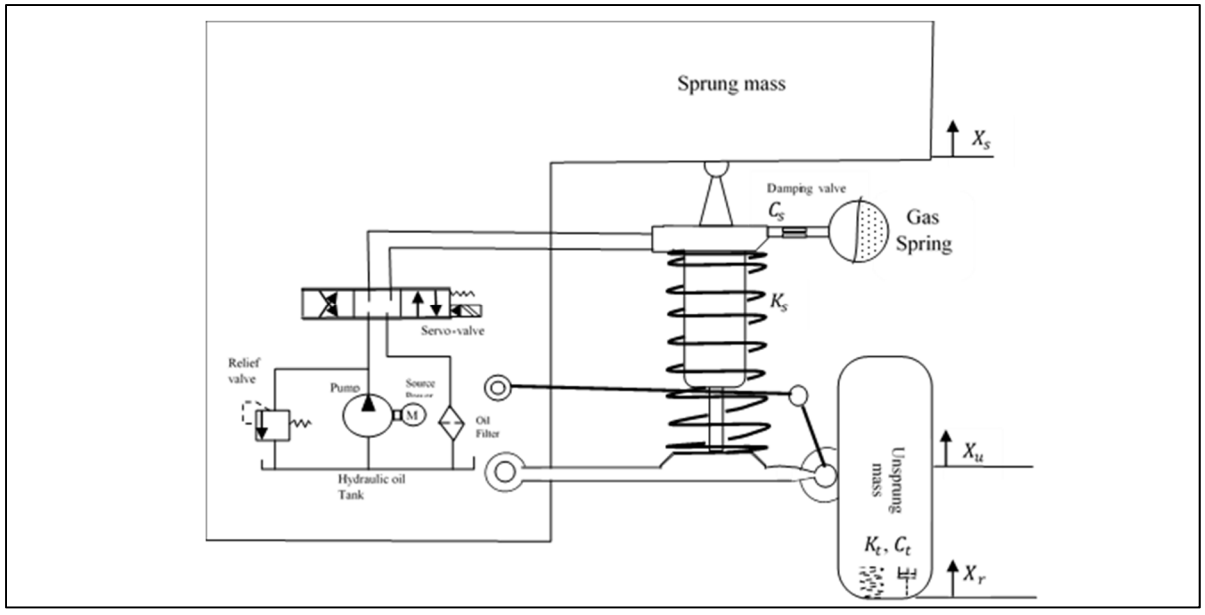

Figure 2.1 A sketch of a quarter-car active suspension

The main purposes of the active suspension in vehicles are to isolate the sprung mass from road perturbations and to provide vehicle handling (stability) at different operation conditions. The hydraulic actuator generates forces by the EHSS to provide a compromise between ride comfort and road holding (Huang et al., 2019). The following are the nomenclatures used for the active suspension system parameters, with accompanying descriptions:

Table 2.1 Nomenclatures with their accompanying descriptions

Quantity	Description	Quantity	Description
m_u	Unsprung mass, Kg	τ_v	Servovalve time constant, s
m_s	Sprung mass, Kg	Λ_e	Effective bulk modulus, N/m^2
K_t	Tire spring stiffness, N/m	C_d	Low discharge coefficient, -
K_s	Suspension spring stiffness,	C_{tp}	Coefficient of leakage, m^5/(Ns)
C_s	Suspension viscous coefficient,	ρ	Hydraulic oil density, kg/m^3
C_t	Tire viscous coefficient, Ns/m	V_t	Actuator volume, m^3
P_s	Pressure supply, N/m^2	K_u	Servovalve amplifier gain, m^2/V
P_L	Operational hydraulic pressure,	X_s	Sprung mass position, m
X_u	Unsprung mass position, m	$\dot{X}_s$	Sprung mass velocity, m/s
$\dot{X}_u$	Unsprung mass velocity, m/s	$\ddot{X}_s$	Sprung mass acceleration, m/s^2
$\ddot{X}_u$	Unsprung mass acceleration,	A_v	Spool valve displacement, m^2
K_{ns}	Nonlinear spring coefficient, $\mathrm{N/m^3}$	$C_{ns}(t)$	Nonlinear time-varying damper coefficient, $\mathrm{Ns^2/m^2}$
ζ	RBFNN compact set	$f_i(\zeta)$	Unknown smooth function (i)
n	State space order system	l	Number of nodes in the hidden
m	Number of variables in the compact set RBFNN	A_p	Hydraulic piston projected area, m^2
φ	The center vector of the receptive field in hidden layer	**b**	The width vector of Gaussian function
g	Acceleration gravity, m/s^2		

Mathematical Modeling

For simplicity, the unsprung mass positions at the wheel and the hydraulic actuator have the same values and directions. The mathematical modeling of the quarter-car of active suspension was developed based on several physical theories. Therefore, many researchers have applied

nonlinear mathematical modeling for a quarter car of active suspension. The sprung and unsprung mass dynamic systems can be modeled (Chin and Huang, 2005).

$$m_s \ddot{X}_s = -K_s(X_s - X_u) - K_{ns}(X_s - X_u)^3 - C_s(\dot{X}_s - \dot{X}_u) - C_{ns}(t)(\dot{X}_s - \dot{X}_u)^2 + A_p P_L + d(t) \quad (2.1)$$

where $d(t)$ is an external disturbance, which bounds by a known constant $d_0 > 0$, $|d(t)| \leq d_0$.

$$m_u \ddot{X}_u = \begin{cases} F_{SU} + F_{Dt} - A_p P_L & \frac{|F_{Dt}|}{(m_s + m_u)\mathrm{g}} \leq 1 \\ F_{SU} - A_p P_L & \frac{|F_{Dt}|}{(m_s + m_u)\mathrm{g}} > 1 \end{cases} \quad (2.2)$$

where F_{Dt} is a dynamic tire force, F_{SU} is the spring and damper forces, $F_{SU} = K_s(X_s - X_u) + K_{ns}(X_s - X_u)^3 + C_s(\dot{X}_s - \dot{X}_u) + C_{ns}(t)(\dot{X}_s - \dot{X}_u)^2$, K_{ns} is the $C_{ns}(t)$ is a nonlinear time varying damping coefficient.

$$F_{Dt} = -K_t(X_u - X_r) - C_t(\dot{X}_u - \dot{X}_r) \quad (2.3)$$

In equation (2.2), the dynamic tire force F_{Dt} must be smaller than suspension weight " $(m_s + m_u)\mathrm{g}$ " to keep road holding; otherwise, the tire will not contact to hold a road surface " tire liftoff phenomenon".

The hydraulic servovalve controlled piston system can be presented as (Merritt, 1967).

$$\frac{V_t}{2\Lambda_e}\dot{P}_L(t) = C_d A_v(t)\sqrt{\frac{P_s - P_L\, sgn(A_v(t))}{\rho}} - A_p(X_s - X_u) - C_{tp}P_L \quad (2.4)$$

The dynamic spool valve area of the hydraulic servovalve system can be introduced (Shaer et al., 2016).

$$\dot{A}_v = \frac{1}{\tau_v}\left(-A_v + K_u u(t)\right) \tag{2.5}$$

Before developing the state-space modelling system, we need to rearrange the previous equations 1-5 as semi-strict-feedback models.

Semi-strict-feedback active suspension

In order to simplify the state modelling, the unsprung mass dynamic uncertainties are lumped into the sprung mass dynamic uncertainties (Chen and Huang, 2005). Thus, the unsprung dynamic uncertainties are ignored to develop the backstepping control approach. Moreover, to ensure the semi-strict-feedback meets requirements, all signs of virtual control coefficients are positive. Accordingly, the maximum operation pressure $(P_L)_{max} \leq \frac{2}{3}P_s \ , \ \forall\, t \geq 0$. Also, the state variables modeling systems $\zeta \equiv \left(X_s, \dot{X}_s, X_u, \dot{X}_u, X_h, X_v\right)$ are measured, estimated (or both) in the presence of perturbed road excitation. The semi-strict feedback state-space modeling system of the quarter-car active suspension has four state variables.

$$\begin{aligned}
&X_1 \equiv X_s, \ \ X_2 \equiv \dot{X}_s, X_3 \equiv C_h P_L, \ X_4 \equiv C_v A_v, \qquad \forall\, [X_1, X_2, X_3, X_4\ ] \in\ \Omega_X \subset R^4 \\
&\dot{X}_1 = X_2 \\
&\dot{X}_2 = X_3 + g_2(\zeta) + d(t) \\
&\dot{X}_3 = X_4 + g_3(\zeta) \\
&\dot{X}_4 = \beta u(t) + g_4(\zeta) \\
&y = \ X_1
\end{aligned} \tag{2.6}$$

Thus, the functions $g_2(\zeta), g_3(\zeta),\ g_4(\zeta)$ and the parameter β are chosen as the following forms.

$$
\begin{aligned}
g_2(\zeta) &\equiv -X_3 - \frac{K_s}{m_s}(X_1 - X_u) - \frac{C_s}{m_s}\left(X_2 - \dot{X}_u\right) + \frac{A_p}{m_s}X_3 \\
g_3(\zeta) &\equiv -X_4 + \frac{2\Lambda_e C_d}{V_t}\, X_4 \sqrt{\frac{P_s - X_3\, sgn(X_4)}{\rho}} - \frac{2\Lambda_e A_p}{V_t}\left(X_2 - \dot{X}_u\right) + \frac{2\Lambda_e C_{tp}}{V_t}\, X_3 \\
g_4(\zeta) &\equiv -\frac{X_4}{\tau_v} \\
\beta &\equiv \frac{K_u}{\tau_v}
\end{aligned}
\tag{2.7}
$$

We need to know the radial basis function neural network aspects in order to approximate the unknown functions $g_i(\zeta)$.

Radial Basis Function Neural Networks

The radial basis function neural network (RBFNN) can approximate nonlinear and unknown bounding functions. In this study, we use a linear RBFNN to approximate the unknown functions of the modelling system. The linear RBFNN has one hidden layer, a fixed size, and fixed moving basis functions (James et al.,2016). The typical structure of the linear RBFNN is three layers "input layer, hidden layer, and output layer," as shown in Figure 2.2.

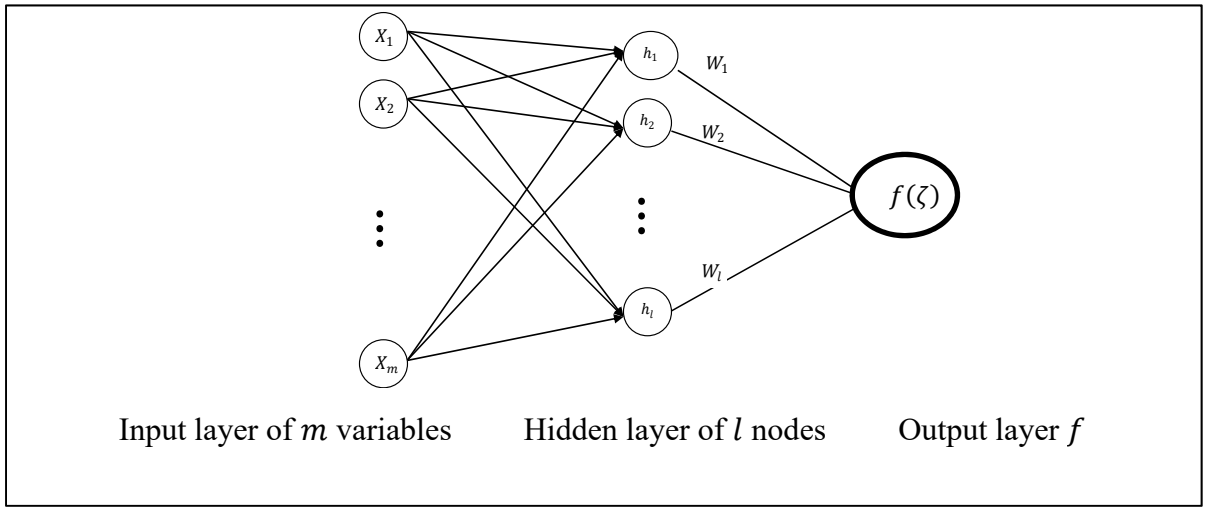

Figure 2.2 Structure of a linear RBFNN, based on the interpolation theory

Therefore, the unknown smooth functions $f_i(\zeta)$ is designed to satisfy the following form.

$$f_i(\zeta) = W_i^T \mathcal{H}_i(\zeta) + \varepsilon_i \ , \quad i = 1,2, \dots, n, \qquad \forall\, \zeta \in \Omega_\zeta \subset \mathbb{R}^m \tag{2.8}$$

where the input vector $\zeta \in \Omega_\zeta \subset \mathbb{R}^m$, the ε_i is the approximation error, the W_i^T is an unknown weight vector, $W_i^T = [W_1 \quad W_2 \quad \dots \quad W_l]_i^T$, the $\mathcal{H}_i(\zeta)$ is a basis function vector, $\mathcal{H}_i(\zeta) = [h_1(\zeta) \quad h_2(\zeta) \quad \dots \quad h_l(\zeta)]_i$. The hidden Gaussian functions $h_i(\zeta), i = 1, \dots, l$ are satisfied.

$$h_i(\zeta) = e^{-\left\{\frac{\|\zeta - \varphi_{i,j}\|^2}{2b_j^2}\right\}}, i = 1, \dots, l, \ \boldsymbol{\zeta} = [\zeta_1, \zeta_2, \dots, \zeta_m], \quad \forall\, \zeta \in \Omega_\zeta \subset \mathbb{R}^l \tag{2.9}$$

where $\varphi_{i,j}$ are centers of the receptive field, b_j is and the width of Gaussian function, $i = 1, \dots, l, j = 1, \dots, m$.

Therefore, approximate smooth functions $\hat{f}_i(\zeta)$ can be estimated by RBFNN (Ge and Wang, 2002) as follows:

$$\hat{f}_i(\zeta) = \widehat{W}_i^T \mathcal{H}_i(\zeta) \ , i = 1,2, \dots, n \ , \qquad \forall\, \zeta \in \Omega_\zeta \subset \mathbb{R}^m \tag{2.10}$$

The optimal weight value of the W of RBFNN is defined to minimize the approximation error (Zhang et al., 2019).

$$W_i := \arg \min_{\widehat{W}_i \in R^n} \left\{ \sup_{\zeta \in \Omega_i} \left\| f_i(\zeta) - \hat{f}_i(\zeta) \right\| \right\} , W_i \text{ is } l \times m, \forall\, \zeta \in \Omega_i \tag{2.11}$$

Hence, a minimal positive design error ε_D could occur (Liu, 2013).

$$\max \left\| \boldsymbol{f}(\zeta) - \hat{\boldsymbol{f}}(\zeta) \right\| \leq \varepsilon_D \tag{2.12}$$

where $\boldsymbol{f}(\zeta) = [f_1(\zeta) \quad f_2(\zeta) \quad \dots \quad f_n(\zeta)]$, and the $\hat{\boldsymbol{f}}(\zeta) = \left[\hat{f}_1(\zeta) \quad \hat{f}_2(\zeta) \quad \dots \quad \hat{f}_n(\zeta)\right]$.

The "centers and widths" of the RBFNN are chosen based on a range of input values (Liu, 2013). Therefore, we use a Gradient Descent learning algorithm to obtain the initial RBFNN parameters such as the centers $\varphi_{i,j}$, widths b_j. The Gradient Descent learning algorithm adjusts the weights w_i, centers $\varphi_{i,j}$, widths b_j numerically to minimize the squared error function E_i. Furthermore, a backpropagation method uses in this algorithm for each $f_i(\zeta), i = 1,2, \dots, n$, as follows (Liu, 2013).

$$\begin{aligned} \mathrm{w}_i(t) &= \mathrm{w}_i(t-1) + \Delta\mathrm{w}_i + \nu\big(\mathrm{w}_i(t-1) - \mathrm{w}_i(t-2)\big) \\ \varphi_{i,j}(t) &= \varphi_{i,j}(t-1) + \Delta\varphi_{i,j} + \nu\left(\varphi_{i,j}(t-1) - \varphi_{i,j}(t-2)\right) \\ \mathrm{b}_j(t) &= \mathrm{b}_j(t-1) + \Delta\mathrm{b}_j + \nu\left(\mathrm{b}_j(t-1) - \mathrm{b}_j(t-2)\right) \end{aligned} \tag{2.13}$$

The momentum factor ν domain is $0 < \nu < 1$. The updated parameters $\Delta\mathrm{w}_i, \Delta\varphi_{i,j}$, and $\Delta\mathrm{b}_j$ are defined.

$$\Delta\mathrm{w}_i = -\psi\frac{\partial E_i}{\partial \mathrm{w}_i}, \qquad \Delta\varphi_{i,j} = -\psi\frac{\partial E_i}{\partial \varphi_{i,j}}, \qquad \Delta\mathrm{b}_j = -\psi\frac{\partial E_i}{\partial \mathrm{b}_j} \tag{2.14}$$

The learning rate ψ domain is $0 < \psi < 1$. The square error function E_i is.

$$E_i = \frac{1}{2}\big(f(\zeta) - y_m(\zeta)\big)_i^2 \tag{2.15}$$

Where y_m is the estimated output RBFNN function.

2.3 Control Law Design

The design of the adaptive neural network control law according to control coordinates Z_i could be defined as follows:

$$\begin{aligned} Z_1 &= X_1 - X_{1d} \\ Z_2 &= X_2 - \propto_1 \\ &\vdots \\ Z_n &= X_n - \propto_{n-1} \end{aligned} \tag{2,16}$$

where $\propto_i$ is a control function of the i state model, the X_{1d} is the desired tracking signal.

The ANNC system is sketched in Figure 2.3. It consists of three paths. The first path is a tracked signal of the desired sprung mass position by implementing a backstepping control system. In the second path, the unknown functions $f_2(\boldsymbol{\zeta}), f_3(\boldsymbol{\zeta}), f_4(\boldsymbol{\zeta})$ and their unknown derivative functions are compensated by using the adaptive RBFNN, and in the third path, the uncertain control signal coefficient has been adapted by a triangularity condition technique in which the β is bounded by upper and lower known values.

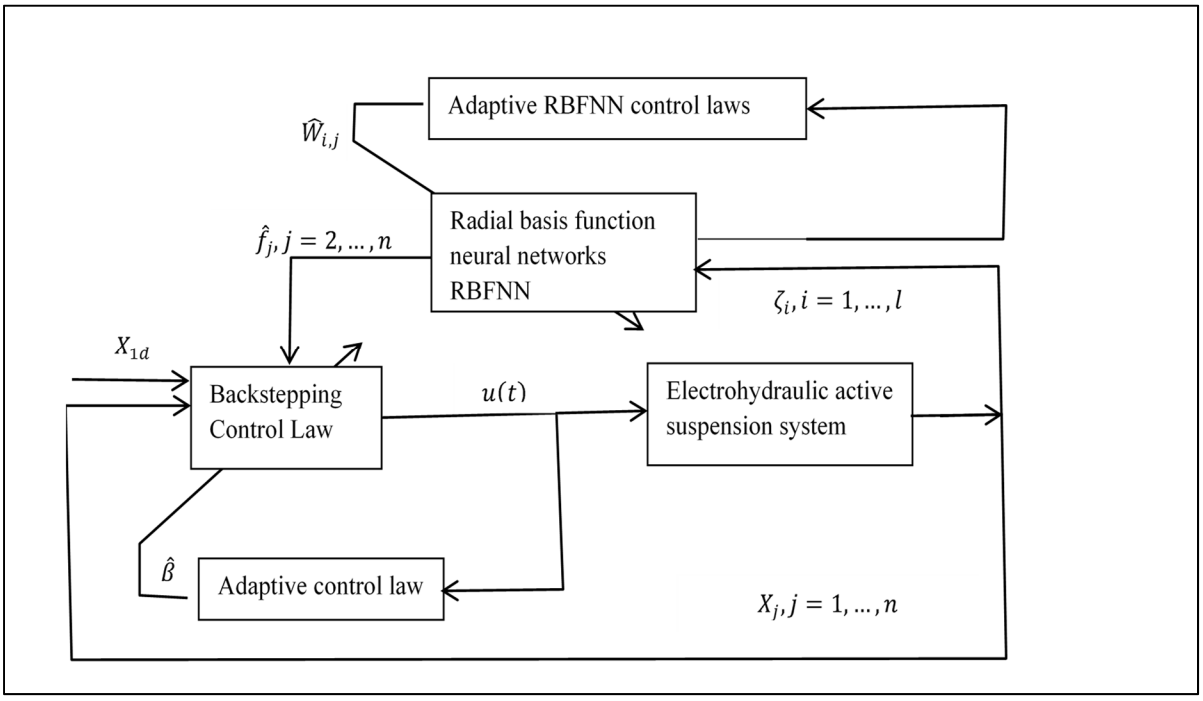

Figure 2.3 The operational Control Law paths of the ANNC

Three control design step procedures (step 1, step i (i=2,3), and step 4) are organized to avoid step repetition, as follows.

Step 1: Sprung mass velocity

$$Z_1 = X_1 - X_{1d} \tag{2.17}$$

To stabilize the controller, let us consider a quadratic Lyapunov function candidate V_1.

$$V_1 = \frac{1}{2} z_1^2 \tag{2.18}$$

The Lyapunov derivative function $\dot{V}_1$ of step 1 becomes

$$\dot{V}_1 = Z_1 \dot{Z}_1 = Z_1 \left(\dot{X}_1 - \dot{X}_{1d} \right) \tag{2.19}$$

To stabilize the system, the derivative control coordinate $\dot{Z}_1$ becomes.

$$\dot{Z}_1 = Z_2 + \propto_1 - \dot{X}_{1d} = -c_1 Z_1 \tag{2.20}$$

where the c_1 is a positive constant.

Then, the virtual control function $\propto_1$ is:

$$\propto_1 = \dot{X}_{1d} - c_1 Z_1 \tag{2.21}$$

Substitute $\propto_1$ into $\dot{V}_1$

$$\dot{V}_1 = Z_1 Z_2 - c_1 Z_1^2 \tag{2.22}$$

Step i (i=2,3)

We can define the virtual control coordinate Z_i as:

$$\dot{Z}_i = \dot{X}_i - \dot{\propto}_{i-1} \tag{2.23}$$

Lemma 2.1: The control derivative function $\dot{\propto}_{i-1}$ produces two parts, namely, a countable part $\dot{\propto}_{(i-1)_c}$ and an uncountable part $\dot{\propto}_{(i-1)_u}$ (Ge and Wang, 2002). The $\propto_{i-1}$ is defined.

$$\propto_{i-1} \equiv \propto_{i-1} \left(X_1, \dots, X_i, \widehat{W}_{i-1}\right) \tag{2.24}$$

Then, the partial derivative of the function $\propto_{i-1}$ is

$$\dot{\propto}_{i-1} = \frac{\partial \propto_{i-1}}{\partial X_1} X_2 + \cdots + \frac{\partial \propto_{i-1}}{\partial X_{i-1}} X_i + \frac{\partial \propto_{i-1}}{\partial \widehat{W}_{i-1}} \dot{\widehat{W}}_{i-1} \tag{2.25}$$

Therefore, the uncountable part $\dot{\propto}_{(i-1)_u}$ consists of unknown smooth functions.

$$\dot{\propto}_{(i-1)_u} = \sum_{k=1}^{i-1} \frac{\partial \propto_{i-1}}{\partial X_k} g_k(X) + \frac{\partial \propto_{i-1}}{\partial \widehat{W}_{i-1}} \dot{\widehat{W}}_{i-1} \tag{2.26}$$

The countable part $\dot{\propto}_{(i-1)_c}$ is a smooth function describes as:

$$\dot{\propto}_{(i-1)_c} = \sum_{k=1}^{i-1} \frac{\partial \propto_{i-1}}{\partial X_k} X_{k+1} \tag{2.27}$$

Thus, the total unknown functions at step i-1 are defined:

$$f_i(X) = g_i(X) - \dot{\propto}_{(i-1)_u} \tag{2.28}$$

The unknown function $f_i(X)$ can be represented by the RBFNN as follows:

$$f_i(X) = W_i^T h_i(\zeta) + \varepsilon_i\,, \qquad \zeta \equiv X, \qquad \forall\, \zeta \in \Omega_\zeta \subset \mathbb{R}^m \tag{2.29}$$

Therefore, the Lyapunov Function candidate V_i design is selected:

$$V_i = V_{i-1} + \frac{1}{2} Z_i^2 + \widetilde{W}_i \, \Gamma_i^{-1} \, \widetilde{\mathrm{W}}_\mathrm{i} \tag{2.30}$$

By applying Lemma 2.1, the Lyapunov derivative function candidate $\dot{V}_i$ becomes:

$$\dot{V}_i = \dot{V}_{i-1} + Z_i\left(X_{i+1} + W_i^T h_i(\zeta) + \varepsilon_i + d_i(t) - \dot{\propto}_{(i-1)_c}\right) + \widetilde{W}_i \, \Gamma_i{}^{-1} \, \dot{\widehat{\mathrm{W}}}_i \tag{2.31}$$

where $d_2(t) = d(t)$,and $d_3(t) = 0$.

Therefore, the selected virtual control $\propto_i$ is:

$$\propto_i = -Z_{i-1} - \delta_i Z_i - \widehat{W}_i^T h_i(\zeta) + \dot{\propto}_{(i-1)_c} \tag{2.32}$$

According to the virtual control functions $\propto_i$ compact set, the control function $\propto_i$ are functions of state variables $X_s, \dot{X}_s, X_u, \dot{X}_u, X_h, and\ X_v$. Constant scaling factors of the operational hydraulic pressure C_h and the servo-valve area C_v are applied to ensure the Gaussian basis function mapping, the as follows:

$$\zeta_1 \equiv X_s, \quad \zeta_2 \equiv \dot{X}_s, \ \zeta_3 \equiv X_u, \quad \zeta_4 \equiv \dot{X}_u, \quad \zeta_5 \equiv C_h P_L, \quad \zeta_6 \equiv C_v A_v$$
$$\forall\, \zeta = [\zeta_1, \zeta_2, \zeta_3, \zeta_4, \zeta_5, \zeta_6] \in \Omega_\zeta \subset \mathbb{R}^6 \tag{2.33}$$

Therefore, the RBFNN input variable l has six input variables.

The adaptive RBFNN law $\dot{\widehat{\mathrm{W}}}_\mathrm{i}$ is defined (Zhang and Zou, 2016; Han and Lee, 2014):

$$\dot{\widehat{\mathrm{W}}}_\mathrm{i} = \Gamma_\mathrm{i} \, Z_i \, h_i(\zeta) - \Gamma_\mathrm{i} \sigma_{\theta_i} \widehat{W}_i \tag{2.34}$$

where Γ_i is a positive definite matrix, and $\sigma_{\theta_i}$is a positive constant.

By substituting equations 9 and 10 into the Lyapunov derivative function $\dot{V}_i$:

$$\dot{V}_i = \dot{V}_{i-1} + Z_{i+1}Z_i + Z_i\varepsilon_i + Z_i d_i(t) - \sigma_{\theta_i}\widetilde{W}_i\widehat{W}_i \tag{2.35}$$

We apply the completing squares (Jiang and Hill, 1999) as follows:

$$\sigma_{\theta_i}\widetilde{W}_i\widehat{W}_i = \sigma_{\theta_i}\left(\widehat{W}_i^T - W_i^T\right)\widehat{W}_i^T = \frac{1}{2}\sigma_{\theta_i}\left|\widehat{W}_i^T - W_i^T\right|^2 + \frac{1}{2}\sigma_{\theta_i}\left|\widehat{W}_i\right|^2 - \frac{1}{2}\sigma_{\theta_i}|W_i|^2 \tag{2.36}$$

Applying Young's inequality [34]:

$$|Z_2|d(t) \leq \frac{Z^2}{2\epsilon} + \epsilon\frac{\{d(t)\}^2}{2}, \quad \delta > 0 \tag{2.37}$$

However, the disturbance $d(t)$ is bounded by a known constant $|d(t)| \leq d_0$

$$\frac{\{d(t)\}^2}{2} \leq \frac{d_0^2}{2} \tag{2.38}$$

Applying inequality (Liu and Wang, 2011) for term $Z_i\varepsilon_i$ in equation (35):

$$|Z_i||\varepsilon_i| \leq |Z_i|\varepsilon_D \tag{2.39}$$

where the ε_D is a positive design error.

To guarantee the Lyapunov candidate $\dot{V}_i$ stability, the designed backstepping constant c_i , which satisfies.

$$c_i \geq \delta_i + \varepsilon_D + \epsilon^{-1} \tag{2.40}$$

where the δ_i is a positive constant of the virtual backstepping coordinate Z_i.
Substituting equations (2.37),(2.39) and (2.40) into equation (2.35):

$$\dot{V}_i \leq -\sum_{j=1}^{n-1} c_j Z_j^2 + Z_n Z_{n-1} - \frac{1}{2}\sigma_{\theta_i}\left|\widehat{W}_i^T - W_i^T\right|^2 - \frac{1}{2}\sigma_{\theta_i}\left|\widehat{W}_i\right|^2 + \frac{1}{2}\sigma_{\theta_i}|W_i|^2 + \epsilon\frac{d_0^2}{2} \quad (2.41)$$

yields

$$\dot{V}_i \leq \sum_{i=1}^{n-1}(-\Pi_i V_i + \Xi_i) + Z_n Z_{n-1} \quad (2.42)$$

where the factors Π_i and Ξ_i are positive values and $\Pi_i := \min\left\{c_i, \frac{\sigma_{\theta_i}}{\eta_{\max}\,\Gamma_i^{-1}}\right\}$, $\Xi_i = \frac{1}{2}\sigma_{\theta_i}|W_i|^2 - \frac{1}{2}\sigma_{\theta_i}\left|\widehat{W}_i^T - W_i^T\right|^2 + \epsilon\frac{d_0^2}{2}$, the $\eta_{\max}$ is the maximum eigenvalue of the positive definite matrix Γ.

Step n, (n=4): Servo-valve dynamic system

In step 4, the control signal design $u(t)$ is designed, and the overall Lyapunov candidate stability is guaranteed. The virtual control coordinate Z_n is selected:

$$Z_n = X_n - \propto_{n-1} \quad (2.43)$$

The overall Lyapunov candidate function V is selected as follows:

$$V = V_{n-1} + \tfrac{1}{2}Z_n^2 + \widetilde{W}_n\,\Gamma^{-1}\,\widetilde{W}_n + \frac{1}{2\mu}\tilde{\beta}^2 \quad (2.44)$$

where the μ is a positive constant.

By using Lemma 2.1, the overall Lyapunov derivative function $\dot{V}$ equation (2.14) becomes:

$$\dot{V} = \sum_{i=1}^{n-1}(-\Pi_i V_i + \Xi_i) + Z_{n-1}Z_n + Z_n\left(\boldsymbol{W}_n h_n(\zeta) + \varepsilon_n + \hat{\beta}u(t) - \dot{\propto}_{(n-1)_c}\right) + \widetilde{\mathrm{W}}_{\mathrm{n}}\frac{1}{\Gamma_{\mathrm{n}}}\dot{\widehat{W}}_{\mathrm{n}} - \tilde{\beta}\, Z_n\, \mathrm{u(t)} + \frac{1}{\mu}\tilde{\beta}\dot{\hat{\beta}} \quad (2.45)$$

Thus, the design control signal $u(t)$ is selected:

$$u(t) = \frac{1}{\hat{\beta}}\left(-Z_{n-1} - \widehat{\boldsymbol{W}}_n h_n(\zeta) + \dot{\propto}_{(n-1)_c}\right) \quad (2.46)$$

The RBF neural network adaptive law $\dot{\widehat{\mathrm{W}}}_{\mathrm{n}}$ is expressed as:

$$\dot{\widehat{\mathrm{W}}}_{\mathrm{n}} = \Gamma_{\mathrm{n}}\, Z_n\, h_n(\zeta) - \Gamma_{\mathrm{n}}\sigma_{\theta_n}\widehat{W}_n \quad (2.47)$$

The $\dot{\hat{\beta}}$ adaptive control law is designed by using the triangularity condition. The triangularity condition technique of the adaptive law is applied to estimate the unknown coefficient of the control signal β. The lower and upper bound known values of the uncertain parameter β is defined as β_{min} and β_{max}, which satisfies:

$$\beta \in \Omega_\beta = \{\beta : \beta_{min} \leq \beta \leq \beta_{max}\} \quad (2.48)$$

Hence, to guarantee $\left(\hat{\beta} - \beta\right)\left(\frac{1}{\mu}\dot{\hat{\beta}} - Z_n \mathrm{u(t)}\right) \leq 0$, a projection-type adaptive law $\dot{\hat{\beta}}$ is applied (Yang et al., 2016).

$$\dot{\hat{\beta}} = Proj(\mu\, Z_n \mathrm{u(t)}) = \begin{cases} 0 & if\ \hat{\beta} = \beta_{max}\ and\ \mu\, Z_n \mathrm{u(t)} > 0 \\ 0 & if\ \hat{\beta} = \beta_{min}\ and\ \mu\, Z_n \mathrm{u(t)} < 0 \\ \mu\, Z_n \mathrm{u(t)} & otherwise \end{cases} \quad (2.49)$$

Similarly to step i, (i=2-n-1), the Lyapunov derivative function $\dot{V}$ of the system yields:

$$\dot{V} \leq \sum_{i=1}^{n} (-\Pi_i V_i + \Xi_i) \tag{2.50}$$

By integrating the overall Lyapunov derivative function $\dot{V}$ in equation (2.18), we obtain:

$$0 \leq V(t) \leq \frac{\Xi}{\Pi} + \left(\mathrm{V}(0) - \frac{\Xi}{\Pi}\right) e^{-\Pi t} \tag{2.51}$$

were the Π and Ξ are positive. Hence, $\dot{\mathbb{Z}}_i$ is thus bounded. Therefore, Z_i, goes to zero automatically when $t \to \infty$.

In conclusion, the $\dot{\mathbb{Z}}_i$ guarantee Barbalat's Lemma (Khalil, 2002), and the $\{Z_1, Z_2, Z_3, Z_4, W_2, W_3, W_4\}$ are uniformly bounded.

2.4 Simulation and result analysis

To illustrate the ANNC algorithms, we consider the following road perturbation design and simulation data for both active and passive suspensions. The simulation data of the active suspension system are posted in Table 2.2.

Table 2.2 Simulation data values of the active suspension mathematical model

$c_1 = 200$	$c_2 = 201$	$c_3 = 203$	$c_4 = 202$	
$C_h = 1 \times 10^{-6}$	$C_v = 1 \times 10^5$	C_s=1000 Ns/m	C_t=800 N/m	
m_s=290 Kg	m_u=59 Kg	K_s=16812 N/m	K_t=190000 N/m	
P_s=10340000	$\Lambda_e = 7.995 \times 10^8$	$A_p = 3.35 \times 10^{-4}\ m^2$		
C_d=0.63	$C_{tp} = 9.047 \times 10^{-13}\ m^5/(Ns)$		τ_v=0.01 s	ρ=867 kg/m^3
$V_t = 135.4 \times 10^{-13}$ m^3		$-5 \leq u(t) \leq 5$	$K_{ns} = 160000$ N/m^2	
$K_u = (2.72 - 3.33) \times 10^{-6}$ m^2/V $\tau_{v\,max} = 0.009$ m2/mA		$C_{ns}(t) = 900 + 200e^{-0.1t}\ Ns^2m^{-2}$		

By using Gradient Descent learning algorithm, the number of nodes l is 5, and the initial $\boldsymbol{\varphi}_i \; and \; \mathbf{b}_i$ are set in the effective range of RBFNN functions. The external disturbance which applies on the sprung mass can be selected as:

$$d(t) = 200(1 - \cos 2\pi t), \text{ Newtons} \tag{2.52}$$

In order to examine the control performance of ANNC, a comparative study is applied between ANNC and another control strategy, which developed in (Chin and Huang, 2005) and called adaptive multi-surface sliding controller (AMSSC). In (Chin and Huang, 2005), a mathematical modeling of a quarter-car active suspension, a road design input and a disturbance force acting on the sprung mass are employed in the comparative study. In Figure 4, the ANNC provides a high control performance, which is more than 99% of compensation at time 5 and 10 seconds. Otherwise, the AMSSC was approximately 88% of compensation at the time of 5 and 10 seconds, as showed in (Chin and Huang, 2005).

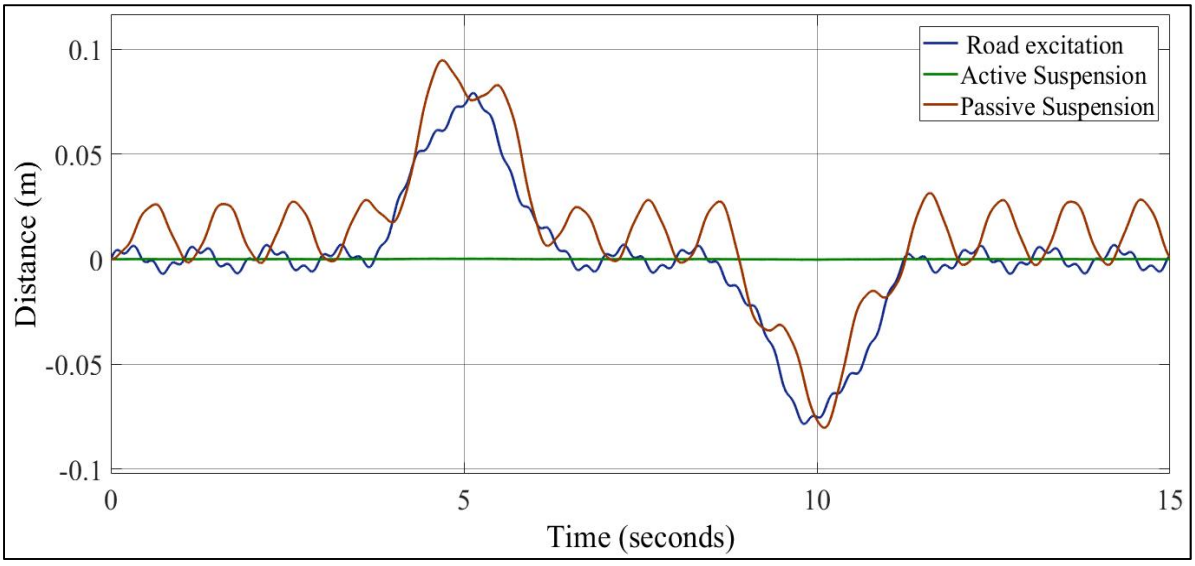

Figure 2.4 Sprung mass positions with Chin's road design

Hence, ANNC can provide high control performance and robustness compared to AMSSC.

In the second part of this study, a comparative study between the proposed controller and the passive suspension is presented (Figure 5 to Figure 18). Both random and bumpy road designs are chosen to be road input excitations. In the random road, a random road input is applied at surface high roughness class D of the International Organization for Standardization (ISO) classifications. In the bumpy road design, the wave length bumpy road λ is always 2 m, the bumpy road amplitude is always 0.025 m. The car velocity is 30 $\frac{Km}{h}$. In Case III, bumpy road designs are created at deferent car velocities. All these cases are chosen to perform the ANNC with passive suspension.

Case I: A random road design

In (Pan et al., 2017), there are series of standards of road roughness classifications of the power spectral density (PSD) that was proposed by the international organization for standardization (ISO), as shown in Table 2.3.

Table 2.3 Standards of road roughness classification using PSD values

Road class	$\theta(10^{-3}m)$	$G(n_0) \times 10^{-6}\, m^3$, $n_0 = 1\, rad/m$	$\xi(rad/m)$
A (very good)	2	1	0.127
B (good)	4	4	0.127
C (averge)	8	16	0.127
D (poor)	16	64	0.127
E (very poor)	32	256	0.127

The random road position PSD can be estimated as

$$G(n) = G(n_0)\left(\frac{n}{n_0}\right)^{-w} \tag{2.53}$$

where n is a space-frequency(m^{-1}), n_0 is a reference space frequency, $G(n)$ is a power spectral density road position, $G(n_0)$ is road roughness coefficient, w is a linear fitting coefficient, w=2.

The random road input can be described as:

$$\dot{X}_r(t) = -\xi\, U\, X_r(t) + w(t) \tag{2.54}$$

where w is a Gaussian white noise wuth spectral density $\Psi_w = 2\xi U\theta^2$, and θ^2 is the road roughness variance, ξ depends on the type of the road surface, and U is vehicle speed.

In this study, the PSD displacement of class D and $U = 108\ km/h$ are selected to design the random road input. The external disturbance on the sprung mass $d(t)$ is also applied. Although the modeling system is highly nonlinear dynamics and largely model uncertainties, the ANNC provides high control performace, as shown in Figure 2.5. On the other hand, the passive suspension is completely unstable due to the stiff modeling system.

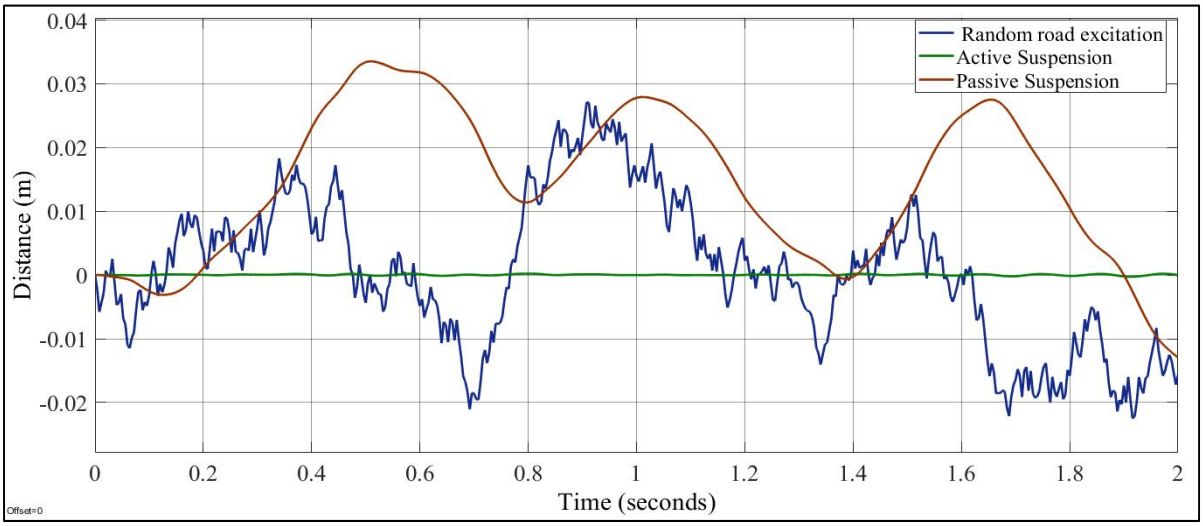

Figure 2.5 Sprung mass position of Case I

The suspension travel is one of the critical performance parameters of the system. In Figure2. 6, There are lots of suspension travel oscillations of the active suspension, which means there is a tradeoff between passenger comfort and suspension travel. Nevertheless, the passive suspension is randomly travelled. Therefore, passive suspension is lost in both passenger comfort, as in Figure 2.5 and suspension travel, as in Figure 2.6. There is a tire liftoff phenomenon in the active suspension system at time 1.7, 1.8 seconds and period 1.91-1.95 seconds, as shown in Figure 2.6.

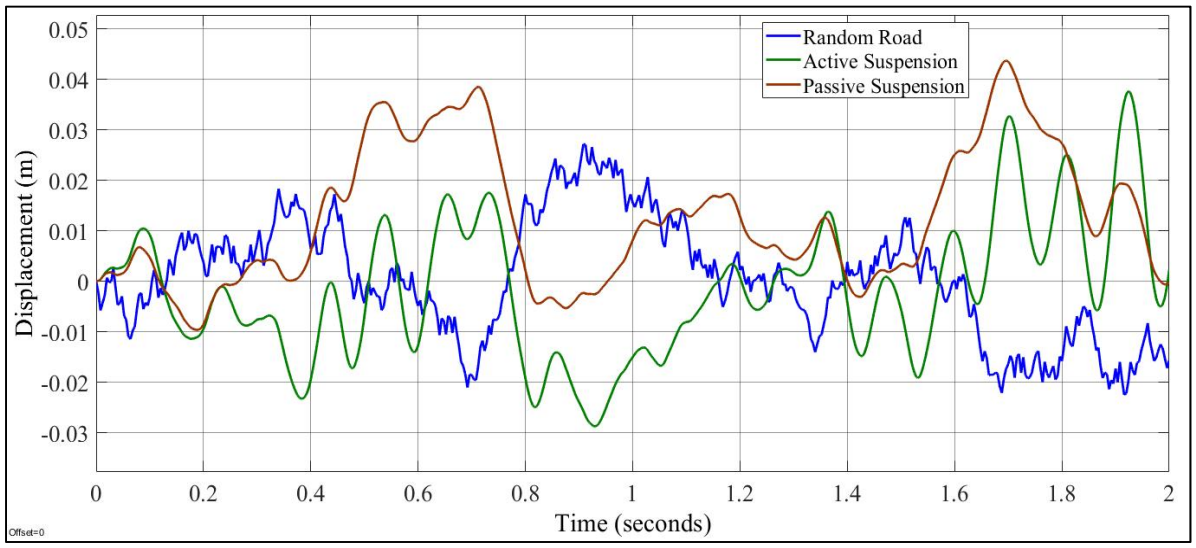

Figure 2.6 Suspension travel of Case I

The tire must contact the road surface to maintain road holding, which the force tire dynamic $\{-K_t(X_u - X_r) - C_t(\dot{X}_u - \dot{X}_r)\}$ must not exceed the suspension weight $\{(m_s + m_u)g\}$ (Pang et al., 2019). In Figure 2.7, the dynamic tire force of the active suspension is fluctuating more than passive suspension, which means there is a compromise between passenger comfort and road holding.

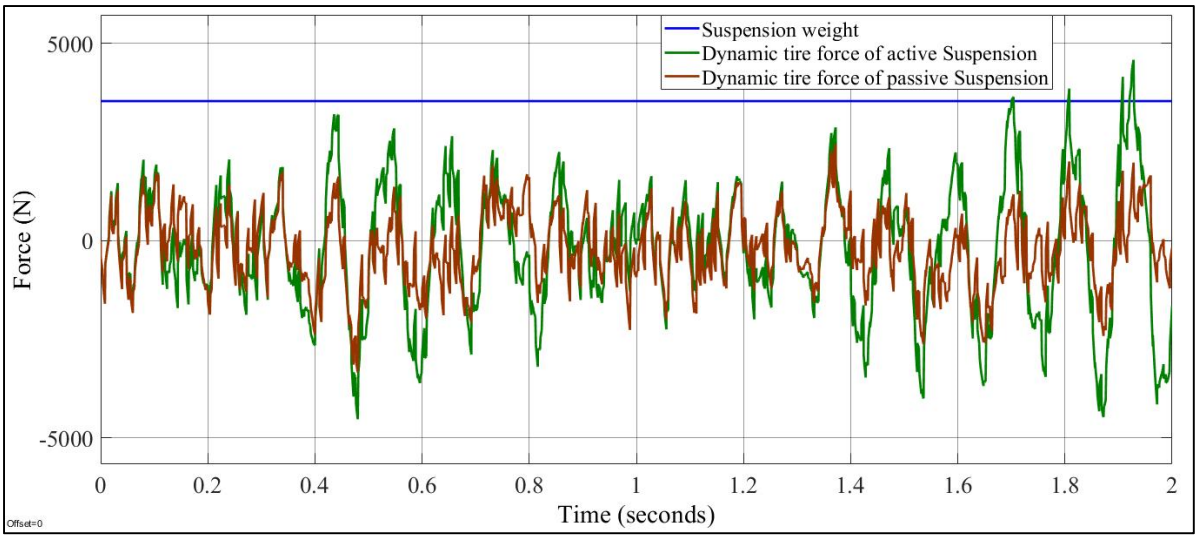

Figure 2.7 Road holding of Case I

Case II: A sinusoidal-shaped of bumpy road signal X_r has been applied in (Mouleeswaran, 2012; Lin and Kanellakopoulos, 1997).

$$X_r = \begin{cases} 0.025\left(\left|1-\cos\frac{2\pi U}{\lambda}\,t\right|\right) & 0 \le t \le \frac{\lambda}{U} \\ 0 & otherwise \end{cases} \tag{2.55}$$

$$d(t) = 200(1-\cos 2\pi t), \text{ Newtons} \tag{2.56}$$

where λ is a bump amplitude, $\lambda = 2$ m, and U is a vehicle velocity, $U = 30\ \frac{Km}{h}$.

Although the simulation of the PID control system has limited performance (Shaer et al., 2016), the proposed control law performs very well. In Figure 8, the proposed controller performs much better than does passive suspension. The sprung mass position active suspension is approximately compensated by 99.57%. On the other hand, the sprung mass position oscillation of the passive suspension is reduced by 20% per cycle at 0.22 seconds.

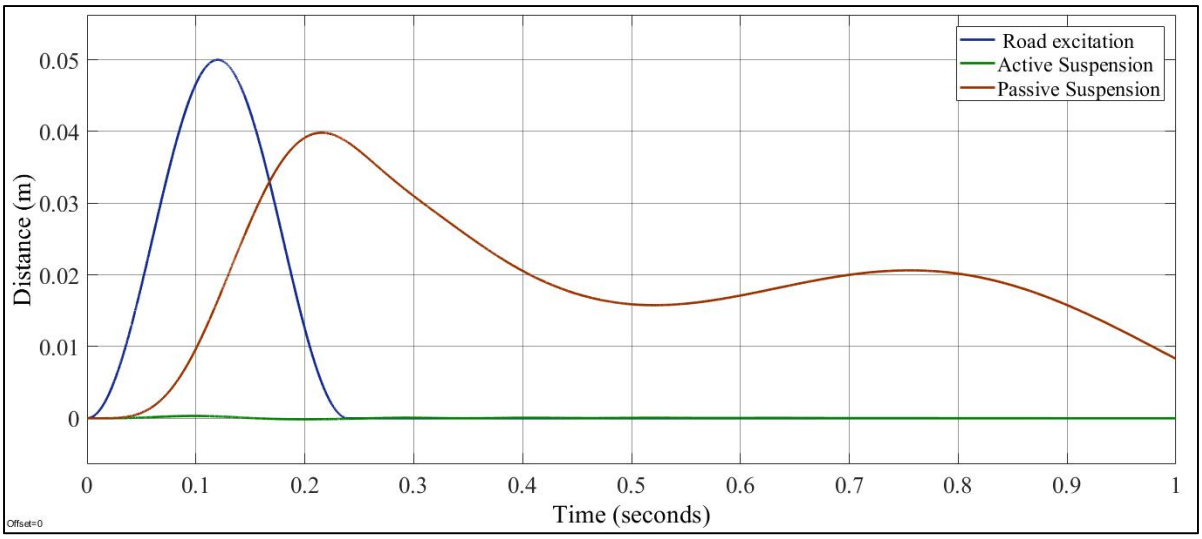

Figure 2.8 Sprung mass position of Case II

In Figure 2.9, the ANNC has a minimal tracking error. The tracking performance is superior to that obtained by the passive suspension.

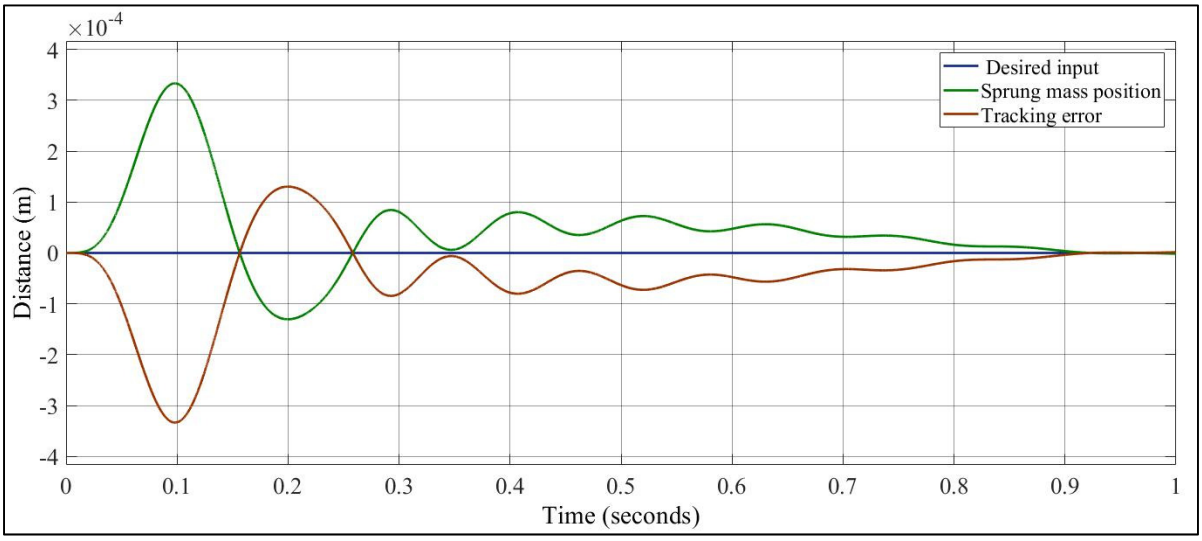

Figure 2.9 Tracking error of active suspension for Case II

In` Figure 2.10, the maximum value of the active suspension travel is -6 cm at 0.12 seconds. Although the ANNC provides the minimum tracking error, the active suspension travel is 1.5 times that of the passive suspension.

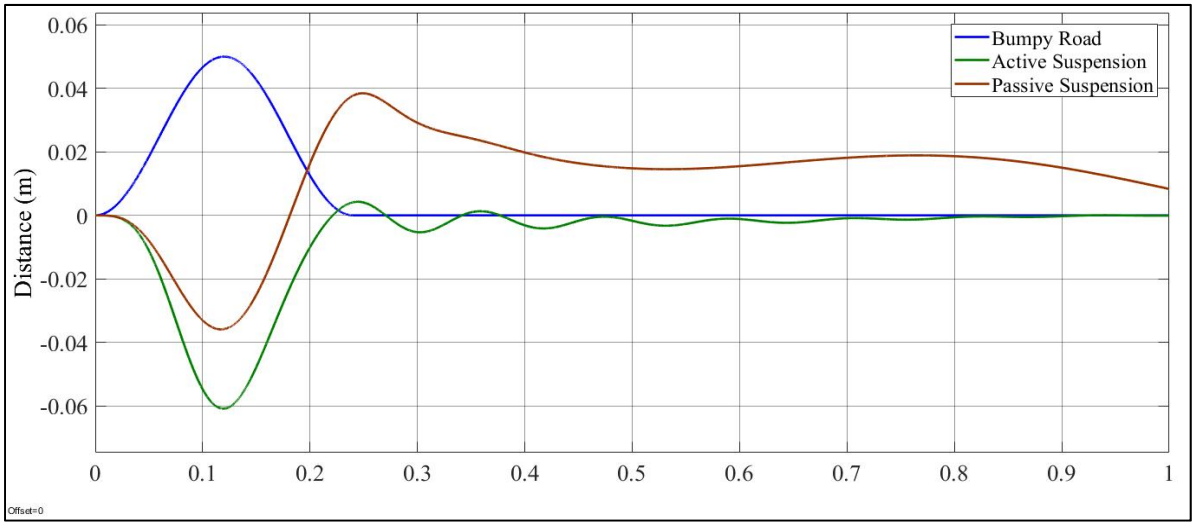

Figure 2.10 Suspension travel of Case II

Figure 2.11 shows the dynamic force behaviors of the tire passive suspension, the tire active suspension, and the suspension weight. Both the active and the passive tire dynamic forces fluctuate below the suspension weight.

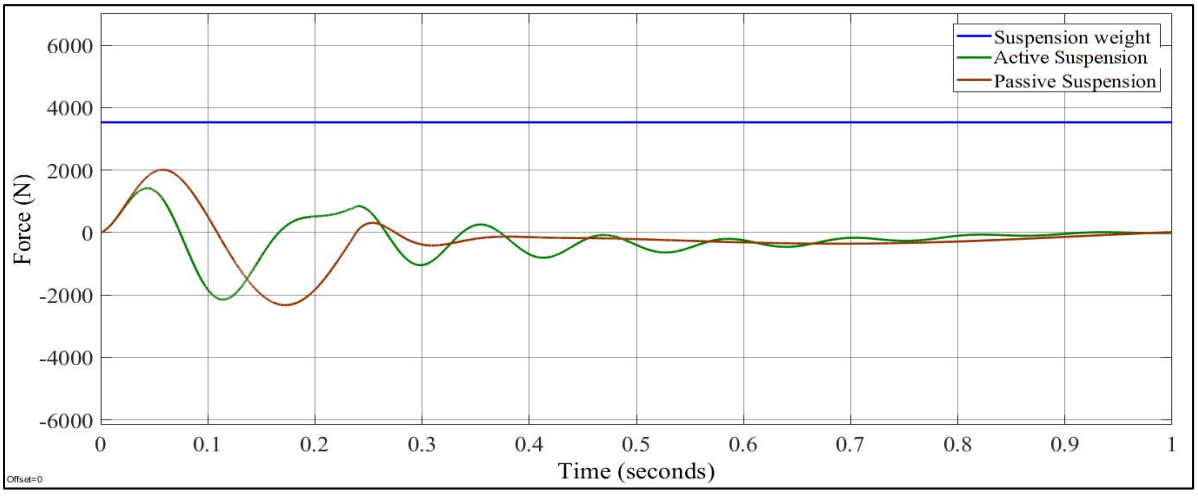

Figure 2.11 Road Holding of Case II

Accordingly, the tire contacts the road; otherwise, the tire passive suspension oscillates more than the tire active suspension.

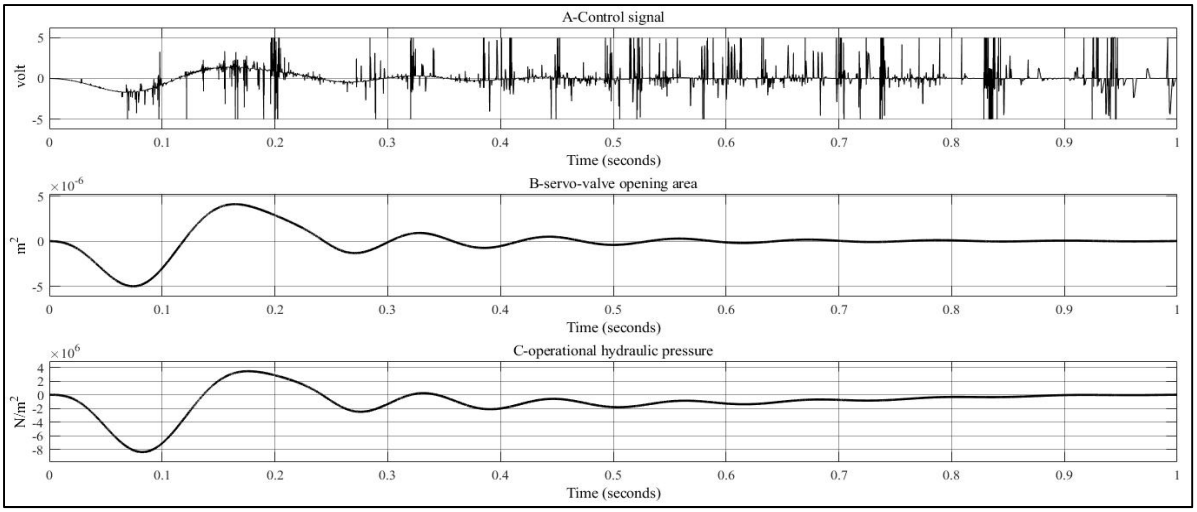

Figure 2.12 A-ANNC control signal, B-servo-valve opening area, C-operational hydraulic pressure of Case II

The control signal, the servovalve operational area, and the operational hydraulic pressures of electrohydraulic servovalve active suspension systems are plotted in separate graphs, respectively, as showed in Figure 2.12. In Figure 2.12A, the behavior of the control signal between two limits of voltage ± 5 Volt. The spool valve opening area and the operational hydraulic pressure are smooth signals.

Case III, bumpy road designs have a wave length of 2 m, the amplitude of 2.5 cm, and the vehicle velocities of 20, 30 and 40 Km/h.

$$X_r = \begin{cases} 0.025\left(\left|1-\cos\frac{2\pi U}{\lambda}\,t\right|\right) & 0 \le t \le \frac{\lambda}{U} \\ 0 & otherwise \end{cases} \tag{2.57}$$

where λ is a bump weave length, $\lambda = 2$ m, and U is a vehicle velocity, $U_{20} = 20\ \frac{Km}{h}$. $U_{30} = 30\ \frac{Km}{h}$ and $U_{40} = 40\ \frac{Km}{h}$

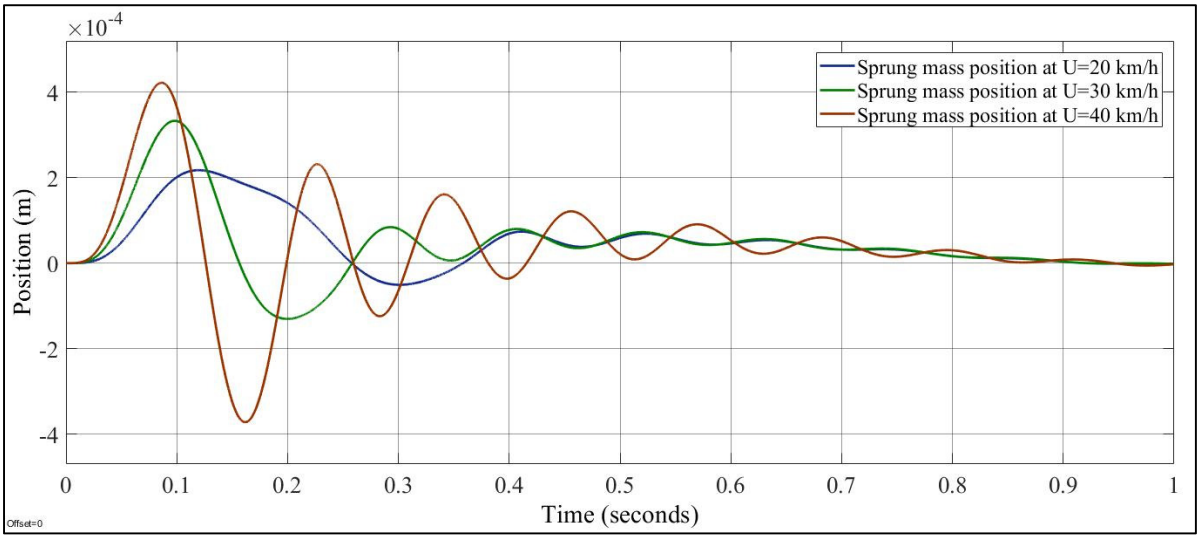

Figure 2.13 Sprung mass position of Case III

In Figure 2.13, the sprung mass position compensation is proportionally degraded depending on bumpy road velocity.

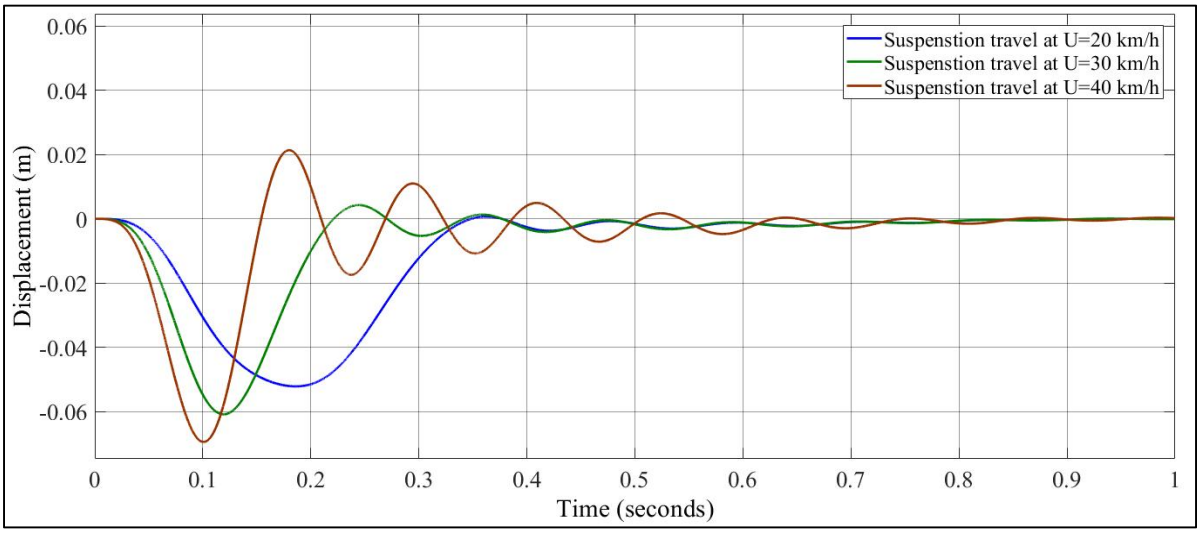

Figure 2.14 Suspension travel of Case III

In Figure 2.14, the suspension travel oscillations are increased with increasing of car velocity. The suspension travel oscillations are approximately 8 % at $U = 20\ km/h$, 10% at $U = 30\ km/h$ and 45 % at $U = 40\ km/h$, respectively. Although the bumpy road amplitude is fixed its value at 0.025 m, the suspension travel is proportionally increased that the maximum travels are -0.05 m of $U = 20\ km/h$, -0.06 m of $U = 20\ km/h$ and -0.074 m of $U = 20\ km/h$. In Figure 2.15, the ANNC cannot maintain road holding at a period of (0.16-0.18) seconds when the velocity of $U = 40\ km/h$, which makes tire liftoff phenomenon.

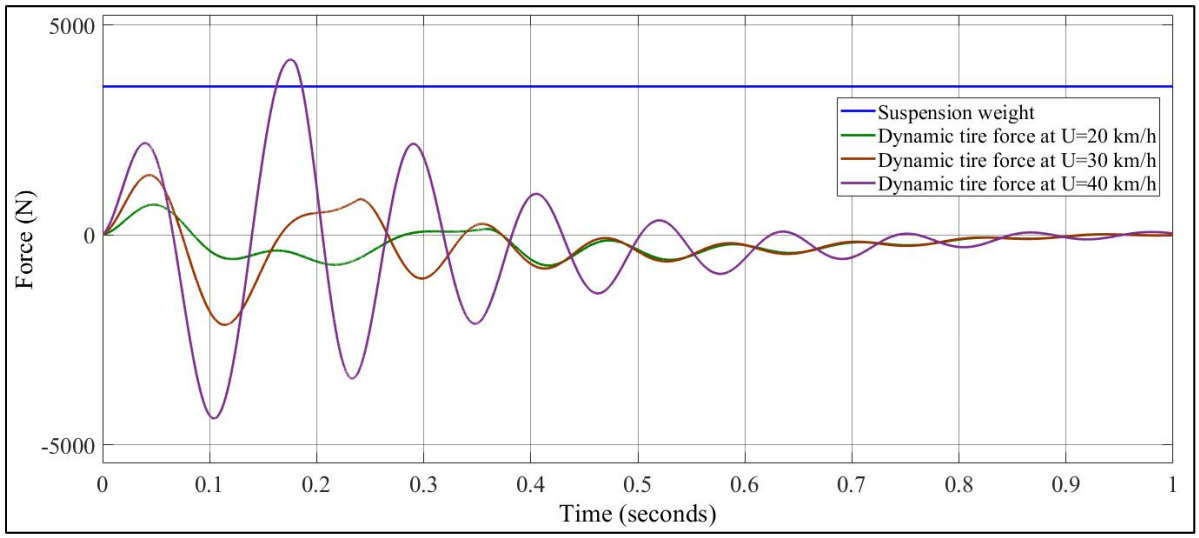

Figure 2.15 Road holding of Case III

In conclusion, the ANNC system provides high control performance, as shown in Figure 2.13; however, it cannot address suspenstion travel limits, as shown in Figure 2.14, and cannot maintain road holding, which makes tire liftoff as shown in Figure 2.15. In (Al Aela et al., 2020), we have considered these restrictions of the active suspension system intensely in that study.

Besides, a frequency response estimation is applied to show the steady state of the active and passive suspension systems. The frequency response is estimated using Simulink tool frequency estimation to the sinusoidal road profile, as shown in Figures 2.16, 2.17, and 2.18.

Figure 2.16 shows a sprung mass acceleration. The active suspension sprung mass acceleration is lower than that of the passive suspension. The sensitive human frequency is about 3-8 Hz (Tuan et al., 2001). Therefore, passenger comfort is highly improved. The sensitive vibration for humans shows a good improvement as well.

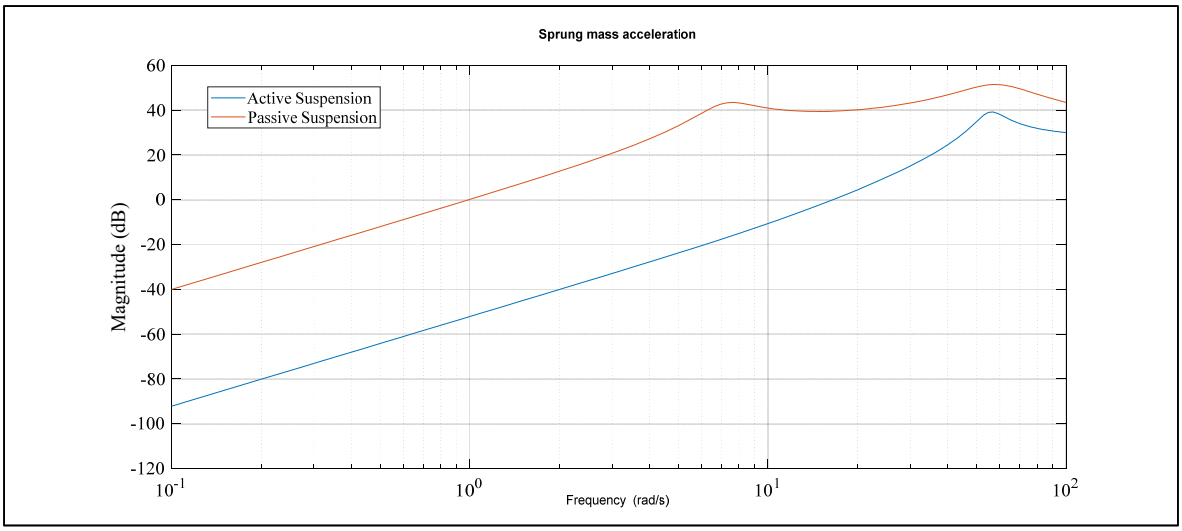

Figure 2.16 Sprung mass acceleration against the road frequency for both active suspension and passive suspension

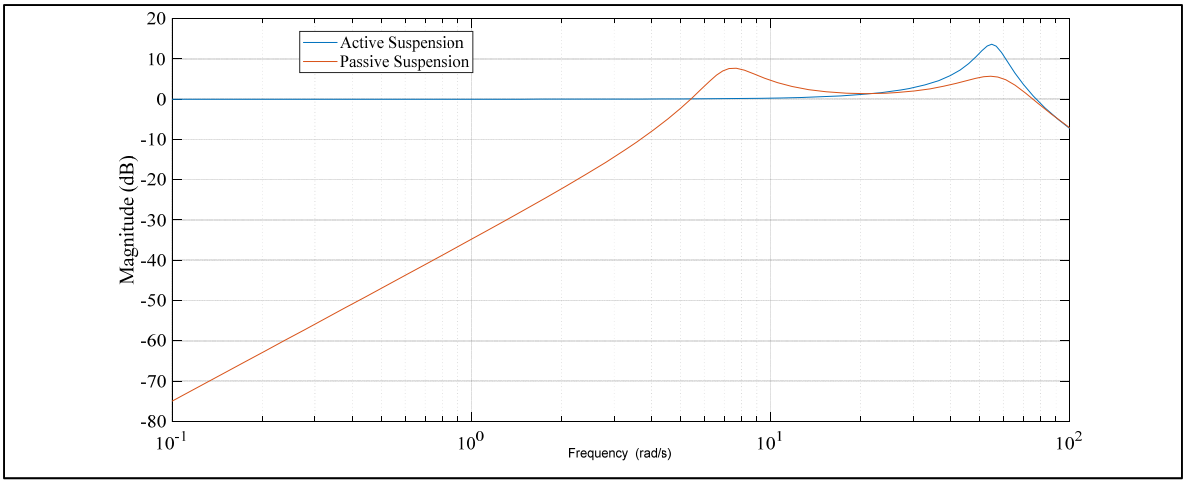

Figure 2.17 Suspension travel (X_s-X_u) against the road frequency for both active suspension and passive suspension

Furthermore, the ANNC achieves a reduction of the suspension travel (X_s-X_u) below 20 rad/s. However, the active suspension shows the worst suspension travel (more than 20 rad/s), as can be seen in Figure 2.17. In Figure 2.18, the sprung mass position active suspension is in negative dB below passive suspension. Hence, the active suspension reduces road perturbations because of the sprung mass attenuation.

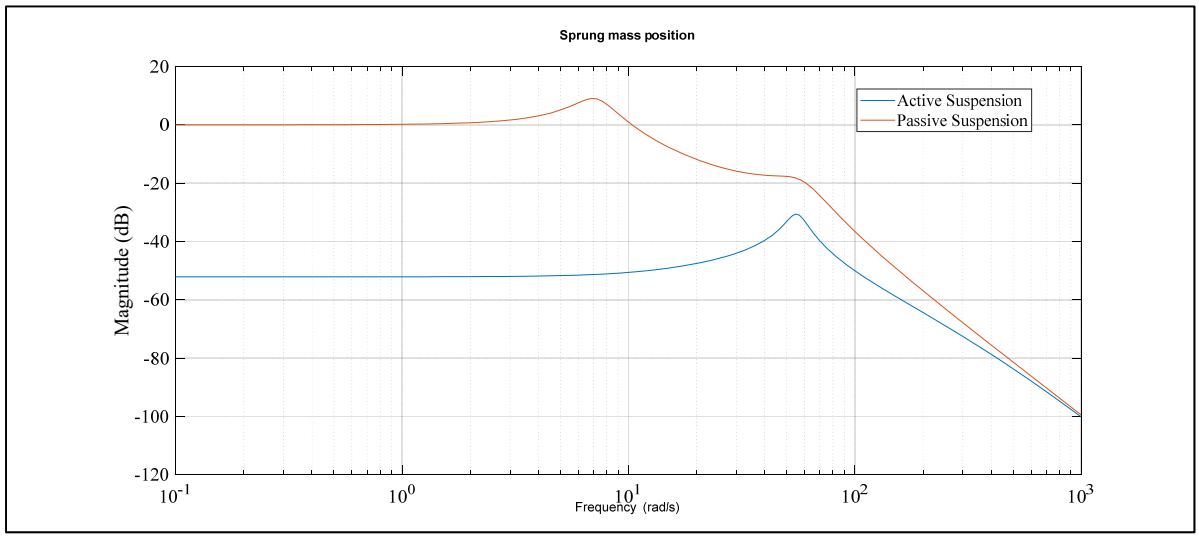

Figure 2.18 Sprung mass position against the road frequency for both active suspension and passive suspension

Therefore, the ANNC has high control compensation compared with passive suspension. A parametric sensitivity analysis is applied to adapt the computed nominal active suspension concerning road perturbation (Michael and Gerdts, 2015). This analysis is presented in Table 2.4. The influence of ANNC compensation is used as a signal property of the sensitivity analysis. The analysis is exclusively applied for each selected parameter by setting the other parameters.

Table 2.4 Sensitivity Analysis

Selected Parameter	Minimum and Maximum parameter values	Unit	Min. - Max. of the sensitivity control compensation %	Compensation Variation %	Control Sensitivity
m_s	250-350	Kg	99.573-99.576	0.002765	Very small
K_s	15120-18480	N/m	99.556-99.59	0.034237	Very small
C_s	900-1100	Ns/m	99.558-99.591	0.033120	Very small
A_p	$(3.015 - 3.4) \times 10^{-4}$	m^2	99.535-99.58	0.044969	Very small
C_{tp}	$(8.1423 - 9.9517) \times 10^{-13}$	$m^5/(Ns)$	99.574-99.574	0.0005147	Very small

The effect of the selected parameters on the control compensation are minimal, as explained in Table 2.4. Therefore, the ANNC has a good robustness with the parametric uncertainties.

2.5 Conclusion

This paper presents an adaptive neural network control (ANNC) for an electrohydraulic servo-valve active suspension in the presence of bumpy road and dynamic nonlinearity and uncertainty systems. The adaptive RBFNN is combined with the backstepping controller to overcome the nonlinearities and uncertainties of the dynamic system, in which an adaptive RBFNN estimates the unknown smooth functions of the modeling system. The unknown coefficient control signal is bounded by using two known parameters. The results show that ANNC system gets 11% of compensation better than AMSSC. Even though the passive suspension is failed to provide passenger comfort and to keep road holding, the ANNC provides a high compensation of 97% of the sprung mass position. However, the ANNC may make tire liftoff phenomenon or hit the suspension travel limits, representing a trade-off between passenger comfort and both road holding and suspension travel limits. The sensitivity analysis of the selected parametric uncertainties shows tiny variations on the ANNC

compensation. Future work will focus on the adaptive control design for a full car active suspension with different operational conditions.

CHAPTER 3

A NOVEL ADAPTIVE AND NONLINEAR ELECTROHYDRAULIC ACTIVE SUSPENSION CONTROL SYSTEM WITH ZERO DYNAMIC TIRE LIFTOFF

Amhmed Mohamed Al Aela [a], Jean-Pierre Kenne [b] and Honorine Angue Mintsa [c]

[a, b] Department of Mechanical Engineering, École de technologie supérieure, 1100, Notre Dame Street West, Montreal Quebec, Canada, H3C 1K3

[c] Department of Mechanical Engineering, Ecole polytechnique de Masuku (EPM), Masuku, Franceville, Haut-Ogooué, Gabon

Paper published in *Journal of Machines MDPI*, July 2020

https://www.mdpi.com/2075-1702/8/3/38

Abstract

In this paper, a novel adaptive control system (NAC) is proposed for a restricted quarter-car electrohydraulic active suspension system. The main contribution of this NAC is its explicit tackling of the trade-off between passenger comfort/road holding and passenger comfort/suspension travel. Reducing suspension travel oscillations is another control target that was considered. Many researchers have developed control laws for constrained active suspension systems. However, most of the studies in the works of the latter have not directly examined the compromise between road holding, suspension travel, and passenger comfort. In this study, we proposed a novel adaptive control system to explicitly address the trade-off between passenger comfort and road holding, as well as the compromise between passenger comfort and suspension travel limits. The novelty of our control technique lies in its introduction of a modeling system for a dynamic landing tire system aimed at avoiding a

dynamic tire liftoff. The proposed control consists of an adaptive neural networks' backstepping control, coupled with a nonlinear control filter system aimed at tracking the output position of the nonlinear filter. The tracking control position is the difference between the sprung mass position and the output nonlinear filter signal. The results indicate that the novel adaptive control (NAC) can achieve the handling of car–road stability, ride comfort, and safe suspension travel compared to that of the other studies, demonstrating the controller's effectiveness.

Keywords: active suspension, road holding, dynamic landing tire, suspension travel, passenger comfort, backstepping control system, adaptive neural networks' control

3.1 Introduction

A vehicle active suspension is a mechanical vibration system. The active suspension aims primarily to minimize the transmission of vertical road forces to the sprung mass (passenger comfort) and to maximize tire–road contact (road holding) (Amer et al., 2011). An active suspension system must operate within safe travel ranges to avoid exceeding the suspension travel limits. Consequently, the hydraulic actuator of the active suspension generates vertical forces to enable a compromise between ride comfort, suspension deflection, and road holding. To ensure passenger comfort, the hydraulic actuator can absorb the road energy transmitted to the sprung mass. Further, the actuator can generate vertical forces to improve car stability and safety. Although the active suspension is an important system in the vehicle structure, it must deal with several challenges. For example, the system has several inherent undesirable dynamic characteristics, such as nonlinear dynamics, parametric uncertainties, and external perturbations (Liu et al, 2013). Moreover, it forces a trade-off between passenger comfort, road holding, and limited suspension travels.

Many control strategies have been applied in vehicle systems, which have multiple modeling systems. A high-precision hydraulic pressure control based on linear pressure drop modulation in valve critical equilibrium state was developed in (Lv et al., 2017). The control methodology

in that study was a sliding mode control based on high-precision hydraulic pressure for an automobile brake system. The experimental tests and validation system showed improvements in the control performance and robustness. In (Xing et Lv, 2019), a dynamic state estimation for the advance brake system of an electric vehicle was implemented by using deep recurrent neural networks. In that study, an integrated time series model based on multivariate deep recurrent neural networks with long short-term memory units was applied for brake pressure estimation of the electric vehicle system. The test results showed the effectiveness of the proposed integrated method. In (Riaz et Khan, 2015), a neuro-fuzzy adaptive control for a full car nonlinear active suspension with onboard antilock braking system was investigated. A comparative study was done between the intelligent control system and passive suspension. The method showed an improvement in control performance.

The vehicle active suspension system is among the systems that have been most studied in recent years. Active suspensions in vehicles serve mainly to isolate the car cabin from road perturbations and provide vehicle handling under different operating conditions. Many researchers have developed control strategies for these systems. Testing and simulation of a motor vehicle suspension were carried out in (Popescu et Mastorakis, 2009). In the study, experiments were done by applying impulse road input perturbation. The results showed reduction of transmitted road energy to the system. Road profiles on a rig for indoor vehicle chassis and suspension durability testing were reproduced in (Chindamo et al., 2017). An impulse road input was applied in the test rig. The results showed control performance improvements. Other studies have been developed for the active suspension system in a bed to overcome the dynamic nonlinearities and parametric uncertainties present. In (Shaer et al., 2016) a sliding mode and fuzzy hybrid control system were developed to overcome dynamic nonlinearities and reduce control chattering for a quarter-car active suspension. There, a fuzzy hybrid control system was designed to track a force and a position and reduce the control chattering. The controller provided control performance improvements. On the other hand, the road holding and the suspension travel limits were not addressed.

Many researchers have also developed control strategies for active suspension systems. For example, in (Pan et al., 2017), an adaptive tracking control was developed to overcome the dynamic nonlinearities for a non-ideal actuator of a quarter-car active suspension. The actuator's nonlinearities of both dead-zone and hysteresis were addressed in that study. The experimental results showed a better balance between isolation performance and energy consumption for the active suspension. Even though several road case designs were applied, road holding was not clearly indicated in results. An adaptive neural networks' control system was designed in (Na et al., 2018). In that study, the road design could not generate the tire liftoff phenomenon to indicate road holding. In (Lin et Kanellakopoulos, 1997), a backstepping control law was investigated to monitor suspension travel by using a nonlinear control filter. The results showed an improvement in control performance. However, road holding was not addressed. A multi-objective control system for a constrained active suspension, designed based on both barrier and quadratic Lyapunov functions, was developed in (Sun et al., 2014), with results showing control performance improvements. However, the system did not address tire liftoff phenomenon. In (Huang et al., 2015), an adaptive control was developed for nonlinear active suspension. While the system provided suspension deflection and road holding, its bumpy road design did not address tire liftoff either. In (Pang et al. 2019), an adaptive backstepping-based tracking controller was investigated for nonlinear half-active suspension. In that study, zero dynamics system was applied to ensure that all dynamic order errors were bounded. Although the results showed improvements in control performance, tire liftoff was not tested. In (Pang et al., 2019), an adaptive backstepping tracking control was developed for an uncertain nonlinear active suspension. The control consisted of a model-reference control combined with coordinated adaptive backstepping control systems. Simulation results showed control performance degradation and, once again, tire liftoff was not examined. In (Pusadkar, 2019), a linear disturbance observer coupled with a sliding mode scheme was developed for an active suspension with a non-ideal actuator. The results showed compensation improvements despite the presence of a dead-zone and hysteresis, as well as modeling uncertainty. In this case as well, the tire liftoff effect was not considered. In (Liu et al., 2019), an adaptive neural networks' control was developed for a restricted quarter-car active suspension. Both the barrier Lyapunov function and zero dynamics system were applied

to prevent any violation of the system's constraints. There was an improvement in the control performance, but the tire liftoff was not evaluated.

As we can see, while previous works showed improvements in control performance, they universally did not examine tire liftoff. Therefore, the results in previous studies cannot indicate road-holding robustness.

In general, high-frequency bumpy road input can generate tire liftoff phenomenon. Thus, road holding can clearly be addressed. In (Huang et al., 2019), an approximation-free control was developed for quarter-car active suspension. In that study, both a random road and a high-frequency bumpy road designs were examined. The results showed an improvement in road holding when the random road design was applied. Even though previous studies were developed, improving in control performance, the researchers did not explicitly address both a trade-off between ride comfort and road holding, and a trade-off between ride comfort and suspension travel limits.

In this study, a novel control system was developed to handle the inherent trade-off between passenger comfort/road holding, passenger comfort/suspension contraction limitation, and passenger comfort/suspension expansion limitation, as well as to overcome the dynamic nonlinearities and parametric uncertainties of quarter-car active suspension systems. The novelty of this study lies in its aim, which is two-fold. On the one hand, it aimed to overcome and prevent the dynamic tire liftoff phenomenon by implementing a new model of a dynamic landing tire system. On the other hand, it aimed to avoid exceeding suspension travel limits. We broke down the suspension deflection into two different suspension travel limits, namely, suspension contraction limitation and suspension expansion limitation. We then redesigned a nonlinear control filter that was introduced in (Lin et Kanellakopoulos, 1996). The redesigned filter became three regions, which are a dead zone, a dynamic landing tire nonlinear function, and a suspension deflection nonlinear function. This design of the nonlinear control filter can accommodate and improve the trade-off between passenger comfort, road holding, and suspension travel. Therefore, the novel adaptive control system (NAC) is an adaptive neural

networks' backstepping control system coupled with the nonlinear control filter. The adaptive neural networks' control system can deal with unknown smooth functions of the modeling system. The summarized contributions of this article are:

1. The NAC was established to achieve passenger comfort while keeping road holding and prevention of exceeding suspension travel limits.
2. The NAC was also designed to reduce suspension travel oscillations.
3. A dynamic landing tire modeling system was developed to evaluate a required tire vertical displacement, which maintains road holding for the car.
4. The suspension travel limits were separately chosen to be suspension contraction limitation and suspension expansion limitation in order to realize operation conditions.
5. In NAC structure, the adaptive radial basis function neural networks were designed to approximate nonlinear and unknown bounding functions in the modeling system.

Finally, simulation examples demonstrated the performance of the NAC in enhancing passenger comfort, maintaining road holding, avoiding reaching suspension travel limits, and reducing suspension travel oscillation.

The rest of the paper is broken down as follows. Section 2 presents the notations used and the problem statement. Section 3 describes the control law design, which includes the nonlinear control filter, the adaptive neural networks' backstepping control design, and zero dynamics system. Section 4 discusses the illustrated example of a comparative study of a filtered active suspension, an unfiltered active suspension, and a passive suspension. Section 5 presents the conclusion and future works.

3.2 Notation and Problem Statement

The primary purpose of the active suspension is to provide a compromise between ride comfort, car–road stability, and safety (Alleyne et Hedrick, 1995). This suspension is mainly composed of a sprung mass, an unsprung mass, a spring suspension, a suspension damper, a tire, an electrohydraulic servovalve system, and other accessories (Kadlicko et Halina, 1994),

as shown in Figure 1. Passenger comfort definition is to isolate the sprung mass from road perturbations. Moreover, road holding definition is to handle vehicle–road stability. The electrohydraulic servovalve system (EHSS) of the active suspension generates hydraulic forces to provide a compromise between ride comfort and road holding. In Table 3.1, the nomenclature for the active suspension system parameters is listed with accompanying descriptions as follows.

Table 3.1 Active suspension parameters and their descriptions

Quantity	Description	Quantity	Description
A_p	Actuator piston area, m^2	ST	Suspension travel, m
A_v	Spool valve projected area, m^2	ST_D	Minimum allowable of suspension travel "contraction", m
b_j	Gaussian function width for RBFNN	ST_E	Maximum allowable of suspension travel "expansion", m.
C_d	Low discharge coefficient, -	V_t	Actuator volume, m^3
C_{tp}	Coefficient of leakage, $m^5/(Ns)$	X_L	The landing tire position, m
c_i	Positive constant, -	X_u	Unsprung mass position, m
C_{sf}	Parameter for static friction	X_s	Sprung mass position, m
C_s	Suspension viscous coefficient, Ns/m	$\dot{X}_s$	Sprung mass velocity, m/s
C_t	Tire viscous coefficient, Ns/m	$\ddot{X}_s$	Sprung mass acceleration, m/s^2
f_i	Unknown function i	$\dot{X}_u$	Unsprung mass velocity, m/s
$\hat{f}_i$	An approximate smooth function i	$\ddot{X}_u$	Unsprung mass acceleration, m/s^2
F_{c0}	Coulomb friction coefficient	W_i	an unknown weight vector for RBFNN
F_{s0}	Static friction coefficient	$\bar{X}_u$	Unsprung mass position nonlinear control filter output, m

g	Gravitational acceleration, m/s^2	δ_0	Positive constant, -
g_i	Unknown modeling function i	σ	Parameter for viscous friction
$K_{u\,min}$	Lower bound control signal gain, m^2/V	τ_v	Servovalve time constant, s
$K_{u\,max}$	Upper bound of control signal gain, m^2/V	β_e	Effective bulk modulus, N/m^2
K_s	Suspension spring stiffness, N/m	ρ	Hydraulic oil density, kg/m^3
K_t	Tire spring stiffness, N/m	κ_{st}	Positive constant, -
l	Number of RFBNN nodes	κ_{Rh}	Positive constant, -
$n_{1,2}$,$m_{1,2,3,4}$	Positive constants	κ_w	Adjustable factor for the road holding ratio 'R_h', -
m_u	Unsprung (wheel) mass, Kg	$\varphi_{i,j}$	centers of the receptive field in RBFNN
m_s	Sprung (body) mass, Kg	ε_N	Positive designed error of RBFNN
m	Number of variables in the compact set	$\propto$	A virtual control function
n	State-space order system	$\boldsymbol{\zeta}$	RBFNN compact set parameters
P_L	Operational hydraulic pressure, N/m^2	NAC	Novel adaptive control
P_s	Pressure supply, N/m^2	ANNC	Adaptive neural networks control system
R_h	Road holding ratio, -	RBFNN	Radial basis function neural networks

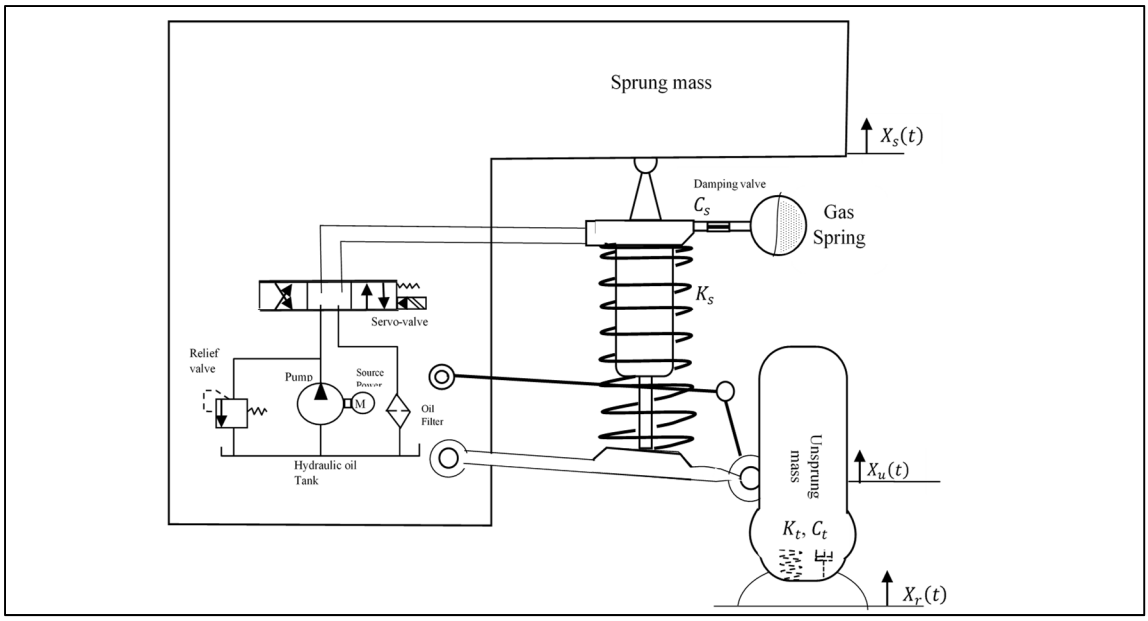

Figure 3.1 Sketch of a quarter-car active suspension

The mathematical modeling of the quarter-car active suspension can be described as shown in Figure 3.1, while the sprung mass of the same is described as in (Kim, 1996):

$$\mathrm{m_s(t)\,\ddot{X}_s = -F_{su} - F_f + A_p P_L} \tag{3.1}$$

The unsprung mass dynamic system with tire liftoff can be modeled as (Kim and RO, 1998).

$$\mathrm{m_u\,\ddot{X}_u} = \begin{cases} \mathrm{F_{su} + F_f - A_p P_L + F_{Dt}} & \mathrm{|F_{Dt}| \le (m_s + m_u)g} \\ \mathrm{F_{su} + F_f - A_p P_L} & \mathrm{|F_{Dt}| > (m_s + m_u)g} \end{cases} \tag{3.2}$$

The spring-damper forces F_{su} can be modeled as:

$$F_{su} = K_s(X_s - X_u) + C_s\left(\dot{X}_s - \dot{X}_u\right) \tag{3.3}$$

The dynamic tire force F_{Dt} is modeled as:

$$F_{Dt} = -K_t(X_u - X_r) - C_t(\dot{X}_u - \dot{X}_r) \tag{3.4}$$

In this study, we considered friction forces, which consisted of a viscous friction, Coulomb friction, and a stiction friction phenomenon (Guglielmino et al., 2008). The friction forces are undesirable effects on the control performance. The friction forces F_f of the hydraulic servosystem can be presented as in (Jelali et Kroll, 2004).

$$F_f = \sigma(\dot{X}_s - \dot{X}_u) + \text{sign}(\dot{X}_s - \dot{X}_u)\left[F_{c0} + F_{s0}\exp\left(-\frac{|(\dot{X}_s - \dot{X}_u)|}{C_{sf}}\right)\right] \tag{3.5}$$

In Equation (3.2), the tire must contact the road surface; otherwise, it loses the road contact (tire liftoff phenomenon). The following formula is used to express road holding:

$$\frac{|\text{Dynamic tire force}|}{\text{Suspension weight}} = \frac{|F_{Dt}|}{(m_s + m_u)g} \leq 1 \tag{3.6}$$

Suspension travel limitations are other suspension restrictions. The maximum allowable suspension deflection can be represented as (Liu et al., 2019):

$$|X_s - X_u| \leq ST_D \tag{3.7}$$

In real operating conditions, both suspension travel limitations do not always equal the same. In this study, the suspension travel limitations became as following the form:

$$ST_E > X_s - X_u > ST_c \tag{3.8}$$

where the ST_c is a suspension travel contraction limit and the ST_E is a suspension travel expansion limit.

The electrohydraulic servovalve system for the hydraulic actuator and the servovalve can be presented as (Chen P and Huang A, 2006):

$$\frac{V_t}{2\beta_e}\dot{P}_L(t) = C_d A_v(t)\sqrt{\frac{P_s - P_L\,\mathrm{sgn}(A_v(t))}{\rho}} - A_p(X_s - X_u) - C_{tp}P_L \tag{3.9}$$

$$\dot{A}_v = \frac{1}{\tau_v}\left(-A_v + K_u u(t)\right) \tag{3.10}$$

In this study, a new modeling for a dynamic landing tire system was developed to avoid the dynamic tire liftoff phenomenon, as shown in Figure 3.2.

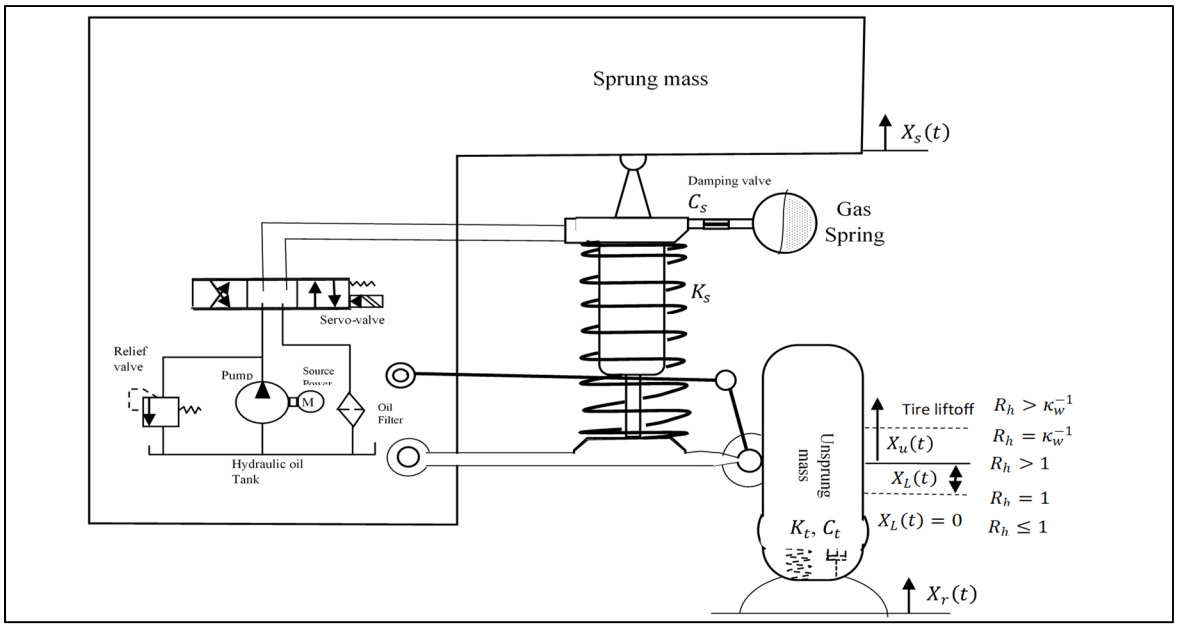

Figure 3.2 Dynamic landing tire system

Dynamic tire liftoff only occurs if the unsprung mass position X_u is higher than the road position X_r. However, Equation (3.6) does not consider this condition. Hence, we can rearrange Equation (3.6):

$$R_h = \frac{\left(K_t(X_u - X_r) + C_t(\dot{X}_u - \dot{X}_r)\right)}{(m_s + m_u)g} \leq 1 \tag{3.11}$$

where R_h is a road holding ratio.

Therefore, the vertical tire displacement $(X_u - X_r)$ can use X_L as a required tire landing position.

$$K_t X_L + C_t \dot{X}_L \leq (m_s + m_u) \tag{3.12}$$

In order to avoid tire liftoff, the tire landing position must be evaluated before the critical road holding ratio '$R_h = 1$'. Thus, the dynamic landing position X_L is created in the following form:

$$\dot{X}_L(t) = \begin{cases} 0 & R_h(t) < 1 \\ \frac{K_t}{C_t}\left(X_L(t) + \frac{\kappa_w(m_s + m_u)g}{K_t}\,(R_h(t) - 1)\right), & \kappa_w^{-1} \geq R_h(t) \geq 1 \end{cases} \tag{3.13}$$

where the κ_w is an adjustable factor for the road holding ratio $(0 \leq \kappa_w \leq 1)$.

Moreover, the differential road holding $\dot{R}_h$ is differentially determined, as follows:

$$\dot{R}_h(t) = \frac{K_t(\dot{X}_u - \dot{X}_r) + C_t(\ddot{X}_u - \ddot{X}_r)}{\kappa_w(m_s + m_u)g}, \qquad R_h(t) \leq \kappa_w^{-1} \tag{3.14}$$

3.3 Control Design

This section consists of three subsections: Nonlinear control filter system, adaptive neural networks' backstepping control system, and zero dynamic systems.

3.3.1 Nonlinear Control Filter

In (Lin et Kanellakopoulos, 1996), a nonlinear control filter was developed to adjust the trade-off between passenger comfort and suspension travel for a quarter-car active suspension system. In this study, we redesigned the nonlinear control filter by modifying a nonlinear tire land function $\phi(X_L)$. The input filter was the unsprung mass position X_u. Therefore, the nonlinear control filter was able to compromise between passenger comfort and road holding and also suspension travel, as follows:

$$\dot{\breve{X}}_u = -\left(\delta_0 + \kappa_{st}\psi(ST) + \kappa_{Rh}\phi(X_L)\right)\left(\breve{X}_u - X_u\right) \tag{3.15}$$

where the symbols δ_0, κ_{st}, and κ_{Rh} are positive constants, and the suspension travel ST, $ST = X_s - X_u$.

The nonlinear function of suspension travel $\psi(ST)$ is a positive nonlinear function.

$$\psi(ST) = \begin{cases} \left(\dfrac{ST - m_2}{m_1}\right)^4, & ST < m_2 \\ 0, & m_3 \geq ST \geq m_2 \\ \left(\dfrac{ST - m_3}{m_4}\right)^4, & ST > m_3 \end{cases} \tag{3.16}$$

where m_2 is a chosen constant $0 \geq m_2 \geq ST_c$, m_3 is a chosen constant $ST_E \geq m_3 \geq 0$, and the m_1 and m_4 are positive constants.

The landing tire nonlinear function $\phi(X_L)$ is a positive nonlinear function and evaluates as follows.

$$\phi(X_L) = \begin{cases} \left(\dfrac{X_L + n_2}{n_1}\right)^4 & \kappa_w^{-1} \geq R_h \geq 1 \\ 0 & R_h < 1 \end{cases} \tag{3.17}$$

where $n_1$and n_1 are positive constants.

It can be concluded that the flow chart of the nonlinear control filter dynamic system is sketched in Figure 3.3. When the filter dead-zone ($R_h < 1, m_3 \geq ST \geq m_2$) was activated, the nonlinear bandwidth filter became a chosen small constant δ_0 to obtain passenger comfort. Otherwise, at least one of the suspension constraints ($m_3 < ST, ST < m_2, \kappa_w^{-1} \geq R_h \geq 1$) was expected; the nonlinear function $\big(\psi(ST), \phi(X_L)\big)$ rapidly increased the filter bandwidth. Thus, the suspension travel became stiff:

The state-space modeling system was built from Equations (3.1), (3.2), (3.9), (3.10), and (3.13)–(3.15). Therefore, the state-space modeling of the filtered active suspension system had nine variables, as follows.

$$X_1 = X_s,\ X_2 = \dot{X}_s, X_3 = C_h P_L,\ X_4 = C_v A_v, X_5 = \breve{X}_u, X_6 = X_u, X_7 = \dot{X}_u, X_8 = X_L, X_9 = R_h$$

$$\dot{X}_1 = X_2 \tag{3.18}$$

$$\dot{X}_2 = -\frac{K_s}{m_s}(X_1 - X_3) - \frac{C_s}{m_s}(X_2 - X_4) + \frac{A_p}{m_s}X_5 \tag{3.19}$$

$$\dot{X}_3 = \frac{2\beta_e C_d}{V_t}\ X_4\sqrt{\frac{P_s - X_3\ \mathrm{sgn}(X_4)}{\rho}} - \frac{2\beta_e A_p}{V_t}(X_2 - X_7) + \frac{2\beta_e C_{tp}}{V_t}\ X_3 \tag{3.20}$$

$$\dot{X}_4 = \frac{1}{\tau_v}\big(-X_4 + K_u\ u(t)\big) \tag{3.21}$$

$$\dot{X}_5 = -\big(\delta_0 + \kappa_{st}\psi(\eta) + \kappa_{Rh}\phi(X_8)\big)(X_5 - X_6) \tag{3.22}$$

$$\dot{X}_6 = X_7 \tag{3.23}$$

$$\dot{X}_7 = \begin{cases} K_s(X_1 - X_6) + C_s(X_2 - X_7)\ - A_p X_3 - K_t(X_6 - X_r) - C_t\big(X_7 - \dot{X}_r\big), & X_9 \leq \kappa_w^{-1} \\ K_s(X_1 - X_6) + C_s(X_2 - X_7)\ - A_p X_3, & X_9 > \kappa_w^{-1} \end{cases} \tag{3.24}$$

$$\dot{X}_8 = \begin{cases} 0 & X_9 < 1 \\ -\frac{K_t}{C_t}\left(X_8 - \frac{\kappa_w(m_s + m_u)g}{K_t}(X_9 - 1)\right), & \kappa_w^{-1} \geq X_9 \geq 1 \end{cases} \quad (3.25)$$

$$\dot{X}_9 = \frac{1}{\kappa_w(m_s + m_u)g}\{-K_t(X_7 - \dot{r}) - K_s C_t(X_1 - X_6) - C_s C_t(X_2 - X_7) + C_t A_p X_3 + C_t K_t(X_6 - X_r) + C_t^2(X_7 - \dot{X}_r) + C_t \ddot{r}\}, \; X_9 \leq \kappa_w^{-1} \quad (3.26)$$

$$y = X_1 - X_5 \quad (3.27)$$

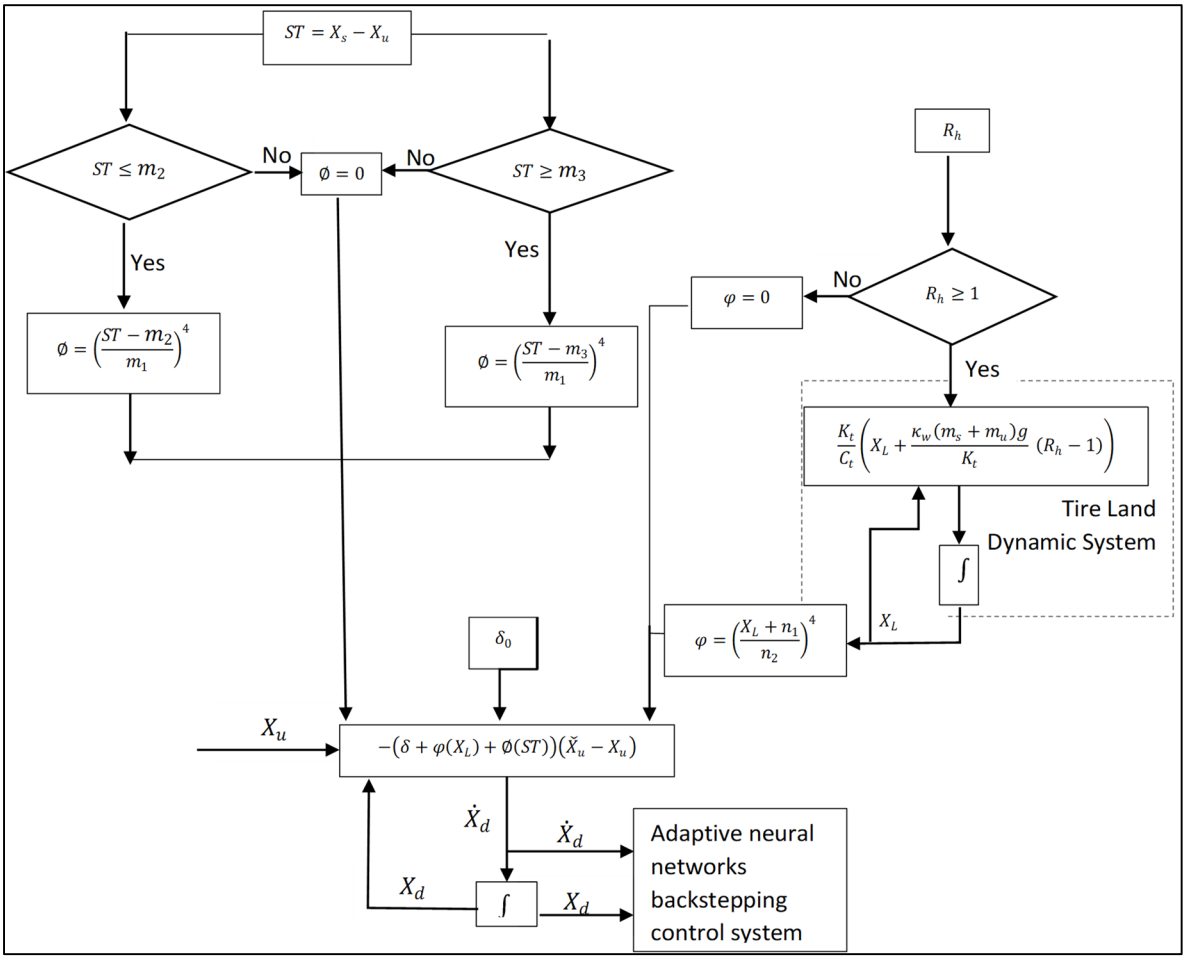

Figure 3.3 Filtered active suspension flow chart

3.3.2 Adaptive Neural Networks' Backstepping Control Design

In this section, an adaptive neural networks' backstepping was developed for the recursive closed-loop system in Equation (3.18). Lyapunov's stability theory was employed to guarantee control stability. One advantages of this technique is that it allows circumventing the unmodeled model uncertainties of multiple dynamic systems. Several research studies have applied the backstepping control technique to overcome the inherent nonlinearities and uncertainties of the system. The backstepping design complicity is to determine regression matrices of uncertain nonlinear functions. In order to linearize the state-space modeling and simplify the backstepping control system, a linear radial basis function neural networks (RBFNN) was implemented, and could deal with unknown functions. Hence, the state space modeling of the adaptive neural networks' control (ANNC) design was reduced to fourth orders.

$$\begin{aligned} \dot{X}_1 &= X_2 \\ \dot{X}_2 &= X_3 + g_2(X) \\ \dot{X}_3 &= X_4 + g_3(X) \\ \dot{X}_4 &= \beta u(t) + g_4(X) \\ y &= X_1 - X_5 , \qquad \forall [X_1, X_2, X_3, X_4] \in \Omega_X \subset R^4 \end{aligned} \tag{3.28}$$

Thus, the functions $g_2(X), g_3(X), g_4(X)$ and the parameter β are chosen as follows.

$$\begin{aligned} g_2(X) &= -X_3 - \frac{K_s}{m_s}(X_1 - X_6) - \frac{C_s}{m_s}(X_2 - X_7) + \frac{A_p}{m_s}X_3 \\ g_3(X) &= -X_4 + \frac{2\beta_e C_d}{V_t} X_4 \sqrt{\frac{P_s - X_3\ \mathrm{sgn}(X_4)}{\rho}} - \frac{2\beta_e A_p}{V_t}(X_2 - X_7) + \frac{2\beta_e C_{tp}}{V_t} X_3 \\ g_4(X) &= -\frac{X_4}{\tau_v} \\ \beta &= \frac{K_u}{\tau_v} \end{aligned} \tag{3.29}$$

In order to approximate the unknown functions $g_i(\zeta)$, we needed to know the aspect of the radial basis function neural network. The radial basis function neural networks (RBFNN) can approximate nonlinear and unknown bounding functions. In this study, we used a linear RBFNN to approximate the unknown functions of the modeling system. The linear RBFNN had one hidden layer, a fixed size, and fixed moving basis functions (Krstic, 1998; Orr, 1996). Therefore, the unknown smooth functions $f_i(\zeta)$ could be presented as (Liu, 2013; Ge et Wang, 2002):

$$f_i(\zeta) = W_i^T H_i(\zeta) + \varepsilon_i, \quad i = 1,2,\dots,n, \quad \forall\, \zeta \in \Omega_\zeta \subset \mathbb{R}^m \tag{3.30}$$

where the input vector $\zeta \in \Omega_\zeta \subset \mathbb{R}^m$, the ε_i is the approximation error, the W_i^T is an unknown weight vector, $W_i^T = [W_1 \quad W_2 \quad \dots \quad W_l]_i^T$, the $H_i(\zeta)$ is a basis function vector, $H_i(\zeta) = [h_1(\zeta) \quad h_2(\zeta) \quad \dots \quad h_l(\zeta)]_i$, and the $h_i(\zeta), i = 1,\dots,l$ are hidden Gaussian functions, which satisfy:

$$h_i(\zeta) = e^{-\left\{\frac{\|\zeta-\varphi_{i,j}\|^2}{2b_j^2}\right\}}, i = 1,\dots,l, \ \boldsymbol{\zeta} = [\zeta_1, \zeta_2, \dots, \zeta_m] \quad \forall\, \zeta \in \Omega_\zeta \subset \mathbb{R}^l \tag{3.31}$$

where the $\{\varphi_{i,j}, b_j, i = 1,\dots,l \text{ and } j = 1,\dots,m\}$ are the centers of the receptive field and the width of Gaussian function, respectively.

Therefore, approximate smooth functions $\hat{\mathbf{f}}_\mathbf{i}(\zeta)$ could be estimated by RBFNN as follows:

$$\hat{f}_i(\zeta) = \widehat{W}_i^T H_i(\zeta), \ i = 1,2,\dots,n \ \forall\, \zeta \in \Omega_\zeta \subset \mathbb{R}^m \tag{3.32}$$

To minimize the approximation error, the optimal weight value 'W_i' of the RBFNN was defined (Zheng Z and Zou Y, 2016).

$$W_i := \arg\min_{\widehat{W}_i \in R^n} \left\{ \sup_{\zeta \in \Omega_i} \left\| f_i(\zeta) - \hat{f}_i(\zeta) \right\| \right\}, \ W_i \text{ is } l \times m, \ \forall\, \zeta \in \Omega_i \tag{3.33}$$

As a result, a tiny positive design error ε_N could have occurred:

$$\max\left\|\mathbf{f}(\zeta)-\hat{\mathbf{f}}(\zeta)\right\| \leq \varepsilon_N \tag{3.34}$$

where $\mathbf{f}(\zeta) = [f_1(\zeta) \quad f_2(\zeta) \quad ... \quad f_n(\zeta)]$ and $\hat{\mathbf{f}}(\zeta) = \left[\hat{f}_1(\zeta) \quad \hat{f}_2(\zeta) \quad ... \quad \hat{f}_n(\zeta)\right]$.

The "centers and widths" of the RBFNN were chosen based on a range of input values. Therefore, we applied a gradient descent learning algorithm to obtain the optimal RBFNN parameters such as the centers $\varphi_{i,j}$, widths b_j, and number of nodes l.

The backstepping control was organized into four backstepping control steps, as follows.

Step 1: Sprung mass velocity

The control coordinate Z_1 was defined as:

$$Z_1 = X_1 - X_5 \tag{3.35}$$

To stabilize the controller, let us consider a quadratic Lyapunov function candidate V_1:

$$V_1 = \frac{1}{2}z_1^2 \tag{3.36}$$

The Lyapunov derivative function $\dot{V}_1$ of step 1 becomes:

$$\dot{V}_1 = Z_1\dot{Z}_1 = Z_1\left(\dot{X}_1 - \dot{X}_5\right) \tag{3.37}$$

To stabilize the system, the derivative control coordinate $\dot{Z}_1$ becomes:

$$\dot{Z}_1 = Z_2 + \propto_1 - \dot{X}_5 = -c_1 Z_1 \tag{3.38}$$

where c_1 is a positive constant.

Then, the virtual control function $\propto_1$ is:

$$\propto_1 = \dot{X}_5 - c_1 Z_1 \tag{3.39}$$

Substitute $\propto_1$ into $\dot{V}_1$:

$$\dot{V}_1 = Z_1 Z_2 - c_1 Z_1^2 \tag{3.40}$$

Step 2: Sprung mass dynamic acceleration

We can define the virtual control coordinate Z_i as:

$$\dot{Z}_i = \dot{X}_i - \dot{\propto}_{i-1} \tag{3.41}$$

Lemma 3.1: The control derivative function $\dot{\propto}_{i-1}$ produces two parts, namely, a countable part $\dot{\propto}_{(i-1)_c}$ and an uncountable part $\dot{\propto}_{(i-1)_u}$ (Han S and Lee J, 2014). The $\propto_{i-1}$ is defined.

$$\propto_{i-1} \equiv \propto_{i-1} \left(X_1, \ldots, X_i, \widehat{W}_{i-1}\right) \tag{3.42}$$

Then, the partial derivative of the function $\propto_{i-1}$ is:

$$\dot{\propto}_{i-1} = \frac{\partial \propto_{i-1}}{\partial X_1} X_2 + \cdots + \frac{\partial \propto_{i-1}}{\partial X_{i-1}} X_i + \frac{\partial \propto_{i-1}}{\partial \widehat{W}_{i-1}} \dot{\widehat{W}}_{i-1} \tag{3.43}$$

Therefore, the uncountable part $\dot{\propto}_{(i-1)_u}$ consists of unknown smooth functions:

$$\dot{\propto}_{(i-1)_u} = \sum_{k=1}^{i-1} \frac{\partial \propto_{i-1}}{\partial X_k} g_k(X) + \frac{\partial \propto_{i-1}}{\partial \widehat{W}_{i-1}} \dot{\widehat{W}}_{i-1} \tag{3.43}$$

The countable part $\dot{\propto}_{(i-1)_c}$ is a smooth function described as:

$$\dot{\propto}_{(i-1)_c} = \sum_{k=1}^{i-1} \frac{\partial \propto_{i-1}}{\partial X_k} X_{k+1} \tag{3.44}$$

Thus, the total unknown functions at step i-1 are defined:

$$\dot{\propto}_{(i-1)_c} = \sum_{k=1}^{i-1} \frac{\partial \propto_{i-1}}{\partial X_k} X_{k+1} \tag{3.44}$$

The unknown function $f_i(X)$ can be represented by the RBFNN as follows:

$$f_i(X) = W_i^T h_i(\zeta) + \varepsilon_i \,, \zeta \equiv X, \forall\, \zeta \in \Omega_\zeta \subset \mathbb{R}^m \tag{3.44}$$

□

Therefore, the Lyapunov function candidate V_2 design is selected:

$$V_2 = V_1 + \frac{1}{2} Z_2^2 + \frac{1}{2} \widetilde{W}_2 \, \Gamma_2^{-1} \, \widetilde{W}_2 \tag{3.45}$$

By applying Lemma 3.1, the Lyapunov derivative function candidate $\dot{V}_2$ becomes:

$$\dot{V}_2 = \dot{V}_1 + Z_2\left(X_3 + W_2^T h_2(\zeta) + \varepsilon_2 - \dot{\propto}_{1_c}\right) + \widetilde{W}_2 \, {\Gamma_2}^{-1} \, \dot{\widehat{W}}_2 \tag{3.46}$$

The adaptive RBFNN law $\dot{\widehat{W}}_2$ is defined (Yang G et al., 2016; Liu J and Wang X, 2012):

$$\dot{\widehat{W}}_2 = \Gamma_2 \, Z_2 \, h_2(\zeta) - \Gamma_2 \sigma_{\theta_2} \widehat{W}_2 \tag{3.47}$$

where the Γ_2 is a positive definite matrix and the $\sigma_{\theta_2}$is a positive constant.

Therefore, the selected virtual control $\propto_2$ is:

$$\propto_2 = -Z_1 - c_2 Z_2 - \widehat{W}_2^T h_2(\zeta) + \dot{\propto}_{1_c} \tag{3.48}$$

By substituting Equations (3.35) and (3.36) into the Lyapunov derivative function $\dot{V}_2$:

$$\dot{V}_2 = -c_1 Z_1^2 - c_2 Z_2^2 + Z_3 Z_2 + Z_2 \varepsilon_2 - \sigma_{\theta_2} \widetilde{W}_2 \widehat{W}_2 \tag{3.49}$$

The function $\dot{V}_2$ is moved to the next step.

Step 3: Hydraulic actuator dynamic system

The virtual control coordinate Z_3 is:

$$Z_3 = X_3 - \propto_2 \tag{3.50}$$

Hence, the Z_3 derivative function becomes

$$\dot{Z}_3 = \dot{X}_3 - \dot{\propto}_2 = X_4 + g_3(X) - \dot{\propto}_2 \tag{3.51}$$

The Lyapunov function candidate V_i design is selected:

$$V_3 = V_2 + \frac{1}{2} Z_3^2 + \frac{1}{2} \widetilde{W}_3 \, \Gamma_3^{-1} \, \widetilde{W}_3 \tag{3.52}$$

By applying Lemma 1, the Lyapunov derivative function candidate $\dot{V}_3$ becomes:

$$\dot{V}_3 = \dot{V}_2 + Z_3\left(X_4 + W_3^T h_3(\zeta) + \varepsilon_3 - \dot{\propto}_{2_c}\right) + \widetilde{W}_3\, \Gamma_3^{-1}\, \dot{\widehat{W}}_3 \tag{3.53}$$

Therefore, the selected virtual control $\propto_3$ is:

$$\propto_3 = -Z_2 - c_3 Z_3 - \widehat{W}_3^T h_3(\zeta) + \dot{\propto}_{2_c} \tag{3.54}$$

By substituting Equation (3.42) into the Lyapunov derivative function $\dot{V}_2$:

$$\dot{V}_3 = -c_1 Z_1^2 - c_2 Z_2^2 - c_3 Z_3^2 + Z_4 Z_3 + Z_2 \varepsilon_2 + Z_3 \varepsilon_3 - \sigma_{\theta_2} \widetilde{W}_2 \widehat{W}_2 - \sigma_{\theta_3} \widetilde{W}_3 \widehat{W}_3 \tag{3.55}$$

The right-side terms in $\dot{V}_3$ are moved to the last step.

Step 4: Servovalve dynamic system

In this step, the control signal design $u(t)$ is designed and the overall Lyapunov candidate stability is guaranteed. The virtual control coordinate Z_4 is selected:

$$Z_4 = X_4 - \propto_3 \tag{3.56}$$

The time derivative Z_4 is:

$$\dot{Z}_4 = g_4(X) + \beta u(t) - \dot{\propto}_3 \tag{3.57}$$

The overall Lyapunov candidate function V is selected as follows:

$$V = V_3 + \tfrac{1}{2} Z_4^2 + \frac{1}{2} \widetilde{W}_4\, \Gamma_4^{-1}\, \widetilde{W}_4 + \frac{1}{2\mu} \tilde{\beta}^2 \tag{3.58}$$

where μ is a positive constant.

By using Lemma 3.1, the overall Lyapunov derivative function $\dot{V}$ Equation (3.46) becomes:

$$\dot{V} = \dot{V}_3 + Z_4\left(W_4^T h_4(\zeta) + \varepsilon_4 + \hat{\beta}u(t) - \dot{\alpha}_{3_c}\right) - \tilde{\beta}\, Z_4\, u(t) + \frac{1}{\mu}\tilde{\beta}\dot{\hat{\beta}} + \widetilde{W}_4\Gamma_4^{-1}\dot{\widehat{W}}_4 \quad (3.59)$$

Thus, the design control signal $u(t)$ is selected:

$$u(t) = \frac{1}{\hat{\beta}}\left(-Z_3 - \widehat{W}_4^T h_4(\zeta) + \dot{\alpha}_{3_c}\right) \quad (3.60)$$

The RBF neural network adaptive law $\dot{\widehat{W}}_4$ is expressed as:

$$\dot{\widehat{W}}_4 = \Gamma_4\, Z_4\, h_4(\zeta) - \Gamma_4\sigma_{\theta_4}\widehat{W}_4 \quad (3.61)$$

The adaptive control law $\dot{\hat{\beta}}$ is designed by the triangularity condition. The triangularity condition technique of the adaptive law is applied to estimate the unknown coefficient of the control signal β. The lower and upper bound known values of the uncertain parameter β is defined as β_{min} and β_{max}, which satisfies:

$$\beta \in \Omega_\beta = \{\beta: \beta_{min} \leq \beta \leq \beta_{max}\} \quad (3.62)$$

Hence, to guarantee $\left(\hat{\beta} - \beta\right)\left(\frac{1}{\mu}\dot{\hat{\beta}} - Z_4 u(t)\right) \leq 0$, a projection-type adaptive law $\dot{\hat{\beta}}$ is applied (Yang G et al., 2016):

$$\dot{\hat{\beta}} = \mathrm{Proj}\left(\mu\, Z_4 u(t)\right) = \begin{cases} 0 & \text{if } \hat{\beta} = \beta_{max} \text{ and } \mu\, Z_4 u(t) > 0 \\ 0 & \text{if } \hat{\beta} = \beta_{min} \text{ and } \mu\, Z_4 u(t) < 0 \\ \mu\, Z_4 u(t) & \text{otherwise} \end{cases} \quad (3.62)$$

According to the control signal $u(t)$ compact set, the $u(t)$ is a function of the state variables $X_s, \dot{X}_s, X_u, \dot{X}_u, P_L,\ X_v, \dot{X}_u, X_L, R_h$. To ensure the Gaussian basis function mapping, the constant

scaling factors of the operational hydraulic pressure C_h and the servovalve area C_v are applied as follows:

$$\zeta_1 \equiv X_s, \zeta_2 \equiv \dot{X}_s, \zeta_3 \equiv C_h P_L, \zeta_4 \equiv C_v A_v\ , \zeta_5 \equiv \breve{X}_u,\ \zeta_6 \equiv X_u, \zeta_7 \equiv \dot{X}_u,\ \zeta_8 \equiv X_L,\ \zeta_9 \equiv R_h$$
$$\forall\ \zeta = [\zeta_1, \zeta_2, \zeta_3, \zeta_4, \zeta_5, \zeta_6, \zeta_7, \zeta_8, \zeta_9] \in \Omega_\zeta \subset \mathbb{R}^9$$

Therefore, the RBFNN input variable m has nine input variables. The $\dot{V}$ becomes

$$\dot{V} = -c_1 Z_1^2 - c_2 Z_2^2 - c_3 Z_3^2 - c_4 Z_4^2 + Z_2\varepsilon_2 + Z_3\varepsilon_3 + Z_4\varepsilon_4 - \sigma_{\theta_2}\widetilde{W}_2\widehat{W}_2 - \sigma_{\theta_3}\widetilde{W}_3\widehat{W}_3 - \sigma_{\theta_4}\widetilde{W}_4\widehat{W}_4 \quad (3.63)$$

Applying inequality (Liu et Wang, 2012) for term $\sum_{i=2}^{4} Z_i\varepsilon_i$ in Equation (3.51):

$$|Z_i||\varepsilon_i| \leq |Z_i|\varepsilon_N \quad (3.64)$$

The RBFNN error function ε_1 is satisfied:

$$\|0, \varepsilon_2, \varepsilon_3, \varepsilon_4\| \leq \varepsilon_N \quad (3.65)$$

where ε_N is a designed positive error.

Applying Young's inequality (Duraiswamy et Chin, 2003):

$$|Z|\varepsilon_N \leq \frac{Z^2}{2\delta} + \delta\frac{{\varepsilon_N}^2}{2}, \delta > 0 \quad (3.66)$$

We apply the completing squares for each step (Jiang et Hill, 1999) as follows:

$$\sigma_{\theta_i}\widetilde{W}_i\widehat{W}_i = \sigma_{\theta_i}\left(\widehat{W}_i^T - W_i^T\right)\widehat{W}_i^T$$

$$= \frac{1}{2}\sigma_{\theta_i}\left|\widehat{W}_i^T - W_i^T\right|^2 + \frac{1}{2}\sigma_{\theta_i}\left|\widehat{W}_i\right|^2 - \frac{1}{2}\sigma_{\theta_i}|W_i|^2 \tag{3.67}$$

$$\dot{V} \leq \sum_{i=1}^{n}(-\Pi_i V_i + \Xi_i) \tag{3.68}$$

where the factors Π_i and Ξ_i are positive values with $\Pi_i := \min\left\{c_i, \frac{\sigma_{\theta_i}}{\eta_{max}\,\Gamma_i^{-1}}\right\}$, $\Xi_i = \frac{1}{2}\sigma_{\theta_i}|W_i|^2 - \frac{1}{2}\sigma_{\theta_i}\left|\widehat{W}_i^T - W_i^T\right|^2 + \delta\frac{{\varepsilon_N}^2}{2}$, and the η_{max} being the maximum eigenvalue of the positive definite matrix Γ.

By integrating the overall Lyapunov derivative function $\dot{V}$ in Equation (3.56), we obtain:

$$0 \leq V(t) \leq \frac{\Xi}{\Pi} + \left(V(0) - \frac{\Xi}{\Pi}\right)e^{-\Pi t} \tag{3.69}$$

where the Π and Ξ are the positive matrices.

The $\dot{Z}_i$ is thus bounded. Therefore, Z_i, goes to zero automatically when $t \to \infty$. In conclusion, the $\dot{Z}_i$ guarantee Barbalat's Lemma [36] and the $(Z_1, Z_2, Z_3, Z_4, W_2, W_3, W_4)$ are uniformly bounded.

3.3.3 Zero Dynamics' System

In Section 3.2, the fourth-order error systems Z_1, Z_2, Z_3, and Z_4 existed to design the adaptive neural networks' backstepping control system. On the other hand, there were nine state-space modelings for the active suspension system in Equation (3.18). The zero dynamics system can find the other five closed-loop systems of the ninth-order error system. In order to obtain the

control output $y = 0$, the minimization force transmits to the sprung mass can be equivalent, as follows:

$$F_{ZD} = A_p X_3 = K_s(X_1 - X_6) + C_s(X_2 - X_7) \tag{3.70}$$

In order to find zero dynamics closed-loop system of the other state-space system $X_5, X_6, X_7, X_8, \text{and } X_9$, the control output y and first and second output derivative functions $\dot{y}, \ddot{y}$ must be zeros, as follows:

$$y = X_1 - X_5 = 0. \tag{3.71}$$

Hence, $X_1 = X_5$

$$\dot{y} = \dot{X}_s - \dot{\dot{X}}_u = 0 \tag{3.72}$$

$$= X_2 + \left(\delta_0 + \kappa_{st}\psi(ST) + \kappa_{Rh}\phi(X_8)\right)(X_5 - X_6) = 0.$$

Then,

$$X_2 = -\left(\delta_0 + \kappa_{st}\psi(ST) + \kappa_{Rh}\phi(X_8)\right)(X_5 - X_6) \tag{3.73}$$

$$\begin{aligned}\ddot{y} = &-\frac{K_s}{m_s}(X_1 - X_6) - \frac{C_s}{m_s}(X_2 - X_7) + \frac{A_p}{m_s}X_3 \\ &+ \left(\kappa_{st}\frac{\partial\psi(ST)}{\partial ST}\dot{ST} + \kappa_{Rh}\frac{\partial\phi(X_8)}{\partial X_8}\dot{X_8}\right)(X_5 - X_6) \\ &+ \left(\delta_0 + \kappa_{st}\psi(ST)\right. \\ &+ \kappa_{Rh}\phi(X_8)\Big)\Big\{-\left(\delta_0 + \kappa_{st}\psi(ST) + \kappa_{Rh}\phi(X_8)\right)(X_5 - X_6) \\ &- X_7\Big\} = 0\end{aligned} \tag{3.74}$$

Substitute Equations (3.71)– (3.74) into state-space Equation (3.18). The zero dynamics' state-space modeling system becomes:

$$\dot{X}_5 = \dot{\tilde{X}}_u = -\left(\delta_0 + \kappa_{st}\psi(ST) + \kappa_{Rh}\phi(X_8)\right)(X_5 - X_6) \tag{3.75}$$

$$\dot{X}_6 = X_7$$

$$\dot{X}_7 = \frac{m_s}{m_u}\Bigg\{-\Bigg(\kappa_{st}\frac{\partial\psi(ST)}{\partial ST}\dot{ST} + \kappa_{Rh}\frac{\partial\phi(X_8)}{\partial X_8}\frac{K_t}{C_t}\left(X_8 - \kappa_w X_{us}\,(X_9 - 1)\right)\Bigg)(X_5 - X_6) - \varrho_f\{-\varrho_f(X_5 - X_6) - X_7\}\Bigg\} + \kappa_w X_{us} X_9 \tag{3.76}$$

$$X_8 = \begin{cases} -\frac{K_t}{C_t}\left(X_8 - \kappa_w X_{us}\,(X_9 - 1)\right) & \kappa_w^{-1} \geq X_9 \geq 1 \\ 0 & X_9 < 1 \end{cases} \tag{3.77}$$

$$\dot{X}_9 = \frac{-1}{\kappa_w(m_s + m_u)g}\Bigg\{K_t X_7 + \frac{C_t}{m_u}\Bigg(m_s\Bigg(\kappa_{st}\frac{\partial\psi(ST)}{\partial ST}\{-\varrho_f(X_5 - X_6) - X_7\} + \kappa_{Rh}\frac{\partial\phi(X_8)}{\partial X_8}\Bigg(-\frac{K_t}{C_t}\left(X_8 - \kappa_w X_{us}\,(X_9 - 1)\right)\Bigg)\Bigg)(X_5 - X_6) + m_s\varrho_f\{-\varrho_f(X_5 - X_6) - X_7\} + m_u\kappa_w X_{us}\,X_9\Bigg) - K_t\dot{r} - C_t\ddot{r}\Bigg\} \tag{3.78}$$

The nonlinear derivative functions of $\frac{\partial\psi(ST)}{\partial ST}$ and $\frac{\partial\phi(X_8)}{\partial X_8}$ satisfy:

$$\frac{\partial\psi(ST)}{\partial ST}=\begin{cases}4\left(\frac{ST-m_2}{m_1}\right)^3, & ST<m_2\\ 0, & m_3\geq ST\geq m_2\\ 4\left(\frac{ST-m_3}{m_4}\right)^3, & ST<m_3\end{cases} \tag{3.79}$$

$$\frac{\partial\phi(X_8)}{\partial X_8}=\begin{cases}4\left(\frac{X_8+n_2}{n_1}\right)^3 & \kappa_w^{-1}\geq R_h\geq 1\\ 0 & R_h<1\end{cases} \tag{3.80}$$

Furthermore, the X_{us} is a static tire deflection defined as:

$$X_{us}=\frac{(m_s+m_u)g}{K_t} \tag{3.81}$$

The positive nonlinear function ϱ_f is a function of the suspension travel and the tire liftoff as follows:

$$\varrho_f(ST,X_8)=\delta_0+\kappa_{st}\psi(ST)+\kappa_{Rh}\phi(X_8)>0 \tag{3.82}$$

Zero dynamic Lyapunov candidate is designed to guarantee its stability. Let us consider the linearized state-space model as:

$$\dot{X}=AX+\emptyset(t) \tag{3.82}$$

The Lyapunov candidate V_0 is suggested:

$$V_0=X^TPX \tag{3.82}$$

Therefore, the zero dynamics' Lyapunov candidate derivative function $\dot{V}_0$ is:

$$\begin{aligned}\dot{V}_0&=\dot{X}^TPX+X^TP\dot{X}\\&=X^T(A^TP+AP)X+2X^TP\emptyset(t)\end{aligned}$$

$$= -X^{T}QX + 2X^{T}P\emptyset(t) \tag{3.83}$$

In the previous equation $\dot{V}_0$, we applied the Young's inequality for the second term on the right side:

$$X^{T}P\emptyset(t) \leq \frac{1}{\xi_0}X^{T}PPX + \xi_0\emptyset^{T}(t)\emptyset(t), \text{ where } \xi_0 > 0 \tag{3.84}$$

Applying inequality, for term $\emptyset^{T}(t)\emptyset(t)$ in Equation (3.84):

$$\emptyset^{T}(t)\emptyset(t) \leq \|\emptyset\|_{\infty}^{2} \tag{3.85}$$

Therefore, the Lyapunov derivative function $\dot{V}_0$ becomes:

$$\dot{V}_0 \leq -X^{T}QX + \frac{1}{\xi_0}X^{T}PPX + \xi_0\|\emptyset\|_{\infty}^{2} \tag{3.86}$$

where ξ_0 is a positive tunable factor:

$$\dot{V}_0 \leq \left[-\lambda_{\min}(P^{-0.5}QP^{-0.5}) + \frac{1}{\xi_0}\lambda_{\max}P\right]V_0 + \xi_0\|\emptyset\|_{\infty}^{2} \tag{3.86}$$

$$\dot{V}_0 \leq \Pi_0 V_0 + \Xi_0 \tag{3.87}$$

By integrating the overall Lyapunov derivative function $\dot{V}_0$ into Equation (3.87), we obtain:

$$0 \leq V_0(t) \leq \frac{\Xi_0}{\Pi_0} + \left(V_0(0) - \frac{\Xi_0}{\Pi_0}\right)e^{-\Pi_0 t} \tag{3.88}$$

Hence, $\dot{X}_i$, $i = 5, \ldots, 9$ is uniformly bounded.

Finally, the flow pattern of the NAC design is sketched in Figure 3.4. There were four control paths, which combined together to build the NAC system.

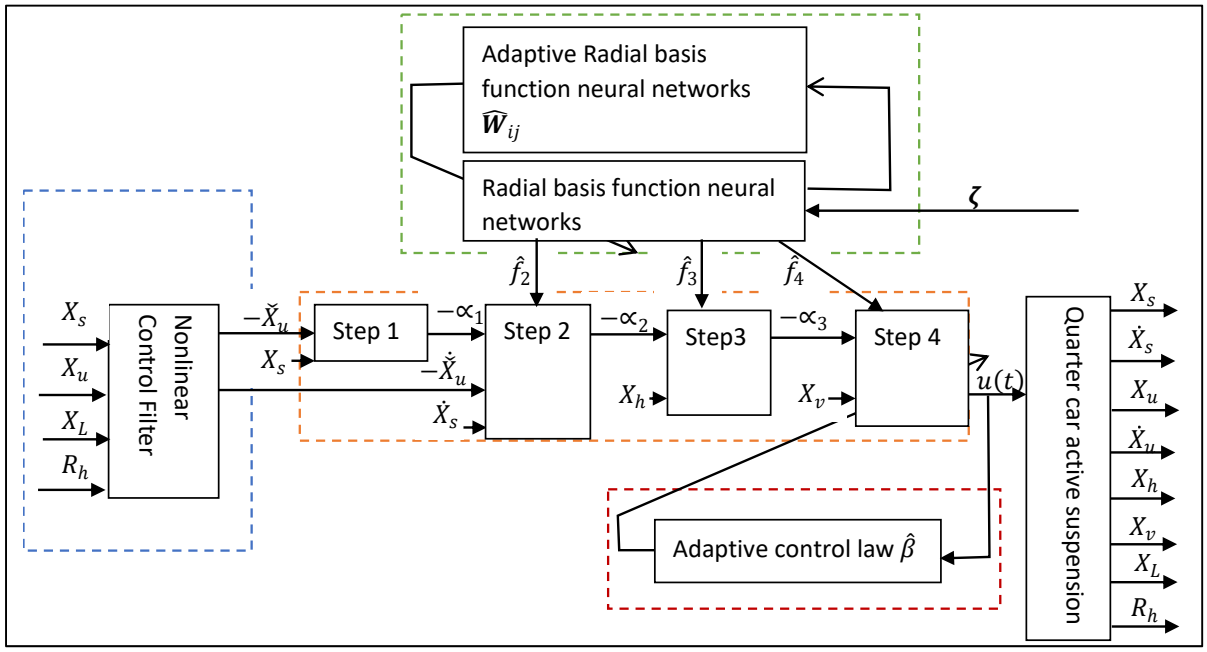

Figure 3.4 Sketch paths of the novel adaptive control 'NAC 'system

The path blue is the nonlinear control filter. The operational backstepping control system is shown in the orange bath. The unknown functions $f_2(\zeta), f_3(\zeta)$, and $f_4(\zeta)$ are approximated by using the green path for the radial basis function neural networks 'RBFNN ' system. The fourth path is the adaptive control law to estimate $\hat{\beta}$.

3.4 Simulation and Results' Discussion

To carry out the NAC control target successfully, we applied a comparative simulation between a filtered active suspension, an unfiltered active suspension, and passive suspension. By definition, the filtered active suspension was controlled by the novel adaptive control system (NAC), while for the unfiltered active suspension, the active suspension was only controlled by the adaptive neural networks control system (ANNC) with no coupling with the nonlinear control filter. To illustrate the comparative study, we considered several road perturbation designs and the active suspension simulation data. The simulation data of the active suspension system are presented in Table 3.2. The ANNC and the active suspension setup data were selected from the control sensitivity and the literature review. The nonlinear control parameters were manually adjusted.

Table 3.2 Simulation data values of the active suspension mathematical model

Data setup			
m_s = 290 Kg.	**m_u = 59 Kg**	**C_s = 1000 Ns/m**	**C_t = 800 N/m**
P_s = 10340000 N/m^2	$\beta_e = 7.995 \times 10^8$ N/m^2	K_s = 16812 N/m	K_t = 190000 N/m
C_d = 0.63	$V_t = 135.4 \times 10^{-13} m^3$	$A_p = 3.35 \times 10^{-4}$ m^2	$C_{tp} = 9.047 \times 10^{-13}$ m^5/(Ns)
$K_u = (2.72 - 3.33) \times 10^{-6}$ m2/mA		ρ =867 kg/m^3	τ_v=0.01 s
The NAC setup is shown below			
$c_1 = 200$	$c_2 = 201$	$c_3 = 203$	$c_4 = 202$
$\Gamma_2 = 27.773$	$\Gamma_3 = 88.33$	$\Gamma_4 = 117.01$	$\sigma_{\theta_2} = 0.000108$
$\sigma_{\theta_3} = 0.00095$	$\sigma_{\theta_4} = 0.0097$	$m_2 = -0.0375$	$m_3 = 0.035$
$m_1 = 0.02$	$m_4 = 0.045$	$n_1 = 0.004$	$n_2 = 0.00001$
$C_v = 1 \times 10^5$	$C_h = 1 \times 10^{-6}$	$\delta_0 = 1.27$	$m = 9$
$ST_c = -0.06$ m	$ST_E = 0.08$ m	$l = 5$	$\kappa_w = 0.7$

First, we analyzed a comparative study about control performance between the filtered active suspension NAC and another control system, which was investigated in [37]. In [37], a high gain observer-based integral sliding mode control 'HGO' was developed for quarter-vehicle active suspension. A bumpy road input design that was used in (Rath J et al., 2017) was applied

for the comparative study. Figure 5 shows the output nonlinear control filter $\check{X}_u$, the estimated sprung mass position $X_{s,}$ and their error. The maximum error of the NAC output was −0.009 m and its percentage of 10% at 1.2 s. In (Rath J et al., 2017), the results showed a high control performance that was less than 1% tracking position error.

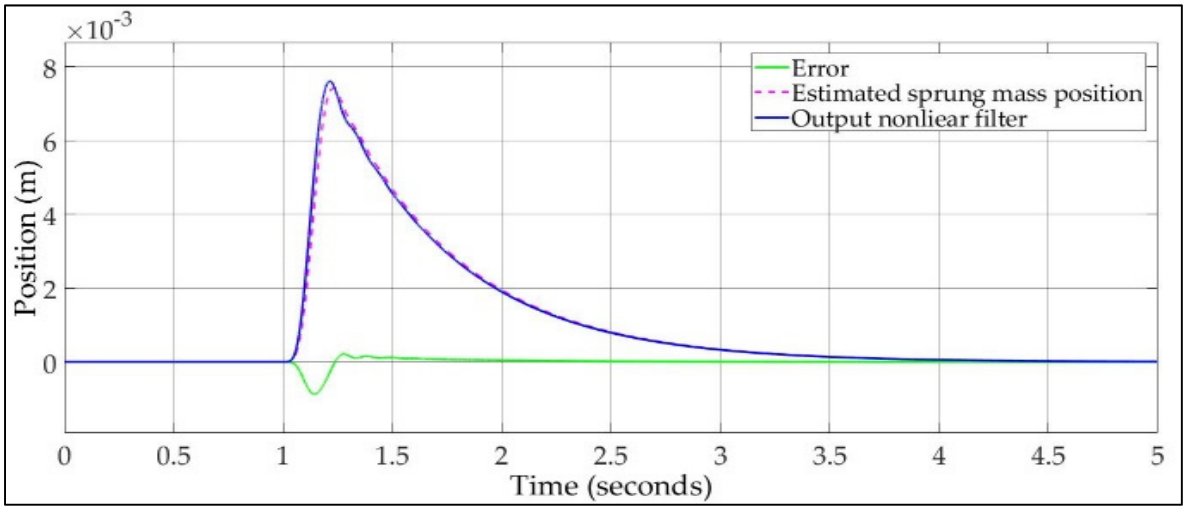

Figure 3.5 The system response of the NAC system

In Figure 6, the estimated sprung mass velocity $\dot{X}_s$, nonlinear filter output time derivative $\dot{\check{X}}_u$, and their error are displayed. The maximum absolute error was 0.01 m/s at 1.15 and 1.25 s. In (Rath J et al., 2017), the velocity tracking error was about 40 m/s at initial time and 18 m/s at 1.25 s. Table 3.3 explains the control performance for both of the NAC and the HGO.

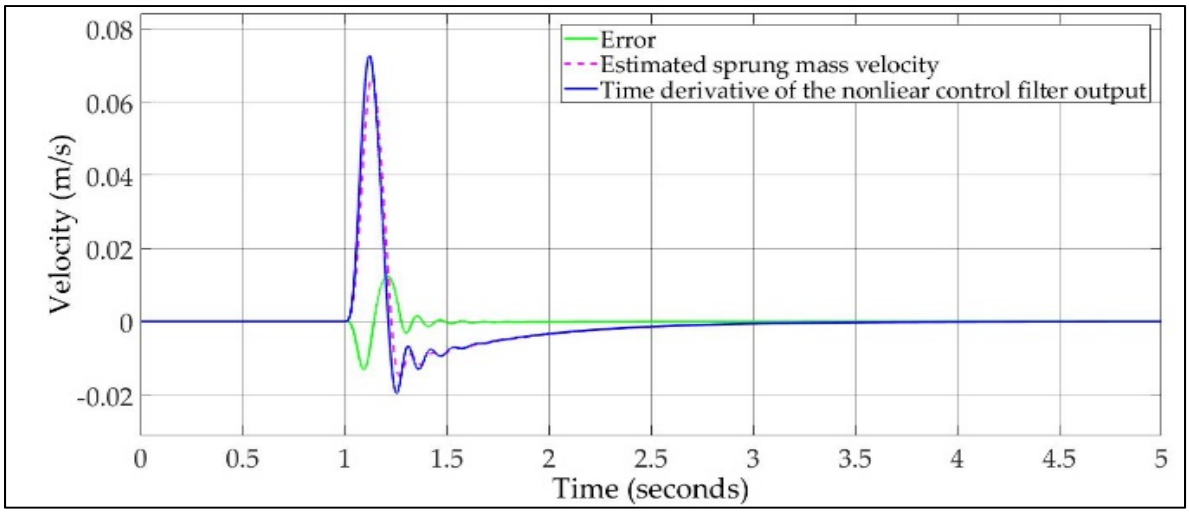

Figure 3.6 The estimated sprung mass velocity and time derivative of the output filter

Table 3.3 Control performance comparative study

	NAC	**HGO**	**Notes**
Maximum position error percentage %	10	>1	
Maximum velocity error percentage %	13	18	
Noise	No	Yes	There was a noise at initial time estimation

Even though the NAC had tiny tracking error in position compared with that in HGO, the NAC had better performance of tracking error velocity, as in Figure 3.6.

Second, we implemented four road design cases in this study, as follows.

Case 1: Road design excitation "bumpy input" had an amplitude of $a = 2.5\,cm$ and a frequency of $8\pi\ \frac{Rad}{S}$

$$X_r = \begin{cases} a(|1 - \cos 8\pi\, t|), & 0.5 \le t \le 0.75\ s \\ 0 & \text{otherwise} \end{cases} \tag{3.89}$$

This case has been used by many researchers in order to stimulate active and passive suspensions. In Figure 3.7, the maximum amplitudes of the dynamic tire force of the filtered active suspension, unfiltered active suspension, and passive suspension are smaller than the suspension weight by 68%, 48%, and 69%, respectively. Also, there was a 39% oscillation reduction in the filtered active suspension versus in the unfiltered active suspension. As result, all dynamic tire forces did not exceed the suspension weight; the filtered and the unfiltered active suspensions and passive suspension held on the road surface.

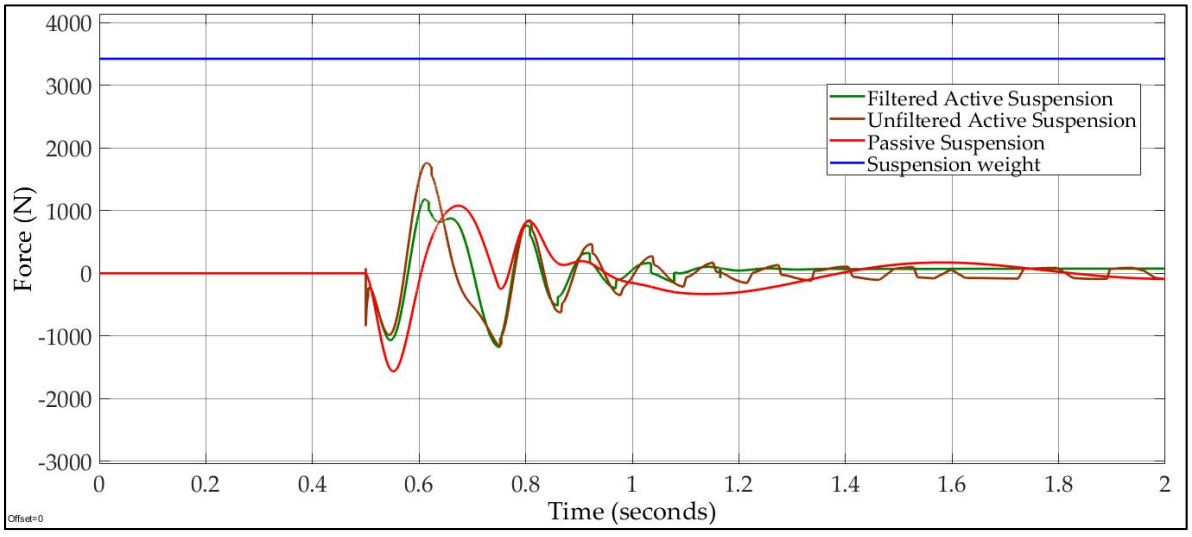

Figure 3.7 Road holding of Case 1

The comparative transient response of both filtered and unfiltered active suspensions are shown in Figure 3.8. Although the sprung mass position of filtered active suspension provided 80% road compensation, as compared to 99.6% with the unfiltered active suspension, the filtered active suspension smoothly decayed to the origin.

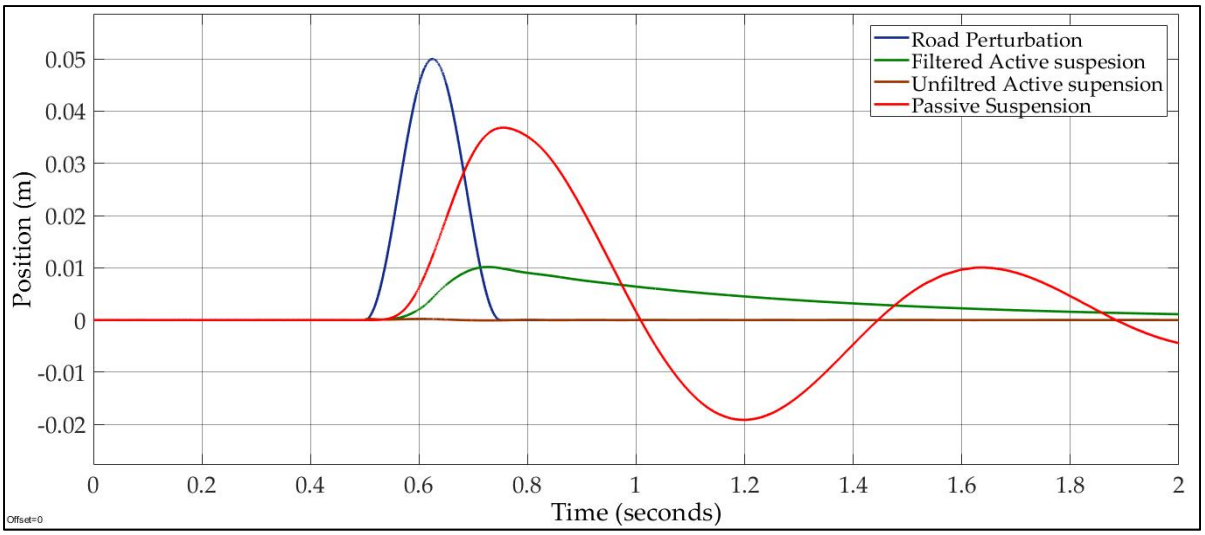

Figure 3.8 Sprung mass position of Case 1

Also, the filtered active suspension provided 75% improvement compensation of that in passive suspension. Therefore, passenger comfort was improved as compared to the case with the passive suspension. In Figure 3.9, there is an improvement in suspension travel for the filtered active suspension versus the unfiltered suspension, in which the maximum values of the filtered and unfiltered suspension travels were −0.052 m at 0.62 s and −0.059 m at 0.62, respectively. The filtered suspension travel oscillation was reduced by 85%, versus 50% with the passive suspension.

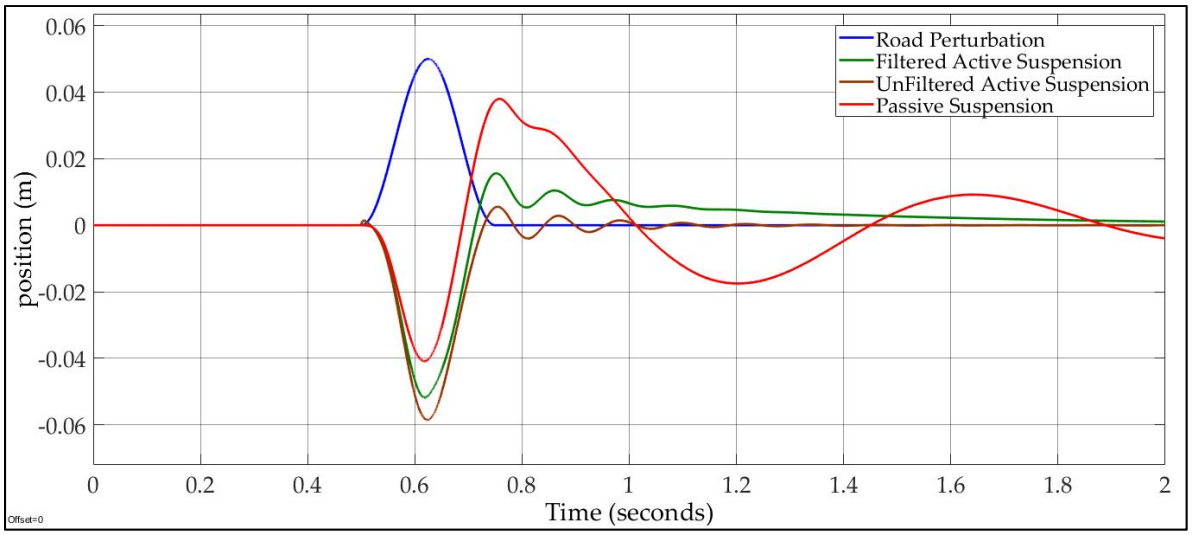

Figure 3.9 Suspension travel of Case 1

In conclusion, both filtered and unfiltered active suspensions obtained good transit responses. The filtered active suspension provided better suspension travel oscillation and a smaller suspension travel compared to the unfiltered active suspension. Also, the reduced suspension travel oscillation with the filtered active suspension was improved by 35% over what was seen in the passive suspension. The vehicle road stability could not be indicated by Case 1, which cannot generate tire liftoff phenomenon. Therefore, we introduced Case 2 for bumpy and pothole impulse road design. The frequency of this case was 16π rad/s, and its amplitude was the same as that in Case 1.

Case 2: Road design excitation "bumpy input" had an amplitude 2.5 cm and a frequency 16π rad/s.

$$X_r = \begin{cases} a(|1-\cos 16\pi\, t|), & 0.5 \le t \le 0.625 \text{ s} \\ -a(|1-\cos 16\pi\, t|), & 2.0 \le t \le 2.125 \text{ s} \\ 0 & \text{otherwise} \end{cases} \tag{3.90}$$

In Figure 3.10, the filtered active suspension kept tire contact with the road surface despite tiny periods of tire liftoff at 0.68 and (2.12–2.13) seconds. On the other hand, the dynamic tire force of the unfiltered active suspension was greater than the suspension weight at four time periods (0.56–0.61), (0.68–0.72), (2.12–2.18), and (2.24–2.26) seconds. The passive suspension dynamic tire force was higher than the weight suspension at (0.57–0.61) seconds' period.

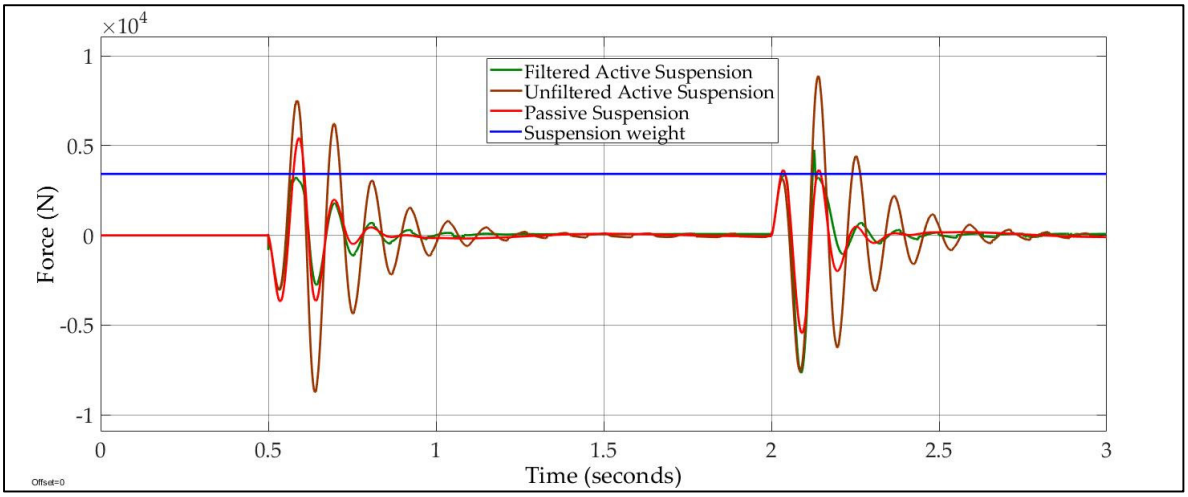

Figure 3.10 Dynamic tire forces vs. suspension weight of Case 2

Thus, both the unfiltered active suspension and passive suspension had tire liftoff phenomenon that may lose car–road stability. The sprung mass position of the filtered active suspension was compensated by 75% on bumpy road and by 88% on the pothole road, and smoothly decayed to origin, despite the road-holding compensation, as shown in Figure 11.

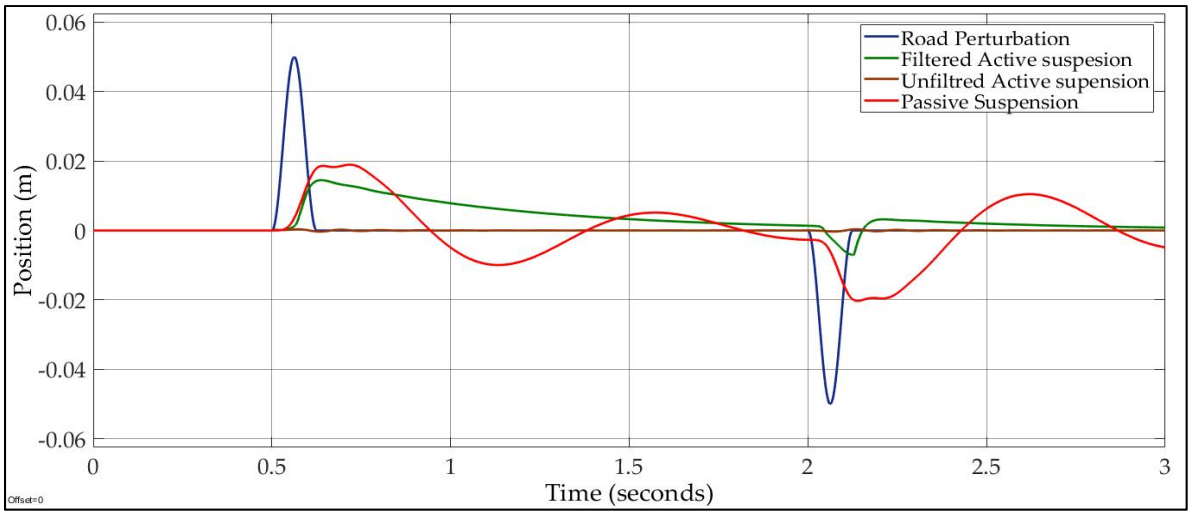

Figure 3.11 Sprung mass position of Case 2

On the other hand, the passive suspension was roughly compensated by about 60%. A frequency response estimation was applied to show the steady state of the filtered and unfiltered active suspension systems. The frequency response was estimated by using the Simulink tool frequency estimation with the sinusoidal road profile, as shown in Figure 12.

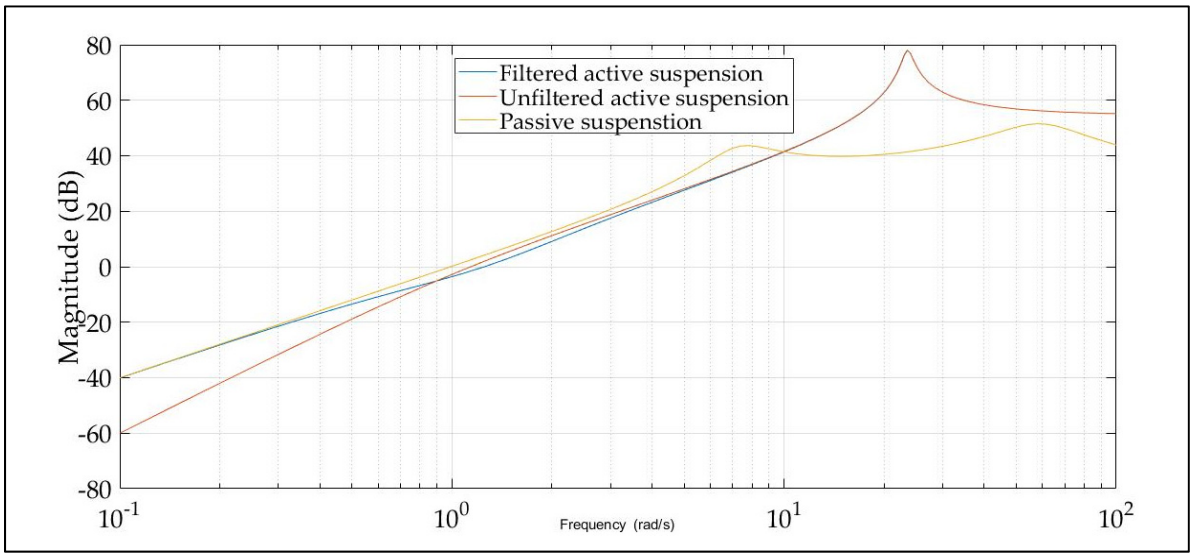

Figure 3.12 Sprung mass acceleration against the road frequency for both filtered and unfiltered active suspension systems of Case 2

The sensitive human frequency was about 18–50 rad/s [38]. In Figure 3.12, there is a compromise between road holding and passenger comfort, with the sprung mass acceleration of the filtered active suspension being higher at the sensitive human frequency domain. The reduction in suspension travel oscillation was also our control target. The suspension travel of the filtered active suspension oscillation was reduced by 87% as compared to 57% with the unfiltered active suspension, as can be seen in Figure 3.13.

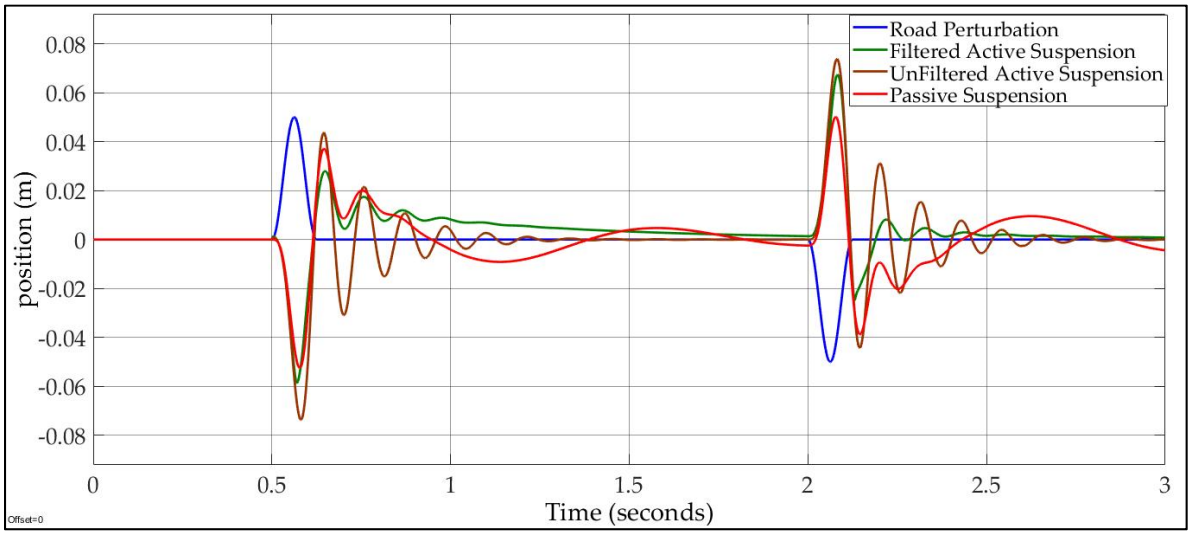

Figure 3.13 Suspension travel of Case 2

The benefits of reducing suspension travel oscillation include the possibility of preventing the suspension travel from reaching its limit, reducing wear in the mechanical suspension system, and saving energy.

The third control objective was to prevent hitting the suspension contraction limit. Hence, we proposed a suspension contraction limit ST_c of −6 cm. The bumpy road design had an amplitude of 3.5 cm and a frequency of 8π rad/s, as in the following case.

Case 3: The road excitation "bumpy input" had an amplitude 3.5 cm and a frequency 8π rad/s.

$$X_r = \begin{cases} a(|1 - \cos 8\pi t|), & 0.5 \leq t \leq 0.75 \text{ s} \\ 0 & \text{otherwise} \end{cases} \quad (3.91)$$

Although there was a trade-off between passenger comfort and suspension deflection, the sprung mass position was compensated by 72% and smoothly decayed to its original position, as shown in Figure 3.14.

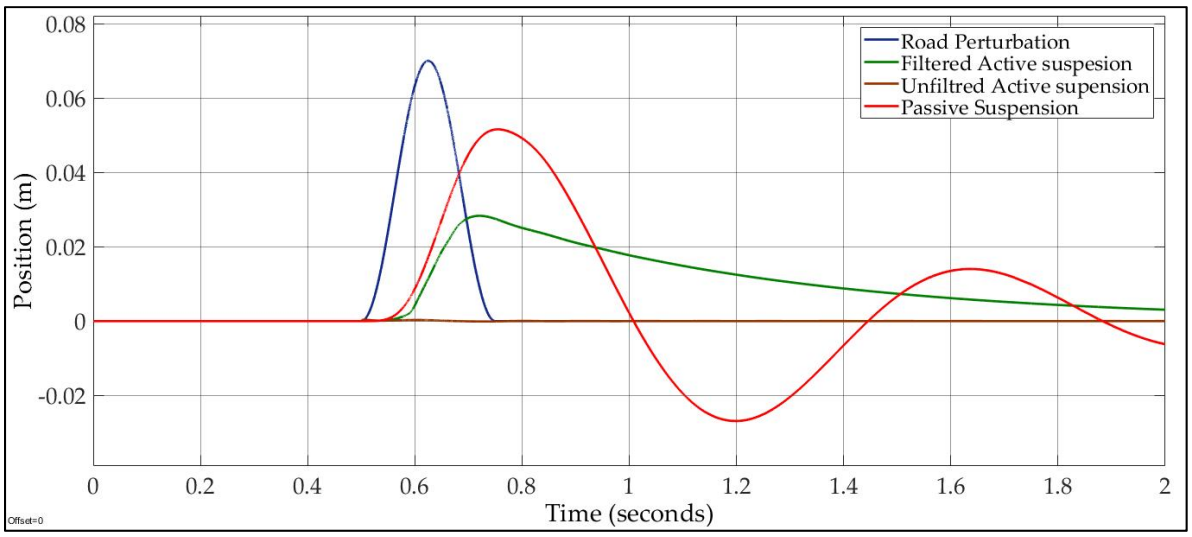

Figure 3.14 Sprung mass position of Case 3

The unfiltered active suspension provided the best compensation, of about 99%. In Figure 3.15, the suspension travel analysis is scoped to indicate the filtered active suspension performance.

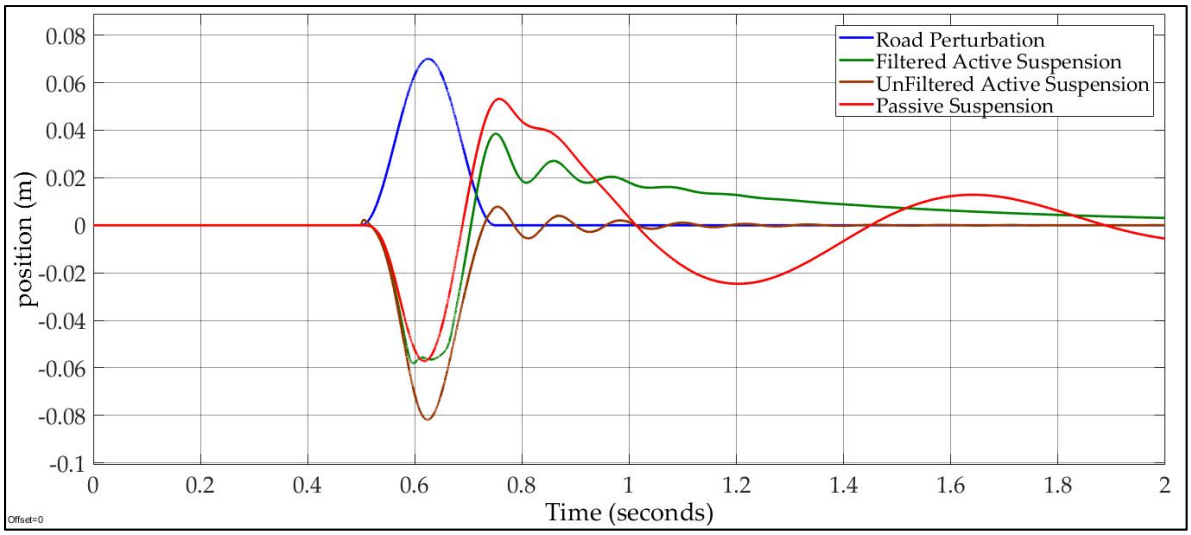

Figure 3.15 Suspension travel of Case 3

Accordingly, the filtered active suspension prevented hitting the suspension travel limit of −0.06 m, as shown in Figure 3.15; otherwise, the unfiltered active suspension hit the suspension travel limit at the (0.58–0.68) seconds' period.

Finally, the fourth control objective was the constrained suspension expansion. The suspension travel expansion limit was rarely addressed in previous studies. In particular, depending on how the vehicle is loaded, the suspension travel expansion limit may not be the same magnitude of the suspension travel contraction limit. The suspension travel expansion limit ST_E is 0.08 m. Therefore, we proposed a suspension travel expansion limit of 8 cm. In Case 4, there were a pothole road perturbation magnitude at −3.5 cm and the frequency of $8\pi\ rad/s$, as follows:

Case 4: The pothole perturbation road design had an amplitude of −4.0 cm and a frequency of 8π rad/s.

$$X_r = \begin{cases} a(|1 - \cos 8\pi t|) & 0.5 \le t \le 0.75 \\ 0 & \text{otherwise} \end{cases} \tag{3.92}$$

In Figure 3.16, the filtered active suspension compensation is 75.5% and 22.5% for the passive suspension.

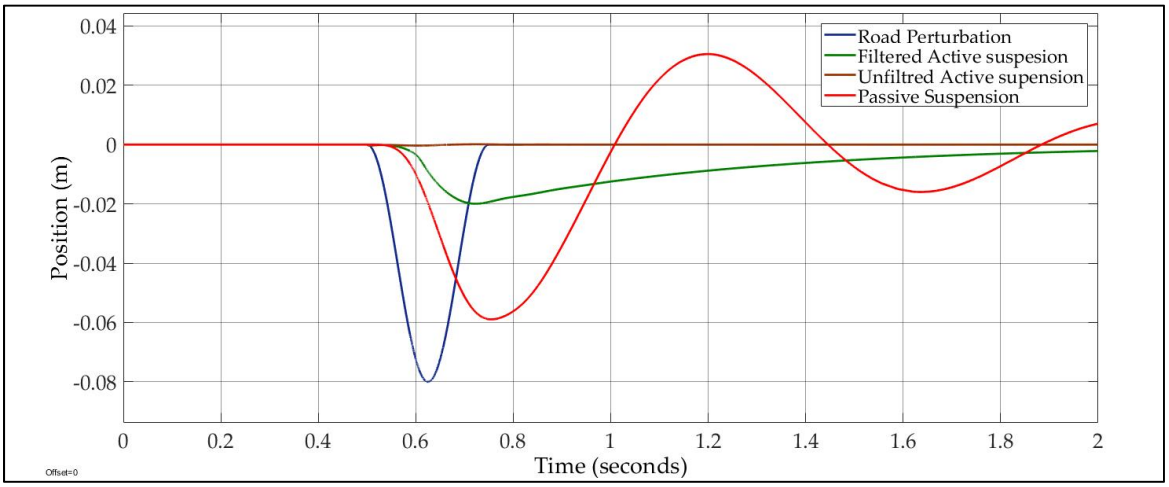

Figure 3.16 Sprung mass position of Case 4

Even though the unfiltered active suspension had the best control compensation of 99%, the unfiltered active suspension travel hit its limitation at about (0.6–0.67) seconds' period, as shown in Figure 3.17. The suspension travel of the filtered active suspension avoided hitting the suspension travel expansion limit ST_E of 0.08 m.

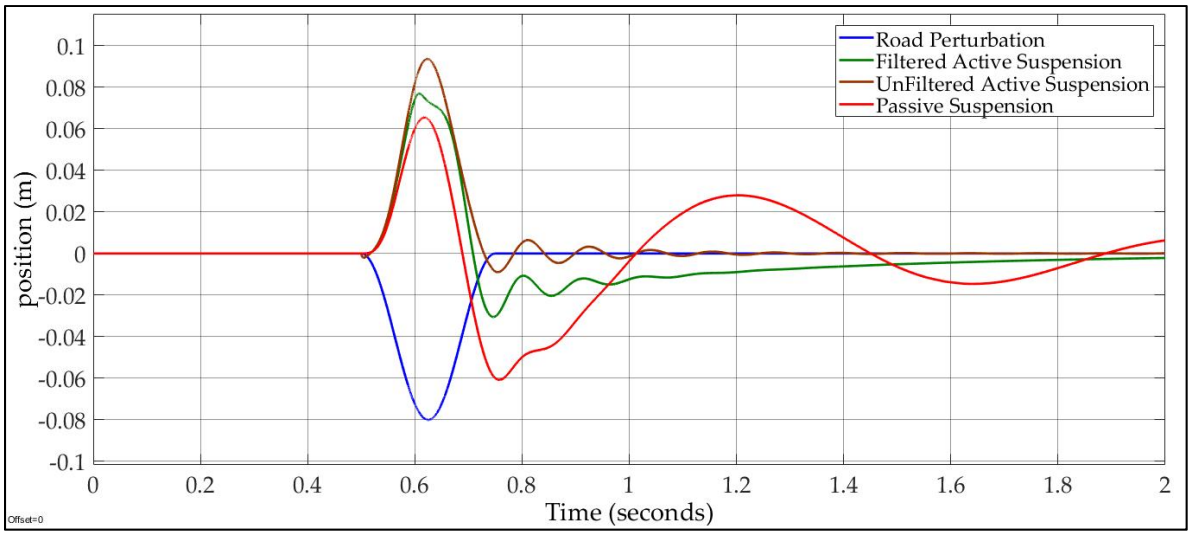

Figure 3.17 Suspension travel of Case 4

On the other hand, the suspension travel of the unfiltered active suspension hit the suspension travel limitation at the (0.06–0.062) seconds' period.

In conclusion, the sprung mass position of the filtered active suspension was smoothly compensated by 75% in Case 1. The suspension travel oscillations were reduced as compared to the unfiltered active suspension. In Case 2, the filtered active suspension provided both passenger comfort and road holding, as shown in Figure 10. On the other hand, the unfiltered active suspension and passive suspension failed to maintain road holding. The filtered active suspension prevented reaching the suspension travel limitations in both Case 3 and Case 4. Hence, the control objectives were successfully addressed.

3.5 Conclusions

This paper presented a novel adaptive neural networks' control system 'NAC' for a restricted active suspension in the presence of several road excitations and dynamic nonlinearity and uncertainty systems. A new control strategy was developed to explicitly address active suspension road holding and suspension travel limits. The NAC consisted of a nonlinear control filter combined with the adaptive neural networks' backstepping control system to

accommodate conflicts between passenger comfort, road holding, and suspension travel. Furthermore, the dynamic modeling system had inherent nonlinearities and uncertainties, which were overcome by the adaptive neural networks' backstepping control system. The results in Case 1 showed that the proposed controller provided a 35% better suspension oscillation than did the passive suspension. In Case 2, the proposed controller explicitly managed the trade-off between passenger comfort and road holding. The NAC provided 75% and 88% compensation based on the bumpy road and the pothole road inputs effects, respectively. In Cases 3 and 4, the suspension travel was displaced by the NAC within allowable displacements. Also, the NAC obtained 72% compensation in Case 3, 75% compensation in Case 4 and smooth decay, and a 22.5% reduced oscillation for the passive suspension.

CHAPTER 4

NONLINEAR CONTROL FILTERS-BASED ROBUST ADAPTIVE BACKSTEPPING OF RESTRICTED FULL CAR ELECTROHYDRAULIC ACTIVE SUSPENSION CONTROL SYSTEM

Amhmed Mohamed Al Aela [a], Jean-Pierre Kenné [b], Honorine Angue Mintsa [c]

[a, b] Department of Mechanical Engineering, École de technologie supérieure,
1100, Notre Dame Street West, Montreal, Quebec, Canada, H3C 1K3
[c] Department of Mechanical Engineering, Ecole polytechnique de Masuku (EPM), Masuku, Franceville, Haut-Ogooué, Gabon

Paper submitted for publication in *journal of Vehicle Dynamic Systems*, May 2021

Abstract

A Robust Adaptive Neural Networks Control (RANNC) is studied for multiple-input-multiple-output (MIMO) nonlinear filtered full car active suspension systems in the presence of both a stiff road perturbation and aerodynamic disturbances. The proposed control system can reduce sprung mass accelerations to improve passenger comfort and indemnify the tyre landing position to maintain road holding. Furthermore, the RANNC has the ability to avoid hitting the suspension travel limits. Several researchers have investigated several control laws for full car active suspension systems. Even though most of them have proved improvements in control performances, there was limited focusing on critical road conditions and aerodynamic perturbations. In this study, the proposed controller is designed to overcome a nonlinearity and uncertainty modelling system and improve active suspension performance. The novelty of this study is to introduce four dynamic tyre land modelling systems to prevent the happening of

dynamic tyre liftoff phenomena. In addition, an aerodynamic disturbance is also considered to guarantee the control robustness. The RANNC consists of adaptive neural networks backstepping control coupled with nonlinear control filters. Therefore, each wheel is monitored by a nonlinear control filter to design the desired control signals. The combinative robust adaptive radial basis function neural networks backstepping control systems can solve unmatched dynamics and deal with the unknown smooth functions. A zero dynamics system is also applied to guarantee system stability. The proposed controller has demonstrated that simulation provides an excellent performance compared with passive suspension and unfiltered active suspension systems.

Keywords: full car active suspension, Backstepping control, nonlinear control filter, adaptive neural networks, aerodynamic perturbations, zero dynamics

4.1 Introduction

A vehicle suspension system is one of the essential systems in the car structure. The car suspension acts as a bridge between a road surface and the vehicle body (sprung mass). The vehicle suspension system can be classified into three categories that are a passive suspension, semi-active suspension, and active suspension systems. The vehicle suspension system can improve ride comfort characteristics, handling performance, and vehicle manoeuvrability. The external perturbations could be generated from the unevenness of the road surface, aerodynamic disturbances, mechanical rotating unbalance of a wheel, a defect in the tyre, and suddenly barking (Gillespie, 1992). In general, improvements in passenger comfort can reduce the vehicle stability and suspension travel safety. In passive suspension, there is a fixed compromising between passenger comfort and road holding. On the other hand, the active suspension system can make a variable compromising between the suspension performance parameters. In this study, we focus on a full car electrohydraulic active suspension system. In general, the full car electrohydraulic active suspension consists of Springs, dampers, a sprung mass, unsprung masses, and an electrohydraulic servovalve system (EHSS). The EHSS can accurately respond to a vertical road disturbance and characterise fast delivery (Sallah, 2015).

Consequently, the active suspension is generally designed to manage conflicting requirements on the suspension performances. However, the active suspension system is known by dynamic nonlinearities and significant system uncertainties. Therefore, lots of studies were developed for active suspension systems to achieve improvements in control performance and robustness.

Several researchers have investigated control laws to provide ride comfort in electrohydraulic active suspension systems. Several control laws such as LQR and H_∞were investigated to improve passenger comfort for active suspension in Shirdel et al. (2010) and Pratheepa (2010) and Yamashita et al. (1994). In that studies, the results showed reduction in sprung mass accelerations. However, EHSS of the active suspension systems were not addressed. A PID was exploited based on a sprung mass position for a quarter car active suspension (Elbayomy et al., 2008). In general, linear controllers can improve ride comfort; however, the dynamic nonlinearities and uncertainties could degrade the control performances.

Many studies were developed nonlinear control laws to overcome dynamic nonlinearities for active suspension systems. An adaptive sliding mode control system was investigated to reduce a sprung mass acceleration in Alleyne et Hedrick (1995). An adaptive multi-surface sliding control system was developed for a non-autonomous quarter car active suspension in Chen et Huang (2005). A backstepping control approach was applied for a full car active suspension to improve the inherent tradeoff between ride comfort and suspension travel (Hu et Liu, 2008). The authors have determined an adaptive neural network control system to enhance passenger comfort and control performance (Al Aela et al., 2020a). In the previous studies, the results showed improvements in ride comfort. However, road holding was not addressed in that studies. Other studies were considered the suspension restrictions of both road holding and limited suspension travel. Adaptive backstepping control schemes were investigated for a quarter car active suspension by Sun et al. (2014) and Huang et al. (2015). However, their EHSS were not considered. In (Al Aela et al., 2020b), the authors have developed a novel adaptive control system (NAC) for nonlinear electrohydraulic active suspension. The results in that study showed that the control system achieves improving passenger comfort, maintaining road holding, avoiding hitting suspension travel limits. Even though the previous

study was showed improvements in the suspension performance, it was only determined for a quarter car active suspension system.

Lots of scientific articles were addressed full vehicle active suspension systems in Yuvapriya et al. (2020 and Wang et al. (2021) and Yatak et Sabin (2021) and Yin et al. (2021). Even though the previous studies were shown improvements in control performance, both the external aerodynamic disturbances and high-frequency road perturbations were not addressed for those studies. The effect of the sudden air turbulence may rock the vehicle. Moreover, a higher car speed and a road geometry can generate high-frequency road perturbation, exceeding the tyre liftoff phenomenon (Al Aela et al., 2020b). Therefore, the full car active suspension modelling system must be precise.

This study proposes a robust adaptive neural networks control system (RANNC) for MIMO nonlinear filtered active suspension system in the attendance of suspension restrictions, aerodynamic disturbances, and high-frequency road perturbations. In (Al Aela et al., 2020b), the authors have modelled new state variables for a quarter car active suspension system, called a dynamic landing tyre system. The dynamic landing tyre system was modelled to maintain road holding. In that study, a nonlinear control filter was designed to estimate the control reference trajectory. In (Al Aela et al., 2020a), the authors have considered a sprung mass external force disturbance to design the control law for a quarter car electrohydraulic active suspension system. Accordingly, an external aerodynamic disturbance is taken into consideration in this study. The external aerodynamic disturbances can be generated by a gusting wind or other vehicle air turbulence. Therefore, the novel feature of the proposed control system in this study uses a dynamic landing tyre modelling system and considers external aerodynamic disturbances for a full car active suspension system. Hence, four nonlinear control filters are implemented in this study to monitor the desired control signals. Therefore, both the dynamic landing tyre position and the suspension travel nonlinear functions are responsible to rapidly increase the filter's bandwidth, which is similar in (Al Aela et al., 2020b). As a result, the RANNC is introduced to asymptotically track the nonlinear control filters to stabilise all the vertical, roll, and pitch sprung mass dynamic systems. The RANNC

is an adaptive Radial Basis Function Neural Networks (RBFNN) backstepping control system coupled with the four nonlinear control filters. The zero dynamics system is also applied to asymptotically guarantee the stability of all non-interacting closed-loop systems. The main contributions of this study are:

1. A precise modelling system is employed for the RANNC design, including a nonlinear modelling system, external aerodynamic disturbances, high-frequency road perturbations, and dynamic landing tyre modelling systems.
2. The RANNC was designed to provide ride comfort while maintaining road holding and avoiding exceeding suspension travel limits.
3. The RANNC can reduce the suspension travel oscillations.
4. The RANNC was developed to overcome dynamic nonlinearities, parametric uncertainties, and uncertain linearities.

Finally, numerical simulation cases are provided to demonstrate the performance and robustness of the RANNC in getting a high control compensation, improving ride comfort, keeping road holding, preventing reaching suspension travel limits, decreasing suspension travel oscillations, and overcoming the system nonlinearities and uncertainties.

The remainder paper is organised as follows. Section 2 introduces the problem statement. In Section 3, control design is presented into two subsections: robust adaptive neural networks backstepping control design and zero dynamics system. Section 4 discusses the simulation of a comparative study between a filtered active suspension, an unfiltered active suspension, and a passive suspension. Section 5 is about the conclusion and future work.

4.2 Problem Statement

Several models of full car active suspension systems were applied to develop control strategies in the literature review. In this study, a nonlinear mathematical modelling system is modelled for full car active suspension, as shown in Figure 4.1.

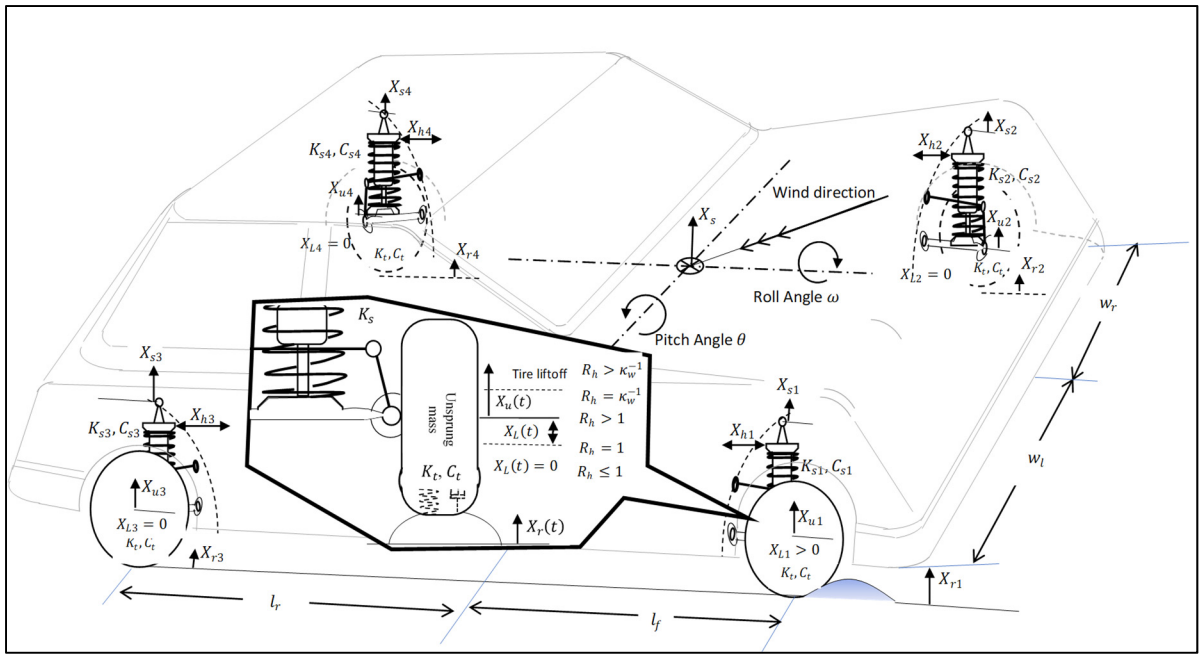

Figure 4.1 Full car active suspension modelling system

There are seven degrees of freedom corresponding to the sprung mass central gravity, such as heave direction, angular pitching direction, angular rolling direction, and the four unsprung mass vertical directions. In addition, the full car electrohydraulic active suspension system consists of a sprung mass, springs, dampers, four unsprung masses, four tyres, and four electrohydraulic servovalves (EHSS) systems. Besides, this study introduces novel modelling systems of both a dynamic landing tyre system and aerodynamic wind external disturbance for full car active suspension. The mathematical modelling system is analysed according to assumptions and dynamic force balances at the car centre gravity.

Let the vertical variables $(X_{s_i}, X_{u_i}, \dot{X}_{s_i}, \dot{X}_{u_i}, X_{h_i})$ of a quarter car i be a sprung mass position, an unsprung mass position, a sprung mass velocity, an unsprung mass velocity and the operational hydraulic pressure, respectively. Therefore, the vertical sprung mass acceleration of the vehicle's central gravity can be represented as follows.

$$\ddot{X}_{s_{cg}} = \frac{1}{M_s}\sum_{i=1}^{4}\left\{-K_{s_i}\left(X_{s_i} - X_{u_i}\right) - F_{ns_i} - C_{s_i}\left(\dot{X}_{s_i} - \dot{X}_{u_i}\right) - C_{ns_i}(t)\left(\dot{X}_{s_i} - \dot{X}_{u_i}\right) - A_{p_i}X_{h_i} + F_{a_i}(t)\right\}, \qquad i = 1,2,3,4 \tag{4.1}$$

where the M_s is the sprung mass (vehicle body), K_{s_i} is the suspension spring stiffness of quarter car i, C_{s_i} and $C_{ns_i}(t)$ are linear and time varying damper coefficients, A_{p_i} a projected position area of hydraulic actuator i. $F_{a_i}(t)$ is a reaction force of aerodynamic perturbation acting on unsprung mass i.

The aerodynamic reaction force $F_{a_i}(t)$ could be produced due to several factors, such as a gusting wind and/or a turbulence wind (Baker, 1991). The turbulence wind can occur the vehicle vibrating, especially when a heavy vehicle passes the car in the opposite direction. Thus, the sudden air turbulence may degrade the control performance. In Appendix B, the aerodynamic forces acting on four wheels road vehicle are described.

The nonlinear spring force F_{ns_i} is mainly due to a limit stop block (Kim et Ro,1998), The F_{ns_i} can be modelled as follows.

$$F_{ns_i} = \begin{cases} 0 & \text{if } \left(X_{s_i} - X_{u_i}\right) \le 0.9 * ST_{C_i} \\ K_{ns}\left(X_{s_i} - X_{u_i}\right)^3 & \text{otherwise} \end{cases} \tag{4.2}$$

where K_{ns} is a nonlinear spring coefficient, ST_{C_i} is a suspension contraction limitation of a quarter car i.

The car body pitch angular acceleration $\ddot{\theta}$ and roll angular acceleration $\ddot{\omega}$ are defined, as follows.

$$\sum \overset{\curvearrowleft}{M_o} = 0$$

$$\ddot{\theta} = \frac{1}{I_\theta}\Bigg\{ l_f \sum_{i=1}^{2} \Big(K_{s_i}(X_{s_i} - X_{u_i}) + F_{ns_i} + C_{s_i}(X_{s_i} - X_{u_i}) + C_{ns_i}(t)(\dot{X}_{s_i} - \dot{X}_{u_i}) - A_{p_i} X_{h_i} + F_{a_i}(t) \Big) - l_r \sum_{i=3}^{4} \Big(K_{s_i}(X_{s_i} - X_{u_i}) + F_{ns_i} + (X_{s_i} - X_{u_i}) + C_{ns_i}(t)(\dot{X}_{s_i} - \dot{X}_{u_i}) - A_{p_i} X_{h_i} + F_{a_i}(t) \Big) \Bigg\}, \qquad i = 1,2,3,4 \tag{4.3}$$

$$\ddot{\omega} = \frac{1}{I_\omega}\Bigg\{ -w_l \sum_{i=1,3} \Big(K_{s_i}(X_{s_i} - X_{u_i}) + F_{ns_i} + C_{s_i}(\dot{X}_{s_i} - \dot{X}_{u_i}) + C_{ns_i}(t)(\dot{X}_{s_i} - \dot{X}_{u_i}) - A_{p_i} X_{h_i} + F_{a_i}(t) \Big) + w_r \sum_{i=2,4} \Big(K_{s_i}(X_{s_i} - X_{u_i}) + F_{ns_i} + C_{s_i}(\dot{X}_{s_i} - \dot{X}_{u_i}) + C_{ns_i}(t)(\dot{X}_{s_i} - \dot{X}_{u_i}) - A_{p_i} X_{h_i} + F_{a_i}(t) \Big) \Bigg\}, \qquad i = 1,2,3,4 \tag{4.4}$$

where I_θ and I_ω are both a pitching and roll moment of inertia ($kg\, m^2$), l_f is a car length from front wheels to the centre of gravity, l_r is a car length from a rear wheel to the centre of gravity, w_l is a car width from lift wheels to the centre of gravity. w_r is a car width from right wheels to the centre of gravity.

The dynamic unsprung mass force acting on a wheel j with tyre liftoff phenomena can be modelled as in Pusadkar et al. (2019).

$$m_{uj}\, \ddot{X}_{uj} = \begin{cases} -F_j - K_t(X_{uj} - X_{rj}) - C_t(\dot{X}_{uj} - \dot{X_{rj}}), & \text{if } R_{h_j} \le 1 \\ -F_j\,, & \text{otherwise} \end{cases}, \qquad j = 1, \dots, 4 \tag{4.5}$$

where F_j is a dynamic sprung mass force at wheel j, K_t is a tyre stiffness, C_t is a tyre damping, m_{uj} is an unsprung mass j, m_{s_j} is the sprung mass equivalence at quarter car j, g is the

acceleration gravity. $X_{rj}$and $\dot{X}_{rj}$ are the vertical road position and velocity. The F_j can be presented as follows.

$$F_i = -K_{s_i}(X_{s_i} - X_{u_i}) - F_{ns_i} - C_{s_i}(\dot{X}_{s_i} - \dot{X}_{u_i}) - C_{ns_i}(t)(\dot{X}_{s_i} - \dot{X}_{u_i}) - A_{p_i}X_{h_i} + F_{a_i}(t)\,, \quad i = 1,2,3,4 \tag{4.6}$$

Road holding quality can provide safe driving, especially during braking, cornering, and swerving. Therefore, the authors have developed a dynamic tyre landing system for a quarter car active suspension (Al Aela et al., 2020b). Therefore, the full car dynamic tyre landing system $\left(\dot{X}_{L_j}, \dot{R}_{h_j}\right)$ can be modeled as the following aspects.

$$\dot{X}_{L_j} = \begin{cases} 0 & \text{if} \quad R_{h_j} < 1 \\ \dfrac{K_t}{C_t}\left(X_{L_j} + \dfrac{\kappa_w\left(m_{s_j} + m_{u_j}\right)g}{K_t}\left(R_{h_j} - 1\right)\right) & \text{if } \kappa_w^{-1} \geq R_{h_j} \geq 1 \end{cases} \tag{4.7}$$

where $j = 1, \ldots, 4$, X_{L_j} is a tyre landing position, R_{h_j} is a road holding factor, κ_w is an adjustable road holding factor of wheel j.

In the dynamic tyre landing equations, the factor κ_w^{-1} is used to adjust the minimum trust weigh that subjects on the road surface. Hence, the R_h should not reach κ_w^{-1}. The equivalent sprung mass m_{s_j} of a quarter car active suspension j can be represented as shown below.

$$\begin{aligned} m_{s_1} &= \frac{1}{2}\frac{\sqrt{l_r^2 + w_r^2}}{\sqrt{l_r^2 + w_r^2} + \sqrt{l_f^2 + w_l^2}}M_s; \quad m_{s_2} = \frac{1}{2}\frac{\sqrt{l_r^2 + w_l^2}}{\sqrt{l_r^2 + w_l^2} + \sqrt{l_f^2 + w_r^2}}M_s \\ m_{s_3} &= \frac{1}{2}\frac{\sqrt{l_f^2 + w_r^2}}{\sqrt{l_f^2 + w_r^2} + \sqrt{l_r^2 + w_l^2}}M_s; \quad m_{s_4} = \frac{1}{2}\frac{\sqrt{l_f^2 + w_l^2}}{\sqrt{l_f^2 + w_l^2} + \sqrt{l_r^2 + w_r^2}}M_s \end{aligned} \tag{4.8}$$

The road holding gradient can represented as follows.

$$\dot{R}_{h_i} = \frac{1}{\kappa_{w,i} W_{us,i}} \left(-\frac{C_t}{m_{u_i}} \left(F_i + K_t \left(X_{u_i} - X_{r_i} \right) \right) + \left(K_t - \frac{C_t^2}{m_{u_i}} \right) \left(\dot{X}_{u_i} - \dot{X}_{r_i} \right) - C_t \ddot{X}_{r_i} \right), \qquad R_{h_i} \leq \kappa_w^{-1}{}_i \tag{4.9}$$

where $i = 1,2,3,4$, $W_{us,i}$ is a quarter car i weight, $W_{us,i} = \left(m_{s_i} + m_{u_i} \right) g$

In Kilicaslan S (2018), the hydraulic servovalve system is modelled as follows.

$$\frac{V_t}{2\beta_e} \dot{P}_{L_j} = C_d A_{v_j} \sqrt{\frac{P_s - P_{L_j} \, sgn(A_{v_j})}{\rho_h}} - A_{p_j} \left(X_{s_j} - X_{u_j} \right) - C_{tp} P_{L_j} \tag{4.10}$$

where $j = 1, \dots, 4$, P_{L_j} is an operational hydraulic pressure variable, A_{v_j} is a opening spool area variable, V_t is a hydraulic actuator volume parameter, β_e is an effective bulk pressure modulus, C_d is low discharge coefficient, $C_{tp}$is a hydraulic leakage coefficient, P_s is a hydraulic pressure supply parameter.

The servovalve dynamic equation can be presented as in Angue-Mintsa et al. (2012).

$$\dot{A}_{v_j} = \frac{1}{\tau_v} \left(-A_{v_j} + K_u u_j(t) \right) \tag{4.11}$$

where $u_j(t)$ is a control signal of quarter car j, τ_v is a servovalve time constant, K_u is a servovalue amplifier gain, $j = 1, \dots, 4$.

Therefore, the sprung mass accelerations of four quarter care active suspension systems $\left(\ddot{X}_{s1}, \ddot{X}_{s2}, \ddot{X}_{s3}, \ddot{X}_{s4} \right)$ are developed according to assumptions of a tiny angular pitch position, a tiny angular roll position, and neglecting the carioles effects as the following forms.

$$\begin{aligned}
\ddot{X}_{s1} &= \ddot{X}_{s_{cg}} + l_f\ddot{\theta} + w_l\ddot{\omega} \\
\ddot{X}_{s2} &= \ddot{X}_{s_{cg}} + l_f\ddot{\theta} - w_l\ddot{\omega} \\
\ddot{X}_{s3} &= \ddot{X}_{s_{cg}} - l_f\ddot{\theta} + w_l\ddot{\omega} \\
\ddot{X}_{s4} &= \ddot{X}_{s_{cg}} - l_f\ddot{\theta} - w_l\ddot{\omega}
\end{aligned} \tag{4.12}$$

Substitute equations (4.1), (4.3) and (4.4) into equations (4.12)

$$\ddot{X}_{s1} = \left(\frac{-1}{M_s} + \frac{l_f^2}{I_\theta} - \frac{w_l^2}{I_\omega}\right)F_1 + \left(\frac{-1}{M_s} + \frac{l_f^2}{I_\theta} + \frac{w_l w_r}{I_\omega}\right)F_2 + \left(\frac{-1}{M_s} + \frac{-l_f l_r}{I_\theta} + \frac{-w_l^2}{I_\omega}\right)F_3 + \left(\frac{-1}{M_s} + \frac{-l_f l_r}{I_\theta} + \frac{w_l w_r}{I_\omega}\right)F_4 \tag{4.13}$$

$$\ddot{X}_{s2} = \left(\frac{-1}{M_s} + \frac{l_f^2}{I_\theta} + \frac{w_l^2}{I_\omega}\right)F_1 + \left(\frac{-1}{M_s} + \frac{l_f^2}{I_\theta} - \frac{w_l w_r}{I_\omega}\right)F_2 + \left(\frac{-1}{M_s} + \frac{-l_f l_r}{I_\theta} + \frac{w_l^2}{I_\omega}\right)F_3 + \left(\frac{-1}{M_s} + \frac{-l_f l_r}{I_\theta} - \frac{w_l w_r}{I_\omega}\right)F_4 \tag{4.14}$$

$$\ddot{X}_{s3} = \left(\frac{-1}{M_s} - \frac{l_f^2}{I_\theta} - \frac{w_l^2}{I_\omega}\right)F_1 + \left(\frac{-1}{M_s} - \frac{l_f^2}{I_\theta} + \frac{w_l w_r}{I_\omega}\right)F_2 + \left(\frac{-1}{M_s} + \frac{l_f l_r}{I_\theta} + \frac{-w_l^2}{I_\omega}\right)F_3 + \left(\frac{-1}{M_s} + \frac{l_f l_r}{I_\theta} + \frac{w_l w_r}{I_\omega}\right)F_4 \tag{4.15}$$

$$\ddot{X}_{s4} = \left(\frac{-1}{M_s} - \frac{l_f^2}{I_\theta} + \frac{w_l^2}{I_\omega}\right)F_1 + \left(\frac{-1}{M_s} - \frac{l_f^2}{I_\theta} - \frac{w_l w_r}{I_\omega}\right)F_2 + \left(\frac{-1}{M_s} + \frac{l_f l_r}{I_\theta} + \frac{w_l^2}{I_\omega}\right)F_3 + \left(\frac{-1}{M_s} + \frac{l_f l_r}{I_\theta} - \frac{w_l w_r}{I_\omega}\right)F_4 \tag{4.16}$$

Let the equivalent inverse mass quantities between brackets be a symbol $\mathcal{M}_{ij}^{-1}$, and substitute equation (4.6) into equations (4.13)-(4.16) as follows.

$$\ddot{X}_{s1} = \sum_{j=1,}^{4} \mathcal{M}_{1j}^{-1} \left\{ K_{s_j} \left(X_{s_j} - X_{u_j} \right) + F_{ns_j} + C_{s_j} \left(\dot{X}_{s_j} - \dot{X}_{u_j} \right) + C_{ns_j}(t) \left(\dot{X}_{s_j} - \dot{X}_{u_j} \right) - A_{p_j} X_{h_j} + F_{a_j}(t) \right\} \quad (4.17)$$

$$\ddot{X}_{s2} = \sum_{j=1,}^{4} \mathcal{M}_{2j}^{-1} \left\{ K_{s_j} \left(X_{s_j} - X_{u_j} \right) + F_{ns_j} + C_{s_j} \left(\dot{X}_{s_j} - \dot{X}_{u_j} \right) + C_{ns_j}(t) \left(\dot{X}_{s_j} - \dot{X}_{u_j} \right) - A_{p_j} X_{h_j} + F_{a_j}(t) \right\} \quad (4.18)$$

$$\ddot{X}_{s3} = \sum_{j=1,}^{4} \mathcal{M}_{3j}^{-1} \left\{ K_{s_j} \left(X_{s_j} - X_{u_j} \right) + F_{ns_j} + C_{s_j} \left(\dot{X}_{s_j} - \dot{X}_{u_j} \right) + C_{ns_j}(t) \left(\dot{X}_{s_j} - \dot{X}_{u_j} \right) - A_{p_j} X_{h_j} + F_{a_j}(t) \right\} \quad (4.19)$$

$$\ddot{X}_{s4} = \sum_{j=1,}^{4} \mathcal{M}_{4j}^{-1} \left\{ K_{s_j} \left(X_{s_j} - X_{u_j} \right) + F_{ns_j} + C_{s_j} \left(\dot{X}_{s_j} - \dot{X}_{u_j} \right) + C_{ns_j}(t) \left(\dot{X}_{s_j} - \dot{X}_{u_j} \right) - A_{p_j} X_{h_j} + F_{a_j}(t) \right\} \quad (4.20)$$

In (Al Aela et al, 2020b), the authors have developed a nonlinear control filter to design the proposed control system's reference trajectories to improve the tradeoff between ride comfort and road holding and suspension travel limits. Therefore, four nonlinear control filters are introduced for the four wheels. The input filter of wheel j is the unsprung mass position X_{u_j} of the wheel j. The effective bandwidth of the nonlinear control filter $\dddot{\breve{X}}_{u_j}$ is nonlinear functions of both a suspension travel nonlinear function $\psi(ST_j)$ and a tyre landing nonlinear function $\phi\left(X_{L_j}\right)$. Hence, the nonlinear control filter can be estimated as the following form.

$$\dddot{\breve{X}}_{u_j} = -\left(\delta_{0_j} + \kappa_{st} \psi(ST_j) + \kappa_{Rh} \phi\left(X_{L_j}\right) \right) \left(\ddot{\breve{X}}_{u_j} - X_{u_j} \right) \quad (4.21)$$

where $j = 1, \dots, 4$, ST is a suspension travel ($ST = X_s - X_u$) , $\check{X}_u$ is a nonlinear control filter output, κ_{st} and κ_{Rh} are positive constants, δ_0 is chosen a positive constant to satisfy the ride comfort requirements.

The nonlinear function $\psi(ST_j)$ satisfies as follows.

$$\psi(ST_j) = \begin{cases} \left(\frac{ST_j - m_2}{m_1}\right)^4, & \text{if} \quad ST_j < m_2 \\ 0, & \text{if } m_3 \geq ST_j \geq m_2 \\ \left(\frac{ST_j - m_3}{m_4}\right)^4, & \text{if} \quad ST_j > m_3 \end{cases} \tag{4.22}$$

where $j = 1, \dots, 4$, m_1, m_2, m_3, m_4 are designed constants.

If ($ST_j < m_2$ or $ST_j > m_3$), the nonlinear function $\psi(ST_j)$ is rapidly activated; else, $\psi(ST_j) = 0$. The $\phi(X_L)$ can be also evaluated as follows.

$$\phi\left(X_{L_j}\right) = \begin{cases} \left(\frac{X_{L_j} + n_2}{n_1}\right)^4, & \text{if } \kappa_w^{-1} \geq R_{h_j} \geq 1 \\ 0, & \text{if} \quad R_{h_j} < 1 \end{cases} \tag{4.23}$$

where n_1 and n_2 are positive constants.

If $\kappa_w^{-1} \geq R_{h_j} \geq 1$, The landing tyre nonlinear function $\phi(X_L)$ is also rapidly activated; elseif $R_{h_j} < 1$, $\phi(X_L) = 0$. If both the nonlinear functions $\left(\psi(ST_j), \phi\left(X_{L_j}\right)\right)$ are inactive, the nonlinear control filter turns into a linear control filter with the bandwidth δ_0.

4.3 Control design

In (Al Aela et al., 2020a, 2020b), the authors have introduced the sprung mass velocity, sprung mass acceleration, the hydraulic actuator, and servovalve dynamic systems as SISO state-space

modelling system for the adaptive neural networks backstepping control design. In this study, a MIMO state-space modelling system is proposed for robust adaptive neural networks backstepping control system (RANNC). The mathematical modelling can be described as a MIMO semi-strict-feedback system as follows.

The sprung mass acceleration equations (4.16)-(4.19) can be represented in terms of unknown functions.

$$\begin{aligned}\ddot{X}_{s1} &= C_h X_{h_1} + f_{s1}(\boldsymbol{X}, t) + D_1(t)\\ \ddot{X}_{s2} &= C_h X_{h_2} + f_{s2}(\boldsymbol{X}, t) + D_2(t)\\ \ddot{X}_{s3} &= C_h X_{h_3} + f_{s3}(\boldsymbol{X}, t) + D_3(t)\\ \ddot{X}_{s4} &= C_h X_{h_4} + f_{s4}(\boldsymbol{X}, t) + D_4(t)\end{aligned} \tag{4.24}$$

where $D_i(t)$ is the effect of the aerodynamic reaction forces acting on m_{s_i}, C_h is a reduced positive factor, $D_i(t) = \mathcal{M}_{i1}F_{a_1}(t) + \mathcal{M}_{i2}F_{a_2}(t) + \mathcal{M}_{i3}F_{a_3}(t) + \mathcal{M}_{i4}F_{a_4}(t)$, $\boldsymbol{X}$ is a reduced state vector, $\boldsymbol{X} = \big(X_{s_1}, X_{u_1}, X_{s_2}, X_{u_2}, X_{s_3}, X_{u_3},\ X_{s_4}, X_{u_4}, \dot{X}_{s_1}, \dot{X}_{u_1}, \dot{X}_{s_2}, \dot{X}_{u_2}, \dot{X}_{s_3}\ \dot{X}_{u_3},\ \dot{X}_{s_4}, \dot{X}_{u_4}, X_{h_1}, X_{h_2}, X_{h_3}, X_{h_4},\ X_{v_1}, X_{v_2},\ X_{v_3}, X_{v_4}\big)$.

The operational pressure gradient $\dot{X}_h$ can be modelled from equations (4.10) and (4.11) as follows.

$$\begin{aligned}\dot{X}_{h1} &= C_v X_{v_1} + f_{h1}(\boldsymbol{X}, t)\\ \dot{X}_{h2} &= C_v X_{v_2} + f_{h2}(\boldsymbol{X}, t)\\ \dot{X}_{h3} &= C_v X_{v_3} + f_{h3}(\boldsymbol{X}, t)\\ \dot{X}_{h4} &= C_v X_{v_4} + f_{h4}(\boldsymbol{X}, t)\end{aligned} \tag{4.25}$$

where the C_v is an amplified positive factor.

Finally, the servovalve modelling can be chosen in teams of unknown functions as follows.

$$\begin{aligned} X_{v1} &= f_{v1}(\boldsymbol{X}, t) + \mathrm{g}_1 u_1(t) \\ X_{v2} &= f_{v2}(\boldsymbol{X}, t) + \mathrm{g}_2 u_2(t) \\ X_{v3} &= f_{v3}(\boldsymbol{X}, t) + \mathrm{g}_3 u_3(t) \\ X_{v4} &= f_{v4}(\boldsymbol{X}, t) + \mathrm{g}_4 u_4(t) \end{aligned} \tag{4.26}$$

By using equations (4.24), (4.25), and (4.26) can be modeled the adaptive neural networks backstepping control system. Therefore, the MIMO state space modelling system for the adaptive neural networks backstepping control system can be modeled from equations (4.24), (4.25), and (4.26) as follows.

$$\mathbf{X_1} = \left[X_{s_1}, X_{s_2}, X_{s_3}, X_{s_4}\right]^T, \mathbf{X_2} = \left[\dot{X}_{s_1}, \dot{X}_{s_2}, \dot{X}_{s_3}, \dot{X}_{s_4}\right]^T, \mathbf{X_3} = \mathrm{C_h}\left[\mathrm{X}_{h_1}, \mathrm{X}_{h_2}, \mathrm{X}_{h_3}, \mathrm{X}_{h_4}\right]^T, \mathbf{X_4} = \mathrm{C_v}\left[\mathrm{X}_{v_1}, \mathrm{X}_{v_2}, \mathrm{X}_{v_3}, \mathrm{X}_{v_4}\right]^T, \boldsymbol{X_i} \in R^{4\times 1}, i = 1,2,3,4$$

$$\dot{\mathbf{X}}_{\mathbf{1}} = \mathbf{X_2} \tag{4.27}$$

$$\dot{\mathbf{X}}_{\mathbf{2}} = \mathbf{X_3} + \boldsymbol{f_2}(x) + \boldsymbol{D}(\boldsymbol{t}) \tag{4.28}$$

$$\dot{\mathbf{X}}_{\mathbf{3}} = \mathbf{X_4} + \boldsymbol{f_3}(x) \tag{4.29}$$

$$\dot{\mathbf{X}}_{\mathbf{4}} = \boldsymbol{f_4}(x) + \mathbf{g}\Phi(u) \tag{4.30}$$

$$\boldsymbol{y} = \mathbf{X_1}, \qquad \forall\, [\mathbf{X_1}, \mathbf{X_2}, \mathbf{X_3}, \mathbf{X_4}] \in \Omega_X \subset R^{4\times 4} \tag{4.31}$$

where $\boldsymbol{y} \in R^{4\times 1}$ is the output vector, $\boldsymbol{\Phi}(u) \in R^{4\times 1}$ is the control input vector, $\boldsymbol{F_2} \in R^{4\times 1}$, $\boldsymbol{F_3} \in R^{4\times 1}$, $\boldsymbol{F_4} \in R^{4\times 1}$, are unknown function matrices, $\boldsymbol{D} \in R^{4\times 1}$, is unknown aerodynamic disturbances. $\mathbf{g} \in R^{4\times 1}$, is unknown control coefficient matrix.

Let the matrix $\mathbf{g}$ be a diagonal parameter matrix $\left(\mathbf{g} = \ diag([\mathrm{g}_1, \mathrm{g}_2, \mathrm{g}_3, \mathrm{g}_4])\right)$, which is a full rank. Hence, the $\mathbf{g}$ is a nonsingular matrix. The g is an uncertain parameter (K_u/τ_v), which has known upper and lower bounding.

Let the external aerodynamic disturbed force $D_{si}(t)$ be bounded by a known positive constant d_{0i}, which is $|D_i(t)| \leq d_{0i}$.

Several researchers have applied radial basis function neural networks in order to approximately linearize the unknown smooth functions and simplify the backstepping control system (Tran et al., 2019). A linear form of radial basis function neural networks (RBFNN) is implemented to approximate the system's unknown functions. The linear RBFNN has one hidden layer, a fixed size, and fixed moving basis functions (Krstic et al., 1995; Orr M, 1996). The unknown smooth nonlinear function $f_i(\zeta)$ can be designed to satisfy the following form.

$$f_i(\zeta) = W_i^T \mathcal{H}_i(\zeta) + \varepsilon_i \ , \quad i = 1,2, \dots, n, \qquad \forall\, \zeta \in \Omega_\zeta \subset \mathbb{R}^m \tag{4.32}$$

where ζ is an input vector, $\zeta \in \Omega_\zeta \subset \mathbb{R}^m$, the ε_i is the approximation error, the W_i^T is an unknown weight vector, $W_i^T = [W_1 \quad W_2 \quad \dots \quad W_l]_i^T$, the $\mathcal{H}_i(\zeta)$ is a basis function vector, $\mathcal{H}_i(\zeta) = [h_1(\zeta) \quad h_2(\zeta) \quad \dots \quad h_l(\zeta)]_i$. In order to minimize the approximation error, the optimal weight value of the W of RBFNN is defined in Zhang et al. (2019):

$$W_i := \arg \min_{\widehat{W}_i \in R^n} \left\{ \sup_{\zeta \in \Omega_i} \left\| f_i(\zeta) - \hat{f}_i(\zeta) \right\| \right\} , W_i \text{ is } l \times m, \forall\, \zeta \in \Omega_i \tag{4.33}$$

where the $h_i(\zeta), i = 1, \dots, l$ are hidden Gaussian functions, l is a number of RFBNN nodes, m is a number of input variables, The $h_i(\zeta)$ satisfies.

$$h_i(\zeta) = exp\left(\frac{-\|\zeta - \varphi_{i,j}\|^2}{2b_j^2} \right), \qquad \forall\, \zeta \in \Omega_\zeta \subset \mathbb{R}^l \tag{4.34}$$

where , $i = 1, \dots, l, j = 1, \dots, m$, $\boldsymbol{\zeta} = [\zeta_1, \zeta_2, \dots, \zeta_m]$, $\varphi_{i,j}$ are centres of the receptive field in RBFNN, b_j^2 is Gaussian function width for RBFNN.

Therefore, the smooth approximation function $\hat{f}_i(\zeta)$can be satisfied as follows.

$$\hat{f}_i(\zeta) = \widehat{W}_i^T \mathcal{H}_i(\zeta), \quad i = 1,2, \dots, n, \qquad \forall\, \zeta \in \Omega_\zeta \subset \mathbb{R}^m \tag{4.35}$$

The deviation ε_N could be occurred under the optimal weight W_i as follows.

$$\left|f_i(\zeta) - W_i^T \mathcal{H}_i(\zeta)\right| = |\varepsilon_i| \leq \varepsilon_N \tag{4.36}$$

where ε_N is a positive designed error for the RBFNN.

4.3.1 Robust Adaptive neural networks backstepping control design

The state-space modelling system has unmodeled model uncertainties. Therefore, a Backstepping control system is applied to solve this issue. The backstepping control is organized into four control steps according to equations (4.27)-(4.31).

Theorem 4.1, if there exists a positive definite Lyapunov function $V(x)$ class $\mathcal{K}$ functions, hence, satisfying $\pi_1(\|x\|) \leq V(x,t) \leq \pi_2(\|x\|)$, and $\frac{\partial V}{\partial t} + \frac{\partial V}{\partial x} f(t,x) \leq -\pi_3(\|x\|)$, where π_1, $\pi_2 : R^n \to R$ are class $\mathcal{K}$ (Chen et al., 2010). Thus, The Lyapunov time derivative function satisfies $\dot{V}(t) = -\boldsymbol{\Lambda V}(t) + \boldsymbol{\Sigma}$.

Proof: there are four steps to guarantee Lyapunov stability $V(x)$ as follows.

Step 1: Sprung mass velocities $\dot{X}_1$

In order to achieve the control contributions, the output nonlinear control filters $\breve{\boldsymbol{X}}_{\boldsymbol{u}} = \left[\breve{X}_{u_1}, \breve{X}_{u_2}, \breve{X}_{u_3} \breve{X}_{u_4}\right]^T$ are represented the four input desired signals of the control system.
The control coordinate vector $\boldsymbol{Z_1}$ is defined as follows.

$$\boldsymbol{Z_1} = \boldsymbol{X_1} - \breve{\boldsymbol{X}}_{\boldsymbol{u}} \tag{4.37}$$

Let us choose a quadratic Lyapunov function candidate V_1 as follows.

$$V_1 = \frac{1}{2}\boldsymbol{Z_1^T}\,\boldsymbol{Z_1} \tag{4.38}$$

The Lyapunov time derivative $\dot{V}_1$ of step 1 is

$$\dot{V}_1 = \frac{1}{2}\boldsymbol{Z_1^T}\,\boldsymbol{\dot{Z}_1} + \frac{1}{2}\boldsymbol{\dot{Z}_1^T}\,\boldsymbol{Z_1} = \boldsymbol{Z_1^T\dot{Z}_1} = \boldsymbol{Z_1^T X_2} - \boldsymbol{Z_1^T\dot{\bar{X}}_u} = \boldsymbol{Z_1^T Z_2} + \boldsymbol{Z_1^T\alpha_1} - \boldsymbol{Z_1^T\dot{\bar{X}}_u} \tag{4.39}$$

Hence, the $\boldsymbol{\dot{Z}_1}$ becomes.

.

$$\boldsymbol{\dot{Z}_1} = \boldsymbol{Z_2} + \boldsymbol{\alpha_1} - \boldsymbol{\dot{\bar{X}}_u} = -\boldsymbol{c_1^T Z_1} \tag{4.40}$$

where the $\boldsymbol{c_1} = \boldsymbol{c_1^T}$ is a positive definite matrix.

Then, the virtual control vector $\boldsymbol{\alpha_1}$ is:

$$\boldsymbol{\alpha_1} = -\boldsymbol{c_1 Z_1} + \boldsymbol{\dot{\bar{X}}_u} \tag{4.41}$$

Substitute equation 23 into $\dot{V}_1$

$$\dot{V}_1 = \boldsymbol{Z_1^T Z_2} - \boldsymbol{Z_1^T c_1 Z_1} \tag{4.42}$$

Step 2: Sprung mass accelerations $\dot{\mathrm{X}}_2$

The control coordinate matrix $\boldsymbol{Z_2}$ is defined as follows.

$$\boldsymbol{Z_2} = \boldsymbol{X_2} - \boldsymbol{\alpha_1} = \boldsymbol{X_2} + \boldsymbol{c_1 Z_1} - \boldsymbol{\dot{\bar{X}}_u} \tag{4.43}$$

Let choose Lyapunov function candidate V_2 as follows.

$$V_2 = V_1 + \frac{1}{2}\boldsymbol{Z_2^T Z_2} + \frac{1}{2}tr\left(\widetilde{W}_2^T\,\Gamma_2^{-1}\,\widetilde{W}_2\right) \tag{4.44}$$

By applying Lemma 3.1 that is in (Al-Aela et al., 2020b). Hence, the Lyapunov candidate derivative time $\dot{V}_2$ becomes:

$$\dot{V}_2 = \dot{V}_1 + \boldsymbol{Z_2^T Z_3} + \boldsymbol{Z_2^T \alpha}_2 + tr(Z_2(W_2^T H_2(\zeta) + \varepsilon_2)) + \boldsymbol{Z_2^T D} - \boldsymbol{Z_2^T \dot{\alpha}_{1_c}} + tr\left(\widetilde{W}_2 \, {\Gamma_2}^{-1} \, \dot{\widehat{W}}_2\right) \tag{4.45}$$

The adaptive RBFNN law $\dot{\widehat{W}}_2$ is defined (Al-Aela et al., 2020b; Han et Lee, 2014):

$$\dot{\widehat{W}}_{2_i} = \Gamma_{2_i} H_{2_i}(\zeta) Z_{2_i} - \Gamma_{2_i} \sigma_{2_i} \widehat{W}_{2_i}, \qquad i = 1,2,3,4 \tag{4.46}$$

Therefore, the selected virtual control $\boldsymbol{\alpha}_2$ can be expressed.

$$\boldsymbol{\alpha}_2 = -\boldsymbol{Z}_1 - \boldsymbol{c_2 Z_2} - \hat{\boldsymbol{f}}_{\boldsymbol{2}} + \dot{\boldsymbol{\alpha}}_{1_c} \tag{4.47}$$

where the $\boldsymbol{c_2}$ is a positive definite matrix, the $\hat{\boldsymbol{f}}_{\boldsymbol{2}}$ is the approximation smooth functions matrix. Substitute equations (4.46) and (4.47) into (4.45). The $\dot{V}_2$ becomes

$$\dot{V}_2 = \dot{V}_1 + \boldsymbol{Z_2^T Z_3} - \boldsymbol{Z_2^T c_2 Z_2} + tr(Z_2 \varepsilon_2) + \boldsymbol{Z_2^T D} - tr\left(\sigma_{w_2} \widetilde{W}_2 \ \widehat{W}_2\right) \tag{4.48}$$

By applying the completing squares as follows:

$$tr\left(\sigma_{w_2} \widetilde{W}_2 \widehat{W}_2\right) = \frac{1}{2}\sigma_{w_2} \left\|\widetilde{W}_2\right\|^2 + \frac{1}{2}\sigma_{w_2} \left\|\widehat{W}_2\right\|^2 - \frac{1}{2}\sigma_{w_2} \|W_2\|^2 \geq \frac{1}{2}\sigma_{w_2} \left\|\widetilde{W}_2\right\|^2 - \frac{1}{2}\sigma_{w_2} \|W_2\|^2 \tag{4.49}$$

Applying inequality for term $tr(Z_2 \varepsilon_2)$

$$|tr(Z_2\varepsilon_2)| \leq \frac{1}{2}\|\varepsilon_2\|^2 + \frac{1}{2}\|Z_2\|^2 \tag{4.50}$$

The inequality is also applied for the aerodynamic perturbations term $\boldsymbol{Z_2^T D}$

$$\boldsymbol{Z_2^T D} \leq \frac{\|Z_2\|^2}{2\epsilon_2} + \epsilon_2\|D(t)\|^2 \leq \frac{\|Z_2\|^2}{2\epsilon_2} + \epsilon_2\|d_0\|^2 \tag{4.51}$$

By substituting equations (4.49), (4.50) and (4.51) into equation (4.48), the Lyapunov derivative function becomes:

$$\dot{V}_2 \leq -\boldsymbol{Z_1^T c_1 Z_1} - \boldsymbol{Z_2^T c_2 Z_2} + \boldsymbol{Z_3^T Z_2} + \frac{1}{2}\sigma_{w_2}\left\{\|W_2\|^2 - \left\|\widetilde{W}_2\right\|^2\right\} + \tfrac{1}{2}\|\varepsilon_2\|^2 + \epsilon_2\|d_0\|^2 \tag{4.52}$$

Step 3: Operational hydraulic gradient of the hydraulic actuators $\dot{\mathrm{X}}_3$

It is a similar procedure that was applied in step 2. Therefore, the Lyapunov function candidate V_3 can be:

$$V_3 = V_2 + \frac{1}{2}\boldsymbol{Z_3^T Z_3} + \frac{1}{2}tr\left(\widetilde{W}_3^T\,\Gamma_3^{-1}\,\widetilde{W}_3\right) \tag{4.53}$$

The time derivative Lyapunov function $\dot{V}_3$ becomes:

$$\begin{aligned}\dot{V}_3 \leq\ & -\boldsymbol{Z_1^T c_1 Z_1} - \boldsymbol{Z_2^T c_2 Z_2} + \boldsymbol{Z_3^T Z_2} + \frac{1}{2}\sigma_{w_2}\left\{\|W_2\|^2 - \left\|\widetilde{W}_2\right\|^2\right\} + \tfrac{1}{2}\|\varepsilon_2\|^2 + \epsilon_2\|d_0\|^2 \\ & + \boldsymbol{Z_3^T Z_4} + \boldsymbol{Z_3^T \alpha_3} + tr(Z_3(W_3^T H_3(\zeta) + \varepsilon_3)) - \boldsymbol{Z_3^T \dot{\alpha}_{2_c}} \\ & + tr\left(\widetilde{W}_3\,{\Gamma_3}^{-1}\,\dot{\widetilde{W}}_3\right)\end{aligned} \tag{4.54}$$

By applying the adaptive RBFNN law equation (4.46), the virtual control $\boldsymbol{\alpha_3}$ can be chosen

$$\boldsymbol{\alpha}_3 = -\boldsymbol{Z}_2 - \boldsymbol{c}_3^T \boldsymbol{Z}_3 - \hat{\boldsymbol{f}}_{\boldsymbol{3}} + \dot{\boldsymbol{\alpha}}_{2_c} \tag{4.55}$$

where the $\hat{\boldsymbol{f}}_{\boldsymbol{3}}$ is a matrix of the approximation smooth functions.
Hence, the $\dot{V}_i$ becomes

$$\dot{V}_3 \leq -\boldsymbol{Z}_1^T \boldsymbol{c}_1 \boldsymbol{Z}_1 - \boldsymbol{Z}_2^T \boldsymbol{c}_2 \boldsymbol{Z}_2 - \boldsymbol{Z}_3^T \boldsymbol{c}_3 \boldsymbol{Z}_3 + \boldsymbol{Z}_3^T \boldsymbol{Z}_4 + \sum_{i=2}^{3} \frac{\sigma_{w\,i}}{2} \left\{ \|W_i\|^2 - \left\| \widetilde{W}_i \right\|^2 \right\} + \frac{1}{2} \sum_{i=2}^{3} \|\varepsilon_i\|^2 + \epsilon_2 \|d_0\|^2 \tag{4.56}$$

Step 4: Servo-valve dynamic system $\dot{\mathrm{X}}_4$

In step 4, the control signal matrix $\boldsymbol{\Phi}(u)$ is designed, and the overall Lyapunov candidate stability is guaranteed. The virtual control vector $\boldsymbol{Z}_4$ is selected:

$$\boldsymbol{Z}_4 = \boldsymbol{X}_4 - \boldsymbol{\alpha}_3. \tag{4.57}$$

The virtual control time derivative $\dot{\boldsymbol{Z}}_4$ is

$$\dot{\boldsymbol{Z}}_4 = \boldsymbol{f}_{\boldsymbol{v}} + \mathbf{g}\, \boldsymbol{\Phi}(u) - \dot{\boldsymbol{\alpha}}_3 \tag{4.58}$$

The system Lyapunov candidate function V can be as the following form:

$$V = V_3 + \frac{1}{2} \boldsymbol{Z}_4^T \boldsymbol{Z}_4 + \frac{1}{2} tr\left(\widetilde{W}_4^T \, \Gamma_4^{-1} \, \widetilde{W}_4 \right) + \frac{1}{2} tr(\Upsilon^{-1} \tilde{\mathbf{g}}^T \tilde{\mathbf{g}}) \tag{4.59}$$

Thus, the $\dot{V}$ can be estimated as follows.

$$\dot{V} = -\boldsymbol{Z_1^T c_1 Z_1} - \boldsymbol{Z_2^T c_2 Z_2} - \boldsymbol{Z_3^T c_3 Z_3} + \boldsymbol{Z_3^T Z_4} + \boldsymbol{Z_4^T \hat{\mathbf{g}} \Phi(u)} - \boldsymbol{Z_4^T \tilde{\mathbf{g}}}\, \emptyset(u)$$
$$+ \sum_{i=2}^{3} \frac{\sigma_{wi}}{2} \left\{ \|W_i\|^2 - \left\|\widetilde{W}_i\right\|^2 \right\} + \frac{1}{2} \sum_{i=2}^{3} \|\varepsilon_i\|^2 + \epsilon_2 \|d_0\|^2$$
$$+ tr\left(Z_4 (W_4^T H_4(\zeta) + \varepsilon_4)\right) - \mathbb{Z}_4^T \dot{\boldsymbol{\alpha}}_{3_c} + tr\left(\widetilde{W}_4^T\, \Gamma_4^{-1}\, \dot{\widehat{W}}_4\right)$$
$$+ tr\left(\Upsilon^{-1} \tilde{\mathrm{g}}^T \dot{\hat{\mathrm{g}}}\right) \tag{4.60}$$

The RBF neural networks adaptive law $\dot{\widehat{W}}_{\mathrm{n,j}}$ is expressed as:

$$\dot{\widehat{W}}_{\mathrm{n,j}} = \Gamma_{\mathrm{n,j}}\, Z_{n,j}\, h_{n,j}(\zeta) - \Gamma_{\mathrm{n,j}} \sigma_{w\, n,j} \widehat{W}_{n,j} \tag{4.61}$$

The adaptive control law $\dot{\hat{\mathrm{g}}}$ is designed by using the triangularity condition. The triangularity condition technique is applied to estimate the unknown coefficient of the control signal g. The uncertain parameter g is bounded by lower and upper known values $(\mathrm{g}_{min}, \mathrm{g}_{max})$, which satisfies $\mathrm{g} \in \Omega_{\mathrm{g}} = \{\mathrm{g}: \mathrm{g}_{min} \leq \mathrm{g} \leq \mathrm{g}_{max}\}$. Hence, to guarantee $\tilde{\mathrm{g}}_j \left(\frac{1}{\Upsilon_j} \dot{\hat{\mathrm{g}}}_j - Z_{n,j} \mathrm{u}_j(\mathrm{t}) \right) \leq 0$, a projection-type adaptive law $\dot{\hat{\mathrm{g}}}$ is applied (Yang et al., 2016).

$$\dot{\hat{\mathrm{g}}}_j = Proj\left(\Upsilon_j\, Z_{n,j} \mathrm{u}_j(\mathrm{t})\right) = \begin{cases} 0, & if\ \hat{\mathrm{g}}_j = \mathrm{g}_{max}\ and\ \Upsilon_j\, Z_{n,j} \mathrm{u}_j(\mathrm{t}) > 0 \\ 0, & if\ \hat{\mathrm{g}}_j = \mathrm{g}_{min}\ and\ \Upsilon_j\, Z_{n,j} \mathrm{u}_j(\mathrm{t}) < 0, \\ \Upsilon_j\, Z_{n,j} \mathrm{u}_j(\mathrm{t}), & otherwise \end{cases} \tag{4.62}$$

The control signals can be chosen

$$\Phi(u) = \hat{\mathbf{g}}^{-1} \left[-\boldsymbol{Z_3^T} - \boldsymbol{c_4 Z_4^T} - \hat{\boldsymbol{f}}_{\boldsymbol{4}} + \dot{\boldsymbol{\alpha}}_{3_c} \right] \tag{4.63}$$

According to the virtual control functions $\boldsymbol{\Omega}_i$ compact set, the control function matrix $\boldsymbol{\alpha}_i$ are functions of state variables matrices $\boldsymbol{X_s, \dot{X}_s, X_u, \dot{X}_u, P_L,\ X_v, \breve{X}_u, X_L, R_h}$. In order to ensure the Gaussian basis function mapping, the constant scaling factors of the operational hydraulic pressure C_h and the servo-valve area C_v are applied as follows:

$\zeta_{1,j} \equiv X_{s,j}$, $\zeta_{2,j} \equiv \dot{X}_{s,j}, \zeta_{3,j} \equiv C_h P_{L,j}$, $\zeta_{4,j} \equiv C_v A_{v,j}$, $\zeta_{5,j} \equiv \ddot{X}_{u,j}$, $\zeta_{6,j} \equiv X_{u,j}$, $\zeta_{7,j} \equiv \dot{X}_{u,j}$, $\zeta_{8,j} \equiv X_{L,j}$, $\zeta_{9,j} \equiv R_{h,j}$,$j = 1, \dots, 4$, $\forall\, \boldsymbol{\zeta} = [\boldsymbol{\zeta}_1, \boldsymbol{\zeta}_2, \boldsymbol{\zeta}_3, \boldsymbol{\zeta}_4, \boldsymbol{\zeta}_5, \boldsymbol{\zeta}_6, \boldsymbol{\zeta}_7, \boldsymbol{\zeta}_8, \boldsymbol{\zeta}_9] \in \Omega_\zeta \subset \mathrm{R}^{9\times 4}$
where $\boldsymbol{\zeta}_i \equiv \{\zeta_{i,1}, \zeta_{i,2}, \zeta_{i,3}, \zeta_{i,4}\}$

Finally, the $\dot{V}$ becomes

$$\dot{V} = -\boldsymbol{Z_1^T c_1 Z_1} - \boldsymbol{Z_2^T c_2 Z_2} - \boldsymbol{Z_3^T c_3 Z_3} - \boldsymbol{Z_4^T c_4 Z_4} - \sum_{i=2}^{4} \frac{\sigma_{wi}}{2} \left\| \widetilde{W}_i \right\|^2 + \sum_{i=2}^{4} \frac{\sigma_{wi}}{2} \|W_i\|^2 + \frac{1}{2} \sum_{i=2}^{4} \|\varepsilon_N\|^2 + \epsilon_2 \|d_0\|^2 \tag{4.64}$$

Hence, the $\dot{V}$ can prove the theorem 4.1 as follows.

$$\dot{V} \leq -\boldsymbol{\Lambda V} + \boldsymbol{\Sigma} \tag{4.65}$$

where the $\boldsymbol{\Lambda}$ and $\boldsymbol{\Sigma}$ remain positive

Furthermore, $\Lambda := \min_{j=1,\dots,4} \left\{ \lambda_{min}(\boldsymbol{c_i}), \frac{\sigma_{wi}}{\lambda_{\max} \Gamma_i^{-1}} \right\}$, $\Sigma = \frac{1}{2} \sum_{i=2}^{4} \frac{\sigma_{wi}}{2} \|W_i\|^2 + \sum_{j=2}^{4} \|\varepsilon_N\|^2 + \epsilon_2 \|d_0\|^2$, the maximum eigenvalue $\lambda_{\max}$ of the positive definite matrix Γ is known

4.3.2 Zero dynamics system

In section 4.3.1, there are four steps to designing the robust adaptive neural networks backstepping control system, which resulted in control coordinate matrices $\{\mathbf{Z_1}, \mathbf{Z_2}, \mathbf{Z_3}, \mathbf{Z_4}\}$. On the other hand, other state modelling systems $\left\{\left(\ddot{\mathrm{X}}_{\mathrm{u}k}, \dot{X}_{u_k}, \ddot{X}_{u_k}, \dot{X}_{L_k}, \dot{R}_{h_k}\right), k = 1,2,3,4\right\}$ must guarantee their stability to ensure control stability. The other state modelling system are described in the equations (4.5), (4.6), (4.7), (4.9), and (4.21).

The zero dynamics closed-loop system can be evaluated by using the control output matrix $\mathbf{y} = \boldsymbol{Z_1}$ and then control output derivative matrices ($\dot{\mathbf{y}} = \mathbf{0}, \ddot{\mathbf{y}} = \mathbf{0}$) as follows.

$$\mathbf{y} = \boldsymbol{Z_1} = \mathbf{X_s} - \breve{\mathbf{X}}_\mathbf{u} = 0$$
$$\mathbf{X_s} = \breve{\mathbf{X}}_\mathbf{u} \tag{4.66}$$

The first derivative output control matrix $\dot{\mathbf{y}}$ becomes

$$\dot{\mathbf{y}} = \dot{\mathbf{X}}_\mathbf{s} - \dot{\breve{\mathbf{X}}}_\mathbf{u} = 0$$
$$\dot{\mathbf{X}}_\mathbf{s} = \dot{\breve{\mathbf{X}}}_\mathbf{u} \tag{4.67}$$

The second derivative control matrix $\ddot{\boldsymbol{y}}$ is:

$$\ddot{\boldsymbol{y}} = \dot{\mathbf{X}}_\mathbf{2} - \ddot{\breve{\mathbf{X}}}_\mathbf{u} \tag{4.68}$$

In order to minimize the sprung mass accelerations $\left\{\left(\ddot{X}_{s_{cg}}, \ddot{\theta}, \ddot{\omega}\ \right) \equiv 0\right\}$, the hydraulic forces of the active suspension $(F_{h1}, F_{h2}, F_{h3}, F_{h4})$ can represent a zero dynamic forces $\left(F_{ZD_1}, F_{ZD_2}, F_{ZD_3}, F_{ZD_4}\right)$ as following form.

$$\begin{aligned} F_{h,i} &= A_{p_i} X_{h_i} = F_{ZD_i} \\ &= -K_{s_i}\left(X_{s_i} - X_{u_i}\right) - F_{ns_i} - C_{s_i}\left(\dot{X}_{s_i} - \dot{X}_{u_i}\right) - C_{ns_i}(t)\left(\dot{X}_{s_i} - \dot{X}_{u_i}\right) \\ &+ F_{a_i}(t), \quad i = 1,2,3,4 \end{aligned} \tag{4.69}$$

It can reorganize the equations (4.13)-(4.16) in matrix form $\ddot{\boldsymbol{X}}_\boldsymbol{s}$ as follows.

$$\ddot{\boldsymbol{X}}_\boldsymbol{s} = \boldsymbol{\mathcal{M}^{-T}}\mathbf{F} \tag{4.70}$$

the $\ddot{\mathbf{y}}$ becomes

$$\ddot{\boldsymbol{y}} = \boldsymbol{\mathcal{M}}^{-T}\mathbf{F} - \ddot{\breve{\boldsymbol{X}}}_u = 0 \tag{4.71}$$

Therefore, the total dynamic forces **F** can be determined as follows.

$$\mathbf{F} = \boldsymbol{\mathcal{M}}^{T}\ddot{\breve{\boldsymbol{X}}}_{\boldsymbol{u}} \tag{4.72}$$

Substituting equations (4.71) and (4.72) into $\ddot{\breve{\boldsymbol{X}}}_{\boldsymbol{u}}$. The $\ddot{\breve{X}}_{u_k}$ becomes:

$$\begin{aligned}\ddot{\breve{X}}_{u_k} = \Bigg\{ -\Bigg(& \kappa_{st}\frac{\partial\psi(\breve{X}_u - X_u)}{\partial(\breve{X}_u - X_u)}\Big(-\big(\delta_0 + \kappa_{st}\psi(\breve{X}_u - X_u) + \kappa_{Rh}\phi(X_L)\big)(\breve{X}_u - X_u) - \dot{X}_u\Big) \\ & + \kappa_{Rh}\frac{\partial\phi(X_L)}{\partial X_L}\frac{K_t}{C_t}\Bigg(X_L - \kappa_w\frac{W_{us}}{K_t}\,(R_h - 1)\Bigg)\Bigg)(\breve{X}_u - X_u) \\ & - \Big(\delta_0 + \kappa_{st}\psi(\breve{X}_u - X_u) \\ & + \kappa_{Rh}\phi(X_L)\Big)\Big\{-\big(\delta_0 + \kappa_{st}\psi(\breve{X}_u - X_u) + \kappa_{Rh}\phi(X_L)\big)(\breve{X}_u - X_u) - \dot{X}_u\Big\}\Bigg\}_k, \\ & k = 1,2,3,4\end{aligned} \tag{4.73}$$

Substituting equation (4.66), (4.67), (4.71) and (4.72) into equations (4.5), (4.7), (4.9) and (4.21). Also, neglecting the effect of the vertical road accelerations $\big(\ddot{X}_{r_1} = 0, \ddot{X}_{r_2} = 0, \ddot{X}_{r_3} = 0, \ddot{X}_{r_4} = 0\big)$. Hence, the zero dynamics state space has linear and nonlinear terms as follows.

$X_5 = \breve{X}_{u1}$, $X_6 = X_{u1}$, $X_7 = \dot{X}_{u1}$, $X_8 = X_{L1}$, $X_9 = R_{h1}$, $X_{10} = \breve{X}_{u2}$, $X_{11} = X_{u2}$, $X_{12} = \dot{X}_{u2}$, $X_{13} = X_{L2}$, $X_{14} = R_{h2}$, $X_{15} = \breve{X}_{u3}$, $X_{16} = X_{u3}$, $X_{17} = \dot{X}_{u3}$, $X_{18} = X_{L3}$, $X_{19} = R_{h3}$, $X_{20} = \breve{X}_{u4}$, $X_{21} = X_{u4}$, $X_{22} = \dot{X}_{u4}$, $X_{23} = X_{L4}$, $X_{24} = R_{h4}$

$$\begin{aligned}\dot{\mathrm{X}}_5 &= -\big(\delta_{0,1} + \kappa_{\mathrm{st}}\psi_1(X_5 - X_6) + \kappa_{\mathrm{Rh}}\phi_1(\mathrm{X}_8)\big)(\mathrm{X}_5 - \mathrm{X}_6) \\ &= -\delta_{0,1}\big(\mathrm{X}_{5,} - \mathrm{X}_{6,}\big) + \mathrm{N}_5(X)\end{aligned} \tag{4.74}$$

$$\dot{X}_6 = X_7 \tag{4.75}$$

$$\dot{X}_{7,} = \frac{\mathcal{M}_{1,1}}{m_{u,1}}\left(\delta_{0_1}{}^2(X_5 - X_6) - \delta_{0_1}X_7\right) + \frac{\mathcal{M}_{1,2}}{m_{u,1}}\left(\delta_{0_2}{}^2(X_{10} - X_{11}) - \delta_{0_2}X_{12}\right)$$
$$+ \frac{\mathcal{M}_{1,3}}{m_{u,1}}\left(\delta_{0_3}{}^2(X_{15} - X_{16}) - \delta_{0_3}X_{17}\right) + \frac{\mathcal{M}_{1,4}}{m_{u,1}}\left(\delta_{0_4}{}^2(X_{20} - X_{21}) - \delta_{0_4}X_{22}\right)$$
$$+ \kappa_{w,1}W_{us,1}X_9 + N_7(X) \tag{4.76}$$

$$X_8 = -\frac{K_t}{C_t}\left(X_8 - \kappa_{w,1}\,X_{us,1}\,(X_9 - 1)\right) \quad \kappa_{w,k}^{-1} \geq X_{9,k} \geq 1 \tag{4.77}$$

$$\dot{X}_9 = \frac{-K_t}{\kappa_{w,1}W_{us,1}}X_7$$
$$- \frac{C_t}{\kappa_{w,1}W_{us,1}}\left\{\frac{\mathcal{M}_{1,1}}{m_{u,1}}\left(\delta_{0_1}{}^2(X_5 - X_6) - \delta_{0_1}X_7\right)\right.$$
$$+ \frac{\mathcal{M}_{1,2}}{m_{u,1}}\left(\delta_{0_2}{}^2(X_{10} - X_{11}) - \delta_{0_2}X_{12}\right) + \frac{\mathcal{M}_{1,3}}{m_{u,1}}\left(\delta_{0_3}{}^2(X_{15} - X_{16}) - \delta_{0_3}X_{17}\right)$$
$$\left. + \frac{\mathcal{M}_{1,4}}{m_{u,1}}\left(\delta_{0_4}{}^2(X_{20} - X_{21}) - \delta_{0_4}X_{22}\right) + \kappa_{w,1}W_{us,1}X_9\right\} + \frac{K_t}{\kappa_{w,1}W_{us,1}}\dot{X}_{r,k}$$
$$+ N_9(X) \tag{4.78}$$

$$\dot{X}_{10} = -\delta_{0,2}\left(X_{10,} - X_{11}\right) + N_{10}(X) \tag{4.79}$$

$$\dot{X}_{11} = X_{12} \tag{4.80}$$

$$\dot{X}_{12,} = \frac{\mathcal{M}_{2,1}}{m_{u,2}}\left(\delta_{0_1}{}^2(X_5 - X_6) - \delta_{0_1}X_7\right) + \frac{\mathcal{M}_{2,2}}{m_{u,2}}\left(\delta_{0_2}{}^2(X_{10} - X_{11}) - \delta_{0_2}X_{12}\right)$$
$$+ \frac{\mathcal{M}_{2,3}}{m_{u,2}}\left(\delta_{0_3}{}^2(X_{15} - X_{16}) - \delta_{0_3}X_{17}\right) + \frac{\mathcal{M}_{2,4}}{m_{u,2}}\left(\delta_{0_4}{}^2(X_{20} - X_{21}) - \delta_{0_4}X_{22}\right)$$
$$+ \kappa_{w,2}W_{us,2}X_{14} + N_{12}(X) \tag{4.81}$$

$$\dot{X}_{13} = -\frac{K_t}{C_t}\left(X_{13} - \kappa_{w,1}\,X_{us,1}\,(X_{14} - 1)\right), \quad \kappa_{w,2}^{-1} \geq X_{14} \geq 1 \tag{4.82}$$

$$\dot{\mathrm{X}}_{14} = \frac{-\mathrm{K_t}}{\kappa_{\mathrm{w},2}\mathrm{W_{us,2}}}\mathrm{X}_{12}$$
$$- \frac{\mathrm{C_t}}{\kappa_{\mathrm{w},1}\mathrm{W_{us,1}}}\left\{\frac{\mathcal{M}_{2,1}}{m_{u,1}}\left(\delta_{0_1}{}^2(X_5 - X_6) - \delta_{0_1}X_7\right)\right.$$
$$+ \frac{\mathcal{M}_{2,2}}{m_{u,1}}\left(\delta_{0_2}{}^2(X_{10} - X_{11}) - \delta_{0_2}\mathrm{X}_{12}\right) + \frac{\mathcal{M}_{2,3}}{m_{u,1}}\left(\delta_{0_3}{}^2(X_{15} - X_{16}) - \delta_{0_3}X_{17}\right)$$
$$\left. + \frac{\mathcal{M}_{2,4}}{m_{u,1}}\left(\delta_{0_4}{}^2(X_{20} - X_{21}) - \delta_{0_4}X_{22}\right) + \kappa_{\mathrm{w},2}\mathrm{W_{us,2}}\mathrm{X}_{14}\right\} + \frac{\mathrm{K_t}}{\kappa_{\mathrm{w},2}\mathrm{W_{us,2}}}\dot{\mathrm{X}}_{r,2}$$
$$+ \frac{\mathrm{C_t}}{\kappa_{\mathrm{w},2}\mathrm{W_{us,2}}}\ddot{\mathrm{X}}_{r,2} + N_{14}(X) \tag{4.83}$$

$$\dot{\mathrm{X}}_{15} = -\delta_{0,3}\left(\mathrm{X}_{15,} - \mathrm{X}_{16,}\right) + \mathrm{N}_{15}(X) \tag{4.84}$$

$$\dot{\mathrm{X}}_{16} = \mathrm{X}_{17} \tag{4.85}$$

$$\dot{\mathrm{X}}_{17} = \frac{\mathcal{M}_{3,1}}{m_{u,3}}\left(\delta_{0_1}{}^2(X_5 - X_6) - \delta_{0_1}X_7\right) + \frac{\mathcal{M}_{3,2}}{m_{u,3}}\left(\delta_{0_2}{}^2(X_{10} - X_{11}) - \delta_{0_2}\mathrm{X}_{12}\right)$$
$$+ \frac{\mathcal{M}_{3,3}}{m_{u,3}}\left(\delta_{0_3}{}^2(X_{15} - X_{16}) - \delta_{0_3}X_{17}\right) + \frac{\mathcal{M}_{3,4}}{m_{u,3}}\left(\delta_{0_4}{}^2(X_{20} - X_{21}) - \delta_{0_4}X_{22}\right)$$
$$+ \kappa_{\mathrm{w},3}\mathrm{W_{us,3}}\mathrm{X}_{19} + N_{17}(X) \tag{4.86}$$

$$\mathrm{X}_{18} = -\frac{\mathrm{K_t}}{\mathrm{C_t}}\left(\mathrm{X}_{18} - \kappa_{\mathrm{w},3}\,\mathrm{X_{us,3}}\,(\mathrm{X}_{19} - 1)\right), \quad \kappa_{\mathrm{w},3}^{-1} \geq \mathrm{X}_{19} \geq 1 \tag{4.87}$$

$$\dot{\mathrm{X}}_{19} = \frac{-\mathrm{K_t}}{\kappa_{\mathrm{w},3}\mathrm{W_{us,3}}}\mathrm{X}_{17}$$
$$- \frac{\mathrm{C_t}}{\kappa_{\mathrm{w},3}\mathrm{W_{us,3}}}\left\{\frac{\mathcal{M}_{3,1}}{m_{u,3}}\left(\delta_{0_1}{}^2(X_5 - X_6) - \delta_{0_1}X_7\right)\right.$$
$$+ \frac{\mathcal{M}_{3,2}}{m_{u,3}}\left(\delta_{0_2}{}^2(X_{10} - X_{11}) - \delta_{0_2}\mathrm{X}_{12}\right) + \frac{\mathcal{M}_{3,3}}{m_{u,3}}\left(\delta_{0_3}{}^2(X_{15} - X_{16}) - \delta_{0_3}X_{17}\right)$$
$$\left. + \frac{\mathcal{M}_{3,4}}{m_{u,3}}\left(\delta_{0_4}{}^2(X_{20} - X_{21}) - \delta_{0_4}X_{22}\right) + \kappa_{\mathrm{w},3}\mathrm{W_{us,3}}\mathrm{X}_{19}\right\} + \frac{\mathrm{K_t}}{\kappa_{\mathrm{w},2}\mathrm{W_{us,2}}}\dot{\mathrm{X}}_{r,3}$$
$$+ N_{19}(X) \tag{4.88}$$

$$\dot{\mathrm{X}}_{20} = -\delta_{0,4}\left(\mathrm{X}_{20,} - \mathrm{X}_{21}\right) + \mathrm{N}_{20}(X) \tag{4.89}$$

$$\dot{\mathrm{X}}_{21} = \mathrm{X}_{22} \tag{4.90}$$

$$\dot{\mathrm{X}}_{22,} = \frac{\mathcal{M}_{4,1}}{m_{u,4}}\left(\delta_{0_1}{}^2(X_5 - X_6) - \delta_{0_1}X_7\right) + \frac{\mathcal{M}_{4,2}}{m_{u,4}}\left(\delta_{0_2}{}^2(X_{10} - X_{11}) - \delta_{0_2}\mathrm{X}_{12}\right)$$
$$+ \frac{\mathcal{M}_{4,3}}{m_{u,4}}\left(\delta_{0_3}{}^2(X_{15} - X_{16}) - \delta_{0_3}X_{17}\right) + \frac{\mathcal{M}_{4,4}}{m_{u,4}}\left(\delta_{0_4}{}^2(X_{20} - X_{21}) - \delta_{0_4}X_{22}\right)$$
$$+ \kappa_{\mathrm{w},4}\mathrm{W}_{\mathrm{us},4}\mathrm{X}_{24} + N_{22}(X) \tag{4.91}$$

$$\dot{\mathrm{X}}_{23} = -\frac{\mathrm{K_t}}{\mathrm{C_t}}\left(\mathrm{X}_{23} - \kappa_{\mathrm{w},4}\,\mathrm{X}_{\mathrm{us},4}\,(\mathrm{X}_{24} - 1)\right), \quad \kappa_{\mathrm{w},4}^{-1} \geq \mathrm{X}_{24} \geq 1 \tag{4.92}$$

$$\dot{\mathrm{X}}_{24} = \frac{-\mathrm{K_t}}{\kappa_{\mathrm{w},4}\mathrm{W}_{\mathrm{us},4}}\mathrm{X}_{22}$$
$$- \frac{\mathrm{C_t}}{\kappa_{\mathrm{w},4}\mathrm{W}_{\mathrm{us},4}}\left\{\frac{\mathcal{M}_{4,1}}{m_{u,4}}\left(\delta_{0_1}{}^2(X_5 - X_6) - \delta_{0_1}X_7\right)\right.$$
$$+ \frac{\mathcal{M}_{4,2}}{m_{u,4}}\left(\delta_{0_2}{}^2(X_{10} - X_{11}) - \delta_{0_2}\mathrm{X}_{12}\right) + \frac{\mathcal{M}_{4,3}}{m_{u,4}}\left(\delta_{0_3}{}^2(X_{15} - X_{16}) - \delta_{0_3}X_{17}\right)$$
$$\left. + \frac{\mathcal{M}_{4,4}}{m_{u,4}}\left(\delta_{0_4}{}^2(X_{20} - X_{21}) - \delta_{0_4}X_{22}\right) + \kappa_{\mathrm{w},4}\mathrm{W}_{\mathrm{us},4}\mathrm{X}_{24}\right\} + \frac{\mathrm{K_t}}{\kappa_{\mathrm{w},4}\mathrm{W}_{\mathrm{us},4}}\dot{\mathrm{X}}_{r,4}$$
$$+ N_{24}(X) \tag{4.93}$$

Therefore, the zero dynamic state space can be represented as follows

$$\dot{\mathbf{X}} = \mathbf{AX} + \mathbf{N} + \mathbf{B}_{\boldsymbol{r}}\dot{\boldsymbol{X}}_{\boldsymbol{r}}\,, \mathbf{A} \to R^{20\times 20}, \mathbf{N} \to R^{1\times 20}, \quad \mathbf{B}_{\boldsymbol{r}} \to R^{1\times 20} \tag{4.94}$$
$$\mathbf{X} = [X_5, X_6, X_7, X_8, X_9, X_{10}, X_{11}, X_{12}, X_{13}, X_{14}, X_{15}, X_{16}, X_{17}, X_{18}, X_{19}, X_{20},$$
$$X_{21}, X_{22}, X_{23}, X_{24}]^{\boldsymbol{T}}$$

Let's suggest zero dynamics Lyapunov candidate V_0 as follows:

$$\mathrm{V}_0 = X^T P\, X \tag{4.95}$$

where P is a positive definite matrix.

Consequently, the zero dynamics Lyapunov time derivative function $\dot{\mathrm{V}}_0$ can be.

$$\begin{aligned}\dot{\mathrm{V}}_0 &= \left(A^T X^T + N^T + B_r^T \dot{X}_r^T\right) PX + X^T P\left(AX + N + B_r \dot{X}_r\right) \\ &= X^T [PA + A^T P] X + N^T PX + X^T PN + B_r^T \dot{X}_r^T PX + X^T P B_r \dot{X}_r \\ &= -X^T QX + 2X^T PN + 2X^T P B_r \dot{X}_r \end{aligned} \tag{4.96}$$

The positive definite matrix Q is existed which the eigenvalues of A are stable (negative real parts). Applying inequality into the terms of $(2X^T PN)$and $\left(2X^T P B_r \dot{X}_r\right)$ as follows.

$$2X^T PN \leq \frac{1}{\epsilon_n} X^T PPX + \epsilon_n N^T N \tag{4.97}$$

$$2X^T P B_r \dot{X}_r \leq \frac{1}{\epsilon_r} X^T PPX + \epsilon_r X_r^T B_r^T B_r \, X_r \tag{4.98}$$

where the ϵ_n and ϵ_r are designed positive constants. Applying (4.97) and (4.98) into (4.96).

$$\dot{\mathrm{V}}_0 \leq -X^T QX + \frac{1}{\epsilon_r} X^T PPX + \epsilon_r \, \dot{X}_r^T B_r^T B_r \, \dot{X}_r + \frac{1}{\epsilon_n} X^T PPX + \epsilon_n N^T N \tag{4.99}$$

$$\dot{\mathrm{V}}_0 \leq -X^T \left(Q - \frac{1}{\epsilon_r} P B_r^T B_r P - \frac{1}{\epsilon_n} PP\right) X + \epsilon_r \, \dot{X}_r^T B_r^T B_r \, \dot{X}_r + \epsilon_n N^T N \tag{4.100}$$

$$\begin{aligned}\dot{\mathrm{V}}_0 \leq -\left[\lambda_{min}(P^{-0.5} Q P^{-0.5}) - \frac{1}{\epsilon_r} \lambda_{max}(P^{0.5} B_r^T B_r P^{0.5}) - \frac{1}{\epsilon_n} \lambda_{max} P\right] \mathrm{V}_0 + \epsilon_r \, \dot{X}_r^T B_r^T B_r \, \dot{X}_r \\ + \epsilon_n N^T N \leq -\Lambda_0 \mathrm{V}_0 + \Sigma_0 \end{aligned} \tag{4.101}$$

where the $\Lambda_0 = \lambda_{min}(P^{-0.5} Q P^{-0.5}) - \frac{1}{\epsilon_r} \lambda_{max}(P^{0.5} B_r^T B_r P^{0.5}) - \frac{1}{\epsilon_n} \lambda_{max} P$, the $\Sigma_0 = \epsilon_r \, \dot{X}_r^T B_r^T B_r \, \dot{X}_r + \epsilon_n N^T N$

So, the solving equation (4.99) can be:

$$0 \leq \mathrm{V}_0(\mathrm{t}) \leq \frac{\Sigma_0}{\Lambda_0} + \left(\mathrm{V}_0(0) - \frac{\Sigma_0}{\Lambda_0}\right) \mathrm{e}^{-\Lambda_0 \, \mathrm{t}} \tag{4.102}$$

Therefore, the $\dot{X}_i$, $\mathrm{i} = 5, \ldots, 24$ are uniformly bounded and then X is stable. Finally, the proposed control system can be sketched, as shown in Figure 2. The output nonlinear control

filters $\left\{\breve{\boldsymbol{X}}_{\boldsymbol{u}} \equiv \left[\breve{X}_{u_1},\ \breve{X}_{u_2}, \breve{X}_{u_3}, \breve{X}_{u_4}\right]^T\right\}$ are represented the control reference trajectories (desired control signals).

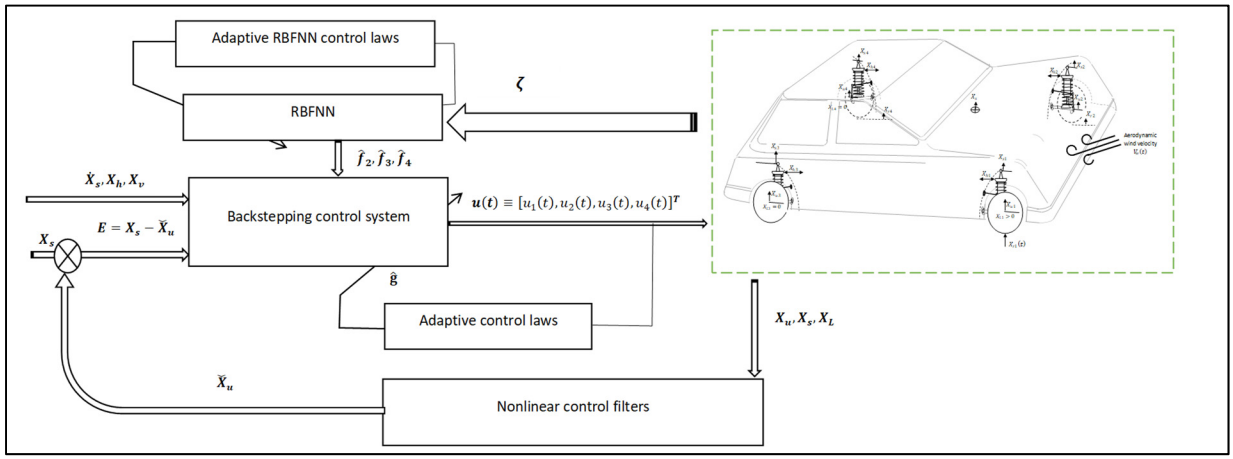

Figure 4.2 Sketch paths of filtered active suspension control system

In the MIMO backstepping control system block, the input tracking error E represents the control coordinate matrix $\boldsymbol{Z_1}$, which is a difference between the sprung mass positions $\left(\boldsymbol{X_s} \equiv \left[X_{s_1},\ X_{s_2}, X_{s_3}, X_{s_4}\right]^T\right)$ and $\breve{\boldsymbol{X}}_{\boldsymbol{u}}$. The adaptive radial basis function neural networks (RBFNN) is proposed to approximate unknown functions $\left(\hat{\boldsymbol{f}}_{\boldsymbol{2}}, \hat{\boldsymbol{f}}_{\boldsymbol{3}}, \hat{\boldsymbol{f}}_{\boldsymbol{4}}\right)$ for the backstepping control system. Finally, the projection-type adaptive control laws are also used to estimate the unknown coefficients of the four control signals **g**.

4.4 Simulation and Results Discussion

A comparative study between the RANNC (filtered active suspension), unfiltered active suspension, and the passive suspension are applied to accomplish the control objectives. The unfiltered active suspension means that the effect of nonlinear control filters was ignored $\left(\breve{\boldsymbol{X}} = 0\right)$ in the control system. Therefore, the authors have considered a sinusoidal wind velocity relative to the vehicle velocity with both bumpy and random road input perturbations. The simulation data was chosen based on the literature review for both filtered

and unfiltered active suspensions. For example, the sprung mass M_s=1200 Kg, front length $l_f = 1.011\ m$, rear length $l_r = 1.803\ m$, right width $w_r = 0.755\ m$, left width $w_l = 0.761\ m$, rolling mass moment of inertia $I_\omega = 460\ Kg\ m^2$, pitching mass moment of inertia $I_\theta = 2160\ Kg\ m^2$, $C_v = 1 \times 10^5$, $C_h = 1 \times 10^{-6}$, the nonlinear damper $C_{ns_i}(t) = 900 + 200e^{-0.1t}\ Ns\ m^{-1}$. The control positive definite matrices are $\mathbf{c_1} = diag([177.6, 186.25, 234, 226.38\ ])$, $\mathbf{c_2} = diag([207, 202.11, 200, 111.5\ ])$, $\mathbf{c_3} = diag([200, 210, 220, 210\ ])$, $\mathbf{c_4} = diag([200, 210, 200, 210\ ])$. In Table 4.1, there are other passive and active suspensions' data.

In this study, the authors have introduced an aerodynamic perturbation of wind velocity. A sinusoidal wind velocity relative to the vehicle speed U_a can be chosen as follows.

$$U_a = \begin{cases} 15(|1 - \cos 2\pi\, t|), & \text{if } 0 \le t \le 1\ s \\ 0 & otherwise \end{cases}, \quad (m/s) \tag{4.103}$$

In addition, two cases of road input design are also introduced in this study to investigate the study contributions as follows.

Case I: Road input bumpy design

Many articles were experienced their control systems by using bumpy road design for input road perturbations. In this study, we have introduced a double bumpy road input. The first bumpy road has a high frequency of $11\pi\ rad/s$, and the other one has $8\pi\ rad/s$.

$$X_{r_1} = \begin{cases} 0.04(|1 - cos\ 11\pi\ t|), & \text{if } 0 \le t \le 0.182\ s \\ 0.025(|1 - cos\ 8\pi\ t|), & \text{if } 3 \le t \le 3.25\ s \\ 0 & otherwise \end{cases}, \qquad X_{r_2} = X_{r_3} = X_{r_4} = 0 \tag{4.104}$$

Table 4.1 Simulation nominal data for passive and active suspensions

	Quantity \ Quarter car	1	2	3	4
Passive and mechanical active suspensions	m_u	59	59	63	63
	$K_s(N/m) \times 10^{-3}$	35	35	38	38
	$C_s(Ns/m) \times 10^{-3}$	1	1	1.1	1.1
	$K_{ns}(N/m^3) \times 10^{-4}$	16	16	16	16
	$K_t(N/m) \times 10^{-4}$	19	19	19	19
	$C_t(Ns/m) \times 10^{-2}$	8	8	8	8
	$\mathrm{ST_c}(m) \times 10^2$	-9	-9	-9	-9
	$\mathrm{ST_E}(m) \times 10^2$	15	15	15	15
	$\kappa_w(-) \times 10^1$	7	7	6.5	6.5
Electrohydraulic servovalve system (EHSS)	$\mathrm{C_d}(-) \times 10^2$	63	63	63	63
	$\mathrm{V_t}(m^3) \times 10^{13}$	135.4	135.4	135.4	135.5
	$C_{tp}(\mathrm{m^5/(Ns)}) \times 10^{13}$	9.047	9.047	9.047	9.047
	$A_p(m^2) \times 10^3$	3.35	3.35	1.15	1.15
	$P_s(N/m^2) \times 10^{-4}$	1,034	1,034	1,034	1,034
	$\beta_e(N/m^2) \times 10^{-8}$	7.990	7.990	7.990	7.990
	$\rho_h(\mathrm{kg}/m^3) \times 10^{-4}$	867	867	867	867
	$K_{u_{min}}(m^2/\mathrm{m}\,A) \times 10^3$	2.7	2.7	2.7	2.7
	$K_{u_{max}}(m^2/\mathrm{m}\,A) \times 10^3$	3.3	3.3	3.3	3.3
	$\tau_v(s) \times 10^3$	5	5	5	5

The comparative study can indicate the control performance and robustness. Thus, the following figures explain the control performance based on the control target.

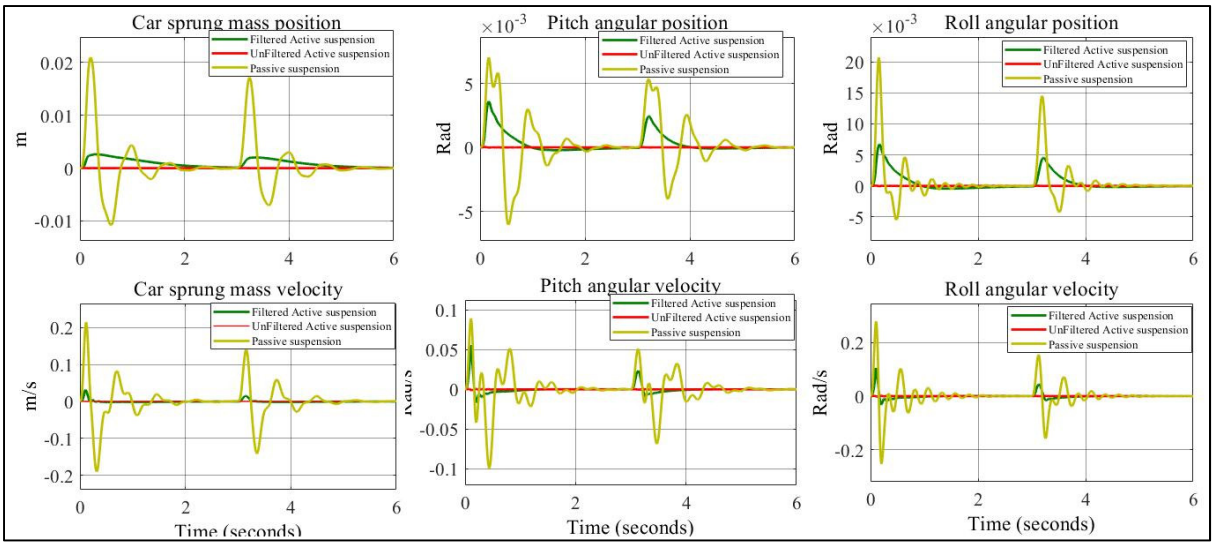

Figure 4.3 Sprung mass (heave, roll, pitch) positions and velocities of Case I

In Figure 3, a comparative study is announced between the filtered active suspension, unfiltered active suspension, and passive suspension systems. The unfiltered active suspension provides the best control compensation. Nevertheless, the filtered active suspension shows a smooth decaying to the origin (equilibrium point) and better compensation than the passive suspension. Therefore, the car sprung mass positions (heave, pitch, roll) of the filtered active suspension are compensated by 86%, 43%, and 62% of that in passive suspension at 0.6 seconds, respectively. The car sprung mass velocities (heave, pitch, roll) of the filtered active suspension are also reduced to 87%, 45%, and 65% of that in passive suspension.

Figure 4.4 shows that both filtered and unfiltered active suspensions can provide better compensation than passive suspension; in quarter 1, the filtered active suspension has a 75% compensation of that in the passive suspension. On the other hand, the unfiltered active suspension provides a 98% compensation related to that in the passive suspension. In Figure 4.4 quarter car 2 and 3, the filtered active suspension makes 86% and 82% compensations compared to the passive suspension and decays smoothly to the origin.

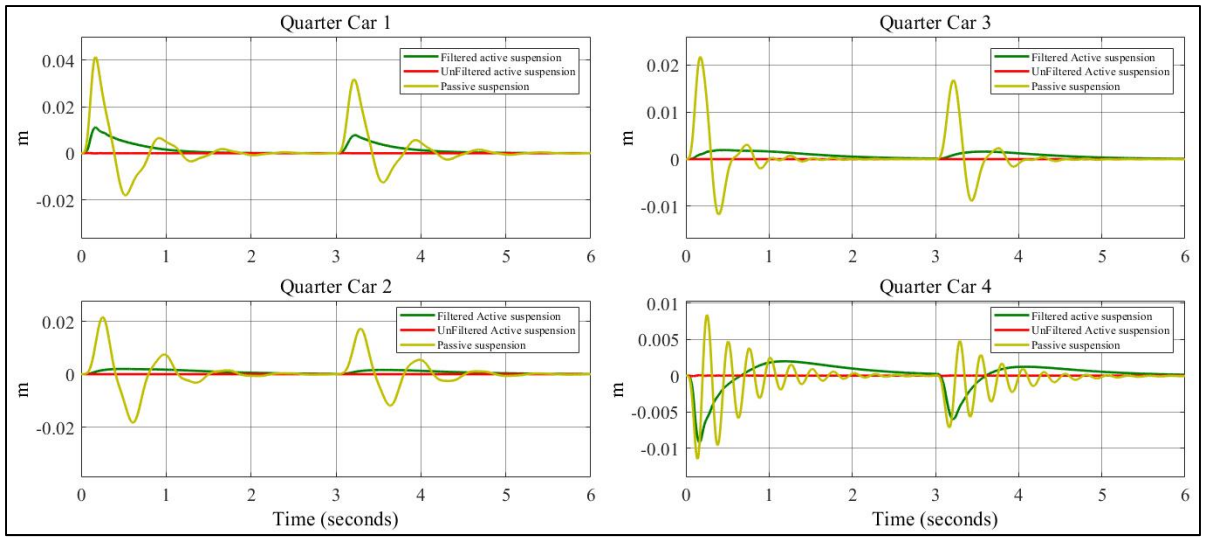

Figure 4.4 Sprung mass positions at the four wheels of Case I

In Figure 4.4 quarter car 4, the suspension direction is expandingly traveling. Otherwise, the other quarter car suspensions in Figure 4.4 are diminishingly traveling.

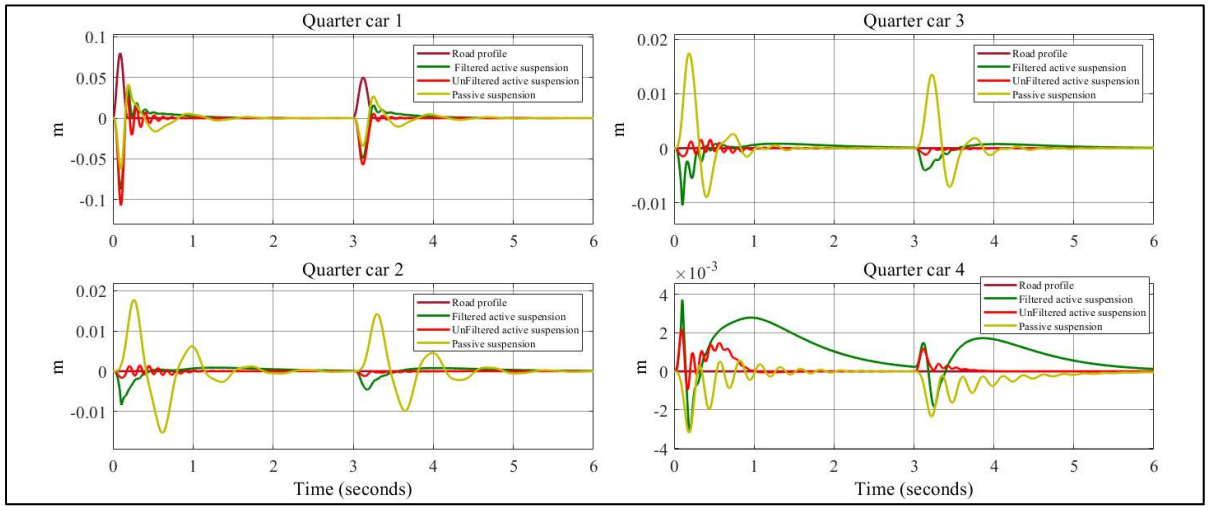

Figure 4.5 Suspension travel of Case I

In this study, the maximum allowable suspension travels are -9 cm for contraction limitation and 15 cm for expansion limitation. Although the unfiltered active suspension provides the best compensation for sprung mass positions, the suspension travel is hitting the suspension

contraction limitation in Figure 4.5 quarter car 1. Hence, the filtered active suspension is succeeded to avoid reaching the suspension contraction limitation that suspension travel value is kept more than -8 cm for the quarter car 1. In contrast, the unfiltered active suspension is failed to avoid hitting the contraction limitation, which reaches less than -12 cm. In Figure 4.5-quarter car 1, the filtered active suspension reduces the suspension travel oscillations ≈ 37% less than the unfiltered active suspension. In Figure 4.5-quarter car 2-4, the filtered active suspension slightly travels more than the unfiltered active suspension because of the control filters' effects.

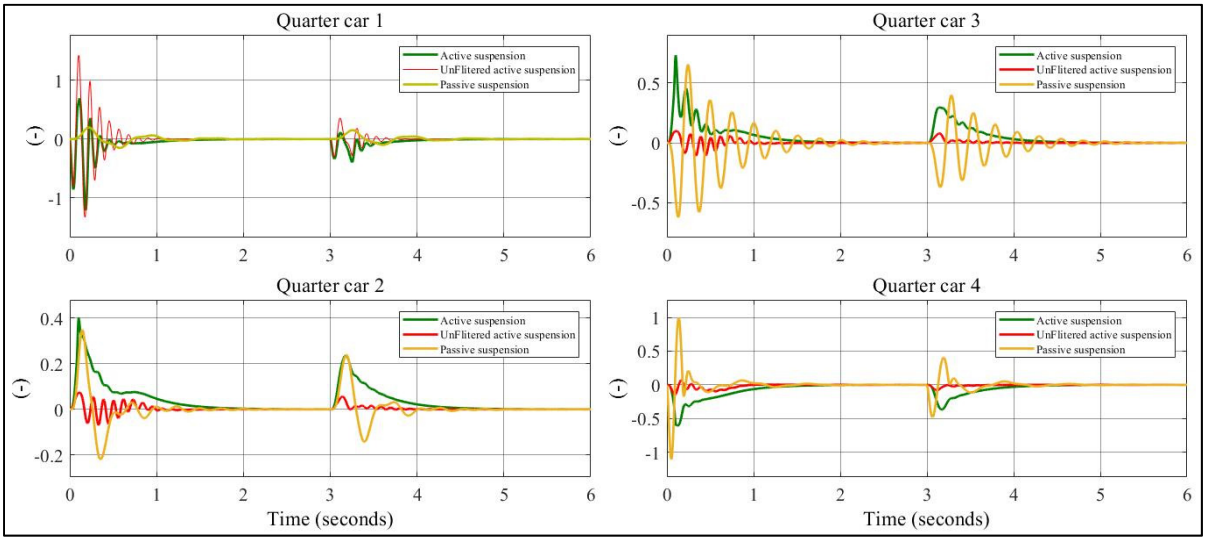

Figure 4.6 Road holding of Case I

Even though the unfiltered active suspension has the best compensation for the sprung mass positions (heaving, angular pitching, and angular rolling) in Figure 4.3 and Figure 4.4, it fails to keep road holding ($R_h > \kappa_w^{-1}$), as shown in Figure 4.6 quarter car 1 at 0.2 seconds. Moreover, the dynamic tyre force of quarter car 1 in Figure 4.6 exceeds 1.4 of the suspension weight. Hence, the dynamic tyre is in the liftoff phenomenon. Also, the passive suspension reaches the critical road holding ($R_h \approx \kappa_w^{-1}$), as shown in Figure 4.6 quarter car 4 at 0.2 seconds. Although the dynamic tyre forces of the filtered active suspension of quarter car 2-4 in Figure 4.6 are more than that in unfiltered active suspension, all quarter car 1-4 maintain road holding.

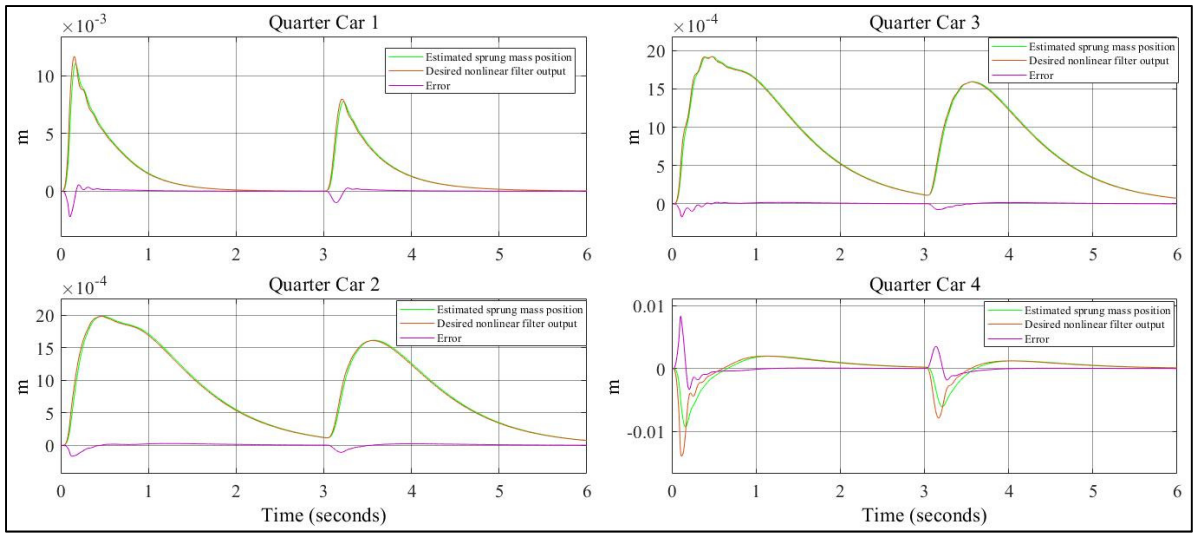

Figure 4.7 The system response of the RANNC

The filtered active suspension provides a high control performance, as shown in Figure 4.6. In Figure 4.7, the maximum error percentage is 15 % for quarter 1, 10 % for quarter 2, 9% for quarter 3, and 35 % for quarter 4. Hence, the minimum control compensations are 85% for quarter car 1, 90% for quarter car 2, 91% for quarter car 3, and 65% for quarter car 4.

Case II: Random road design

The international organization for standardization (ISO) has classified the standards of road roughness using the power spectral density (PSD) (Pan et al., 2017). Thus, there are a series of standards of road roughness, as shown in Table 4.3.

The power spectral density of a random road position can be evaluated as follows.

$$G(n) = G(n_0)\left(\frac{\text{space frequency}(n)}{\text{reference space frequency}(n_0)}\right)^{-\alpha} \tag{4.105}$$

The linear fitting coefficient α is usually equal 2. Therefore, The random road design can be described as follows.

$$\dot{X}_r(t) = -\xi\, U_c\, X_r(t) + \alpha(t) \tag{4.106}$$

Table 4.3 Road roughness standardization using PSD values

Road class	$\theta(10^{-3}m)$	$G(n_0) \times 10^{-6}\, m^3, n_0 = 1\, rad/m$	$\xi(rad/m)$
A (very good)	2	1	0.127
B (good)	4	4	0.127
C (average)	8	16	0.127
D (poor)	16	64	0.127
E (very poor)	32	256	0.127

In this study, both a poor road class D and a vehicle speed $U_c = 108\, km/h$ are selected to design the random road input. The conflicting suspension performances (ride comfort, road holding, suspension travel) are addressed based on the random road and the aerodynamic perturbations, as shown in Figures 4.8-4.10.

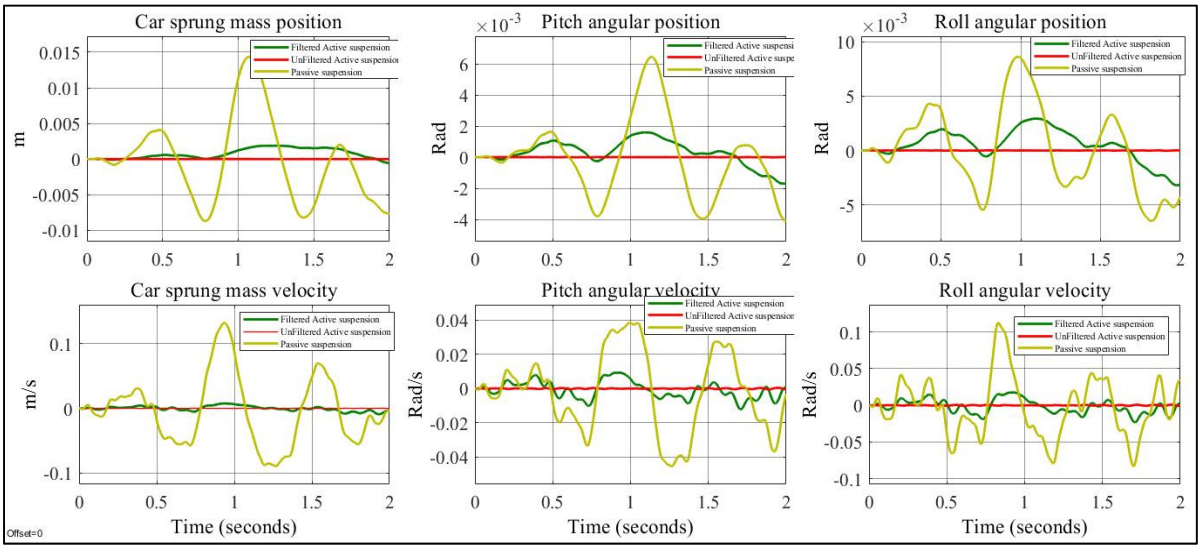

Figure 4.8 Sprung mass (heave, roll, pitch) positions and velocities of Case II

Even though the filtered active suspension is better compensation than passive suspension, it produces small degradations in passenger comfort compared to the unfiltered active suspension, as shown in Figure 4.8. The degradations of the filtered active suspension are produced from the nonlinear control filters' outputs. Therefore, the maximum percentage improvements in the sprung positions (heaving, pitch angular, and roll angular) are approximately 86%, 69%, and 63% of that in passive suspension, respectively. As well as the sprung mass dynamic positions, the maximum percentage compensation of the dynamic velocities are 99%, 75%, and 82% of that in passive suspension, respectively.

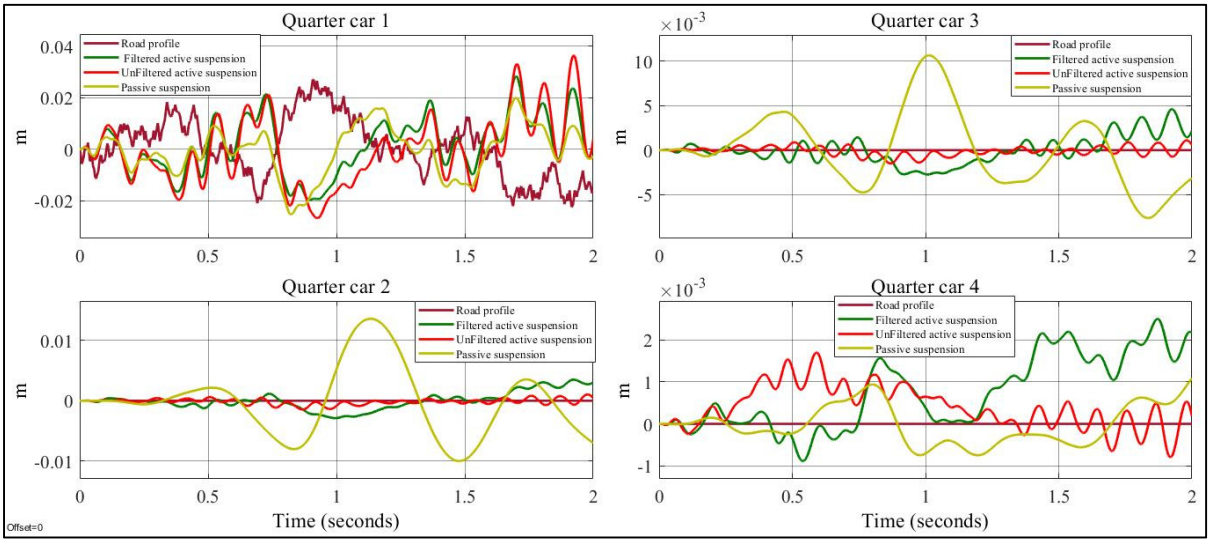

Figure 4.9 Suspension travel of Case II

Quarter car 1 in Figure 9 shows that the suspension travel oscillation of the filtered active suspension is reduced 20% more than the unfiltered active suspension. However, the suspension travel in the filtered active suspension is quietly more oscillations than the unfiltered active suspension, as shown in quarter car 2, 3, and 4.

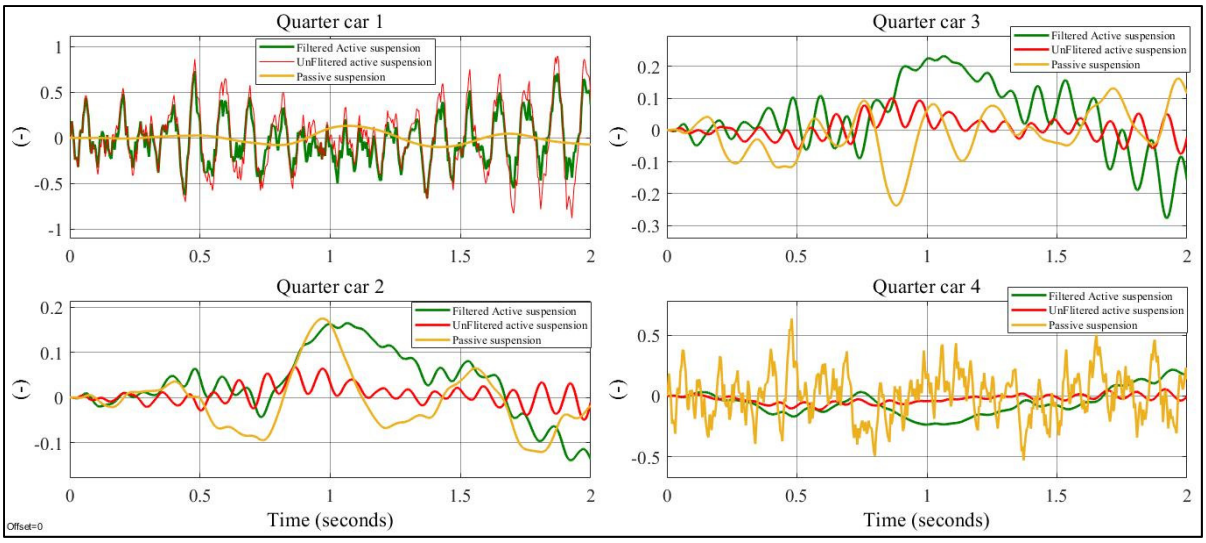

Figure 4.10 Road holding of Case II

Figure 10 quarter car 1 shows a 15% improvement of road holding than in the unfiltered active suspension. Because of the nonlinear control filters' effects, some road holding variations are held under the safe regions for quarter car 2, 3, and 4. On the other hand, the unfiltered active suspension provides a high passenger comfort as shown in Car sprung mass positions (heave, pitch, and roll) of Figure 8. However, both road holding and suspension travel oscillations of the unfiltered active suspension are degraded performance as shown in Quarter 1 of both Figure 8 and Figure 9. In general, filtered active suspension can achieve passenger comfort, road holding, and suspension travel safe.

4.5 Conclusion

This paper presents a robust adaptive neural networks control system (RANNC) for a MIMO nonlinear full car active suspension in enhancing passenger comfort, maintaining road holding, preventing reaching suspension travel limits, and overcoming dynamic nonlinearities and system uncertainties. Consequently, four nonlinear control filters are developed to track the reference trajectories of the full car active suspension system. However, dynamic nonlinearities and uncertainties are naturally lumped into unknown functions in the unmatched dynamic modelling system in the MIMO full car active suspension. Thus, robust adaptive neural

networks backstepping control system is developed to cope with these phenomena. The zero dynamic systems are also applied to stabilise the state space variables that were not guaranteed stability by the robust adaptive neural networks backstepping Lyapunov candidate function. Therefore, the nonlinear control filters are coupled with robust adaptive neural networks backstepping control system to design the RANNC. The results showed that the filtered active suspension was smoothly compensated the sprung mass positions compared with that in passive suspension. The filtered active suspension compensations were 86% of the heave position, 43% pitch angular position, and 62% of the angular roll position at 0.6 seconds in Case I. Moreover, the unfiltered active suspension provided a 98% compensation of that in passive suspension. Nevertheless, the unfiltered active suspension failed maintaining road holding, hitting suspension travel limits and reducing suspension travel oscillations. In Case II, a random road design was applied. The sprung mass (heaving, pitching, and rolling) positions were compensated by 86%, 69%, 63 of those in passive suspension. Future work could focus on the practical validation of the filtered active suspension in terms of real-time. Another future work might be to develop an adaptive control strategy for a vehicle dynamic system to improve the compromise between passenger comfort, road holding, suspension travel, braking, and longitudinal

CONCLUSION

In this research, several control systems are proposed for several electrohydraulic active suspension systems. Therefore, the first contribution is to determine a control law for a quarter car electrohydraulic active suspension system to isolate the sprung mass from vertical road energies. Thus, an adaptive radial basis function neural network backstepping control system was designed to deal with the unmatched nonlinear dynamic system. The proposed control law is able to deal with the dynamic nonlinearities and the system uncertainties. Furthermore, the unknown coefficient of the control signal was adaptively bounded by using the triangularity condition technique. The simulation results show that the proposed control system achieves 97% compensation, which approximately ignored the road energy perturbations. Nevertheless, the proposed controller could not maintain road holding and avoid exceeding suspension travel limits. This issue was solved in the second control strategy. The simulation results show that the ANNC gives an excellent control compensation compared to passive suspension.

The second published article has developed a dynamic physical system called a dynamic landing tire system. The dynamic landing tire system was formed instead of a dynamic tire force condition. The dynamic landing tire system contains two state variables: a landing tire position and a road holding ratio. We have also considered nonsymmetric suspension travel limits instead of that in most previous studies to realize operation conditions. Accordingly, the second part of the second contribution was to develop a nonlinear control filter to track the suspension restrictions by using both a suspension travel nonlinear function and a dynamic landing tire position nonlinear function. Thus, the second proposed control strategy was the combined nonlinear control filter with the first proposed control system (adaptive radial basis function neural networks backstepping control system). Four Cases of simulation comparative study were addressed between filtered active suspension, unfiltered active suspension, and passive suspension. The simulation results show that the control system can perfectly manage the compromise between passenger comfort, road holding, suspension travel limits, suspension travel oscillations, dynamic nonlinearities, and system uncertainties.

Even though the second control strategy successfully achieved the second contribution objectives, it was for SISO nonlinear of a quarter car electrohydraulic active suspension system. Therefore, the third contribution was to establish a control law for full car electrohydraulic active suspension. Hence, we have developed a robust adaptive neural networks backstepping control system for MIMO nonlinear of full car electrohydraulic filtered active suspension system in the presence of both a stiff road perturbation and external aerodynamic disturbances. The simulation results show that the proposed control systems are successfully achieved the control objectives of improving passenger comfort, maintaining road holding, avoiding reaching suspension travel limits, reducing suspension travel oscillations, overcoming both the dynamic nonlinearities and system uncertainties.

RECOMMENDATIONS

The real operation conditions are generally nonlinear and sometimes very complex. Therefore, future work will focus on the practical validation of the filtered active suspension systems in terms of real-time. All the active suspension components must be within the range to avoid the control performance limitations. Finally, the optimization analysis can be applied to improve control performance by setting the control parameters.

Even though the nonlinear control filter represented the desired control signal, a noise control signal started increasing with increasing road input high frequency and reaching suspension travel limits. The nonlinear control filter functions are fourth power. Therefore, we may select other smooth nonlinear functions to reduce the control signal noise.

In addition, the proposed control strategies successfully achieved their contributions. However, huge state variables of the compact set must be measured and/or observed. Therefore, adaptive observer systems must be developed to reduce the measured sensors. It also emphasizes that the dynamic tire landing system must be measured by designing a sensor or evaluated by developing an observer.

Several benefits can also be obtained from the dynamic tire landing system, such as improving car braking and longitudinal acceleration. Therefore, future work might also be to develop an adaptive control strategy for a dynamic vehicle system to improve the compromise between passenger comfort, road holding, suspension travel, braking, and longitudinal acceleration.

APPENDIX

In (Baker III, 1991), the aerodynamic forces acting on the vehicle's four wheels road can be described as follows.

The aerodynamic reaction force acting on wheel 1 can be represented:

$$F_{a_1}(t) = \Bigg\{ C_R\left(\frac{q}{2(w_r + w_l)}\right) + \frac{q(C_D - C_p)}{2(l_f + l_r)} - \frac{l_r \acute{C}_L}{2(l_f + l_r)} + \gamma\left(\frac{qC_f\left(l_f \acute{C}_L - q(C_D - C_p)\right)}{2(w_r + w_l)(l_f + l_r)} + \frac{qC_f\left(l_r \acute{C}_L - q(C_D - C_p)\right)}{2(w_r + w_l)(l_f + l_r)}\right) + \delta\frac{qC_f\left(l_r \acute{C}_L - q(C_D - C_p)\right)}{2(w_r + w_l)(l_f + l_r)}\Bigg\}\frac{1}{2}\rho_a \mathrm{A}_a U_a^2 \quad (\mathrm{A}.1)$$

where C_R is mean rolling moment coefficient, C_D is mean aerodynamic drag coefficient, C_p is mean pithing moment coefficient, C_f is lateral friction coefficient, $\acute{C}_L$ is modified lift force coefficient, q is the Hight of car centre gravity (m), δ is steering angle (rad), A_a is a reference aerodynamic area (m^2), ρ_a is air density, γ is a ratio between lateral displacement velocity and the vehicle speed, and U_a is mean wind velocity.

The aerodynamic reaction force acting on wheel 2 can be represented:

$$F_{a_2}(t) = \Bigg\{ -C_R\left(\frac{q}{2(w_r + w_l)}\right) + \frac{q(C_D - C_p)}{2(l_f + l_r)} - \frac{l_r \acute{C}_L}{2(l_f + l_r)} - \gamma\left(\frac{qC_f\left(l_f \acute{C}_L - q(C_D - C_p)\right)}{2l_r(w_r + w_l)(l_f + l_r)} + \frac{qC_f\left(l_r \acute{C}_L - q(C_D - C_p)\right)}{2(w_r + w_l)(l_f + l_r)}\right) - \delta\frac{qC_f\left(l_r \acute{C}_L - q(C_D - C_p)\right)}{2(w_r + w_l)(l_f + l_r)}\Bigg\}\frac{1}{2}\rho_a \mathrm{A}_a U_a^2 \quad (\mathrm{A}.2)$$

The aerodynamic reaction force acting on wheel 3 can be represented:

$$F_{a_3}(t) = \left\{ C_R\left(\frac{q}{2(w_r + w_l)}\right) - \frac{q(C_D - C_p)}{2(l_f + l_r)} - \frac{l_f \acute{C}_L}{2(l_f + l_r)} \right.$$
$$+ \gamma\left(-\frac{qC_f\left(l_f \acute{C}_L - q(C_D - C_p)\right)}{2(w_r + w_l)(l_f + l_r)} + \frac{qC_f\left(l_r \acute{C}_L - q(C_D - C_p)\right)}{2(w_r + w_l)(l_f + l_r)} \right)$$
$$\left. + \delta\frac{qC_f\left(l_r \acute{C}_L - q(C_D - C_p)\right)}{2(w_r + w_l)(l_f + l_r)} \right\} \frac{1}{2}\rho_a \mathrm{A}_a U_a^2 \qquad \text{(A. 3)}$$

The aerodynamic reaction force acting on wheel 4 can be represented:

$$F_{a_4}(t) = \left\{ -C_R\left(\frac{q}{2(w_r + w_l)}\right) - \frac{q(C_D - C_p)}{2(l_f + l_r)} - \frac{l_f \acute{C}_L}{2(l_f + l_r)} \right.$$
$$- \gamma\left(\frac{qC_f\left(l_f \acute{C}_L - q(C_D - C_p)\right)}{2(w_r + w_l)(l_f + l_r)} + \frac{qC_f\left(l_r \acute{C}_L - q(C_D - C_p)\right)}{2(w_r + w_l)(l_f + l_r)} \right)$$
$$\left. - \delta\frac{qC_f\left(l_r \acute{C}_L - q(C_D - C_p)\right)}{2(w_r + w_l)(l_f + l_r)} \right\} \frac{1}{2}\rho_a \mathrm{A}_a U_a^2 \qquad \text{(A. 4)}$$

In this study, all parameters in equations (A.1) -(A.4) are assumed to constant values except the wind velocity relative to the vehicle speed U_a.

BIBLIOGRAPHY

Abdalla, Wissam H., Al-Mutar and Turki Y. 2015. « Quarter Car Active Suspension System Control Using PID Controller tuned by PSO ». *Iraq J. Electrical and Electronic Engineering*, vol. 11, p. 151-158.

Abdelkareem, M., 2018. « Energy harvesting sensitivity analysis and assessment of the potential power and full car dynamics for different road modes ». *ELSEVIER Mechanical Systems and Signal Processing*, vol. 110, p. 307-332.

Abd El-Nasser, S. Ahmed, Ahmed S. Ali, Nouby Ghazaly, G. Abd el-Jaber. 2015. « PID controller of active suspension system for a quarter car model ». *International Journal of Advances in Engineering & Technology*, vol. 8, p. 899-909.

Ahmed, A., A. Ali, G. Jaber. 2015. PID controller of active suspension system for a quarter car model. *IJAET/International journal of advances in engineering and technology*, p. 899-910.

Al Aela, A., J-P. Kenne, H. Mintsa. 2020a. « Adaptive neural network and nonlinear electro-hydraulic active suspension control system ». *SAGE Journal of Vibration and Control*, vol. 0: p. 1-17.

Al Aela, Amhmed Mohamed, Jean-Pierre Kenne et Honorine Angue Mintsa. 2020b. « A Novel Adaptive and Nonlinear Electrohydraulic Active Suspension Control System with Zero Dynamic Tire Liftoff ». *MDPI Machines*, vol. 8, nº 3, p. 38.

Ali, Hassan. 1986. « Fundamental studies of passive, active and semi-active automobile suspensions systems ». Leeds.

Alkhatib, R., G. N. Jazar, et M. F. Golnaraghi. 2004. « Optimal design of Passive Linear Suspension Using Genetic Algorithm ». *Journal of Sound and vibration*, vol. 275, p. 665-691.

Alleyne, Andrew, et J. Karl Hedrick. 1995. « Nonlinear Adaptive Control of Active Suspensions ». *IEEE Transactions on control systems technology*, vol. 3, p. 94-101.

Alleyne, Andrew, et Rui Liu. 2000. « A simplified approach to force control for electro-hydraulic systems ». *Pergamon Control engineering practice*, vol. 8, p. 9.

Amer, N.H., R. Ramli, Mahadi, M. Abidin. 2011. « A Review on Control Strategies for Passenger Car Intelligent Suspension System ». In *Proceedings of the International Conference on Electrical, Control and Computer Engineering*, (Pahang, Malaysia), 21–22 June 2011.

Angue Mintsa, Honorine, R. Venugopal, et Jean-Pierre Kenne. 2011. « Adaptive Position Control of an Electrohydraulic Servo System With Load Disturbance Rejection and Friction Compensation ». *ASME Journal of dynamic systems measurement and control,* vol. 133

Angue-Mintsa, Honorine, R. Venugopal, Jean-Pierre Kenne. 2012. « Feedback Linearization Based Position Control of an electrohydraulic servo system with supply pressure uncertainty ». *IEEE Transactions on control systems technology*, vol. 20, nº 4, p. 1092-1099.

Araki, M. 2002. « PID controller ». In *Encyclopedia of Life Support Systems (EOLSS) for Control systems, robotics and automation*, vol. II, 23p.

Baker, C. 1991. « Ground vehicles in high cross winds part III of the interaction of aerodynamic forces and the vehicle system ». *Journal of Fluids and Structures*, vol. 5, p. 221-241.

Baumal, A. E., J. J. McPhee, P. H. Calamai. 1998. « Application of genetic algorithms to the design optimization of an active vehicle suspension system ». *ELSEVIER/Computer methods in applied mechanics and engineering*, vol. 163, p. 87-94.

Chen, M., S. Ge, B. How. 2010. « Robust Adaptive Neural Network Control for a Class of Uncertain MIMO Nonlinear Systems With Input Nonlinearities ». *IEEE Transactions on neural networks*, vol. 21, p. 796-13.

Chen, P.C., et A. Huang. 2006. « Adaptive sliding control of active suspension systems with uncertain hydraulic actuator dynamics ». *Vehicle System Dynamics*, vol. 44, p. 357–368.

Chen, PC, et Huang AC. 2005. « Adaptive Multiple-surface Sliding Control of Hydraulic Active Suspension Systems Based on the Function Approximation Technique ». *SAGE/Vibration and Control*, vol. 11, p. 685–706.

Chindamo, D., Gadola M., et Marchesin F. 2017. « Reproduction of real-world road profiles on a four-poster rig for indoor vehicle chassis and suspension durability testing ». *Adv. Mech. Eng*, vol. 9, p. 1-10.

De Queiroz, Marcio S., Darren M., Dawson Siddharth, P. Nagarkatti, et Fumin Zhang. 2000. *Lyapunov-Based Control of Mechanical Systems*. Springer-Science + Business Media, sous la dir. de Levine, William S. 321 p.

Desai, Nikhil, et Bharatbhushan Kale. 2016. « A review work on suspension systems models, and control strategies for suspension systems ». *Journal of Emerging Technologies and Innovative Research (JETIR)*, vol. 3, nº 10, p. 371-376.

Du, Haiping, James Lam, Weihua Li, et Nong Zhang. 2013. « Robust active control of an integrated suspension system ». In *Handbook of vehicle suspension control systems*. Institution of Engineering and Technology.

Du, K. L., et M. Swamy. 2014 . « *Neural networks and statistical learning* ». Springer

Duraiswamy, Shivkumar, George Chiu. 2003. « Nonlinear Adaptive Nonsmooth Dynamic Surface Control of Electro-Hydraulic Systems ». In *IEEE the American control conference* (Denver, Colorado), p. 3287-3292.

Elbayomy, Karam M., Jiao Zongxia, et Zhang Huaqing. 2008. « PID Controller Optimization by GA and Its Performances on the Electro-hydraulic Servo Control System ». *ELSEVIER Chinese Journal of Aeronautics*, vol. 21, nº 2008, p. 378-384.

Fijalkowski, BT. 2011. *Automotive Mechatronics Operational and Practical Issues*, II. Poland: Springer, 517p.

Fukao, T, Yamawaki A, et Adachi N. 1999. « Nonlinear and H_∞ Control of Active Suspension Systems with Hydraulic Actuators ». In *Proceedings of the 38th Conference on Decision & Control*. (Phoenix, Arizona USA), p. 5125-5129. IEEE.

Ge, S., J. Wang. 2002 . « Robust Adaptive Neural Control for a class of perturbed strict Feedback nonlinear systems ». *IEEE Transactions on Neural Networks* , vol.13, nº 6, p. 1409-1419.

Gillespie, Thomas. 1992. *Fundamental of Vehicle dynamics*. SAE International, 519 p.

Guglielmino, Emanuele, Tudor Sireteanu Charles, W Stammers, Gheorghe Ghita, et Marius Giuclea. 2008. *Semi-active Suspension Control*. Springer.

Han, S., et J. Lee. 2014 . « Recurrent fuzzy neural network backstepping control for the prescribed out put tracking performance of nonlinear dynamic systems ». *ELSEVIER ISA Transactions* , vol. 53, nº 1, p. 33-43.

Hanafi, D. 2010. « PID Controller Design for Semi-Active Car Suspension Based on Model from Intelligent System Identification ». In *Second International Conference on Computer Engineering and Applications*.

Hrovat, D. 1997. « Survey of Advanced Suspension Developments and Related Optimal Control Applications ». *Pergamon/ Automatica*, vol. 33, p. 1781–1817.

Hu, JW, et Lin JS. 2008. « Nonlinear Control of Full-Vehicle Active Suspensions with Backstepping Design Scheme ». In *the International Federation of Automatic Control*. (Seoul, Korea). p. 3404-3409

Huang, Y, Na J, Wu X, Liu X, et Guo Y. 2015. « Adaptive control of nonlinear uncertain active suspension systems with prescribed performance ». *ELSEVIER/ISA Transactions*, vol. 54, p. 145-155.

Huang, Y., J. Na, X. Wu et G. Gao. 2019. « Approximation-Free Control for Vehicle Active Suspensions With Hydraulic Actuator ». *IEEE Transactions on Industrial Electronics,* vol. 65, nº 9, p. 7258-7267.

Hussin, Mat, Ab Talib, Z Intan, Mat Darus. 2013. « Self-Tuning PID Controller for Active Suspension System with Hydraulic Actuator ». *IEEE Symposium on Computers & Informatics*. p. 86-91

Jiang, Z., D. Hill. 1999. « A Robust Adaptive Backstepping Scheme for Nonlinear Systems with Unmodeled Dynamics ». *IEEE Transations on Automatic Control* , vol. 44, nº 9, p. 1705-17011.

Jurgen, Ronald K. (1 volume (pages multiple) : illustrations). 1999. *Automotive electronics handbook*, 2nd ed. Coll. « McGraw-Hill handbooks ». New York, N.Y.: McGraw-Hill.

Karlsson, N, A. Teel, D. Hrovatt. 2001.« A Backstepping approach to Control of Active Suspensions ». In *the 40th IEEE, Conference on Decision and Control.* (Orlando, Florida USA), December 2001, p. 4170-4175.

Kaddissi, C., Jean-Pierre Kenne, S. Saad. 2011. « Indirect Adaptive Control of an Electrohydraulic Servo System Based on Nonlinear Backstepping ». *IEEE/ASME Transactons on Mechatronics,* vol. 16, nº 6, p. 1171-1178

Keller, James M., Derong Liu, and David B. Fogel. 2016. « Radial-Basis Function Networks ». In *Fundamentals of Computational Intelligence: Neural Networks, Fuzzy Systems, and Evolutionary Computation*, sous la dir. de James M. Keller, Derong Liu, and David B. Fogel. The Institute of Electrical and Electronics Engineers: Published 2016 by John Wiley & Sons, Inc.

Kim, C., et P. Ro. 1998. « A sliding mode controller for vehicle active suspension systems with non-linearities ». *Proc. Inst. Mech. Eng., Part D. J. Automobile. Engngineering*, vol. *212*, 14p.

Khalil, H. 2002. « *Nonlinear Systems* » Prentice Hall , (Upper Saddle River, NJ, USA), 767p.

Kilicaslan, S. 2018. « Control of active suspension system considering nonlinear actuator dynamics ». *Springer Nonlinear Dynamics*, vol. 91: p. 1383–1394.

Kim, ES. 1996. « Nonlinear indirect adaptive control of a quarter car active suspension ». In *International Conference on Control Applications*. (Dearborn, MI), p. 61-67. IEEE.

Koch, G. 2011. « Adaptive Control of Mechatronic Vehicle Suspension Systems ». Munchen.

Krstic, M., Kanellakopoulos et Kokotovic. 1995. « *Nonlinear and Adaptive Control Design* ». John Wiley and sons.

Lin, Jung-Shan, et Ioannis Kanellakopoulos. 1997. « Nonlinear Design of Active Suspension ». In *34th IEEE Conference on decision and control*. (New Orleans, LA, USA). Vol. 17, p. 45-59.

Liu, H., H. Gao, P. Li. 2013. « *Handbook of Vehicle Suspension Control Systems* ». Institution of Engineering and Technology IET, (London, UK).

Liu, J. 2013. *Radial Basis Function (RBF) Neural Network Control for Mechanical Systems*. Heidelberg New York Dordrecht London: Springer. 374p.

Liu, J. 2018. « Intellegent control design and MATLAB simulation ». Springer

Liu, J., et X. Wang. 2011. « *Advanced Sliding Mode Control for Mechanical Systems* ». Springer TSINGHUA University Press.

Liu, Y. J., Q. Zeng, S. Tong, C. Chen, L. Liu. 2019. « Adaptive neural network control for active suspension systems with time-varying vertical displacement and speed constraints ». *IEEE Trans. Ind. Electronics*, vol. 66, p. 9458–9466.

Lugner, Peter. 2019. *Vehicle Dynamics of Modern Passenger Cars*, 582. Springer International Publishing AG, 382p.

Lv, C., Wang H., Cao D. 2017. « High-precision hydraulic pressure control based on linear pressure drop modulation in valve critical equilibrium state ». *IEEE Trans. Ind. Electron*, vol. 64, p. 7984-7993.

Michael, J., M. Gerdts. 2015. « Pro-active optimal control for semi-active vehicle suspension based on sensitivity updates ». *Vehicle System Dynamics.* Vol. 53, nº 12, p. 1721–1741, DOI: 10.1080/00423114.2015.1081953

Merritt, H. 1967. *Hydraulic control systems*. John Wiley and Sons, 358 p.

Mouleeswaran, Senthilkumar. 2012. « Design and development of PID controller-based active suspension system for automobiles ». *INTECH*, p. 71-98.

Na, J., Y. Huang, X. Wu, G. Gao, G. Herrmann, J. Jiang. 2018. « Active adaptive estimation and control for vehicle suspensions with prescribed performance ». *IEEE Trans. Control Syst. Technol*, vol. 26, p. 2064–2077.

Orr, M. 1996. « *Introduction to Radial Basis Function Networks* ». University of Edinburg: Scotland, Britain.

Pan, H., W. Sun, X. Jing, H. Gao, J. Yao. 2017. « adaptive tracking control for active suspension systems with non-ideal actuators ». *Elsevier/Journal of sound and vibration* vol. 399, p. 2-20

Pang, H., X. Zang, et Z. 2019. « Adaptive backstepping-based tracking control design for nonlinear active suspension system with parameter uncertainties and safety constraints ». *ISA Trans,* vol. 88, p. 23–36.

Pang, H., X. Zhang, J. Chen et K. Liu. 2019. « Design of a coordinated adaptive backstepping tracking control for nonlinear uncertain active suspension system ». *ELSEVIER Applied Mathematical Modelling.* Vol. 76, p. 479–494.

Pedro, Jimoh O., Muhammed Dangor, Olurotimi Dahunsi, M. Montaz Ali. 2018. « Dynamic neural network-based feedback linearization control of full-car suspensions using PSO ». *ELSEVIER Applied Soft Computing*. vol. 70, nº 2018, p. 723–736.

Popescu, M.C., et Mastorakis N. 2009. « Testing and simulation of a motor vehicle suspension ». *Int. J. Syst. Appl. Eng. Dev*, vol. *3*, p. 2074–1308.

Pratheepa, B. 2010. « Modeling and Simulation of Automobile Suspension System ». *IEEE*, p. 377-382.

Pusadkar, U., S. Chaudari, P. Shendge, S. Phadke. 2019. « Linear disturbance observer based sliding mode control for active suspension systems with non-ideal actuator ». Elsevier *Journal of sound and vibration*, vol. 442, p. 428–444.

Qin, Y., M. Dong, C. Xiang, T. Kareemulla, J. Rath, C. Sentouh et J. Popieul. 2017. « Adaptive Robust Active Suspension Control based on Intelligent Road Classifier ». In: *56th Annual Conference on Decision and Control/ IEEE.* (Melbourne, Australia), 12-15 Dec. 2017, p. 861-866.

Rajamani, Rajesh. 2012. *Vehicle Dynamics and Control*, Second. US: Springer Mechanical Engineering Series, 516 p.

Rath, J., M. Defoort, H. Karimi, K. Veluvolu. 2017. « Output feedback active suspension control with higher order terminal sliding mode ». *IEEE Trans. Ind. Electron*, vol. 64, p. 1392–1403.

Rettig, Uwe, et Oskar Stryk. 2005. « Optimal and Robust Damping Control for Semi-Active Vehicle Suspension ». In *5th EUROMECH Nonlinear Dynamics Conference (ENOC 2005)*. (Eindhoven, Netherlands).

Riaz, S., et Khan L. 2015. « Neuro-fuzzy adaptive control for full car nonlinear active suspension with onboard antilock braking system ». *Arab J. Sci. Eng*, vol. 40, p. 3483–3505.

Savitski, Dzmitry, Dmitrij Schleinin, Valentin Ivanov, et Klaus Augsburg. 2017. « Sliding mode approach in semi-active suspension control ». In *Sliding Mode Control of Vehicle Dynamics*, sous la dir. de Ferrara, Antonella.

Sallah, S., M. Rahmat, M Othman, et K. Danapalasingm. 2015. « Review of modeling and control design of hydraulic actuator systems ». *International journal on smart sensing and intelligent systems*, vol. 8, nº 1, p. 30.

Satoh, Masaharu, Naoto Fukushima, Yousuke Akatsu, Itaru Fujimura, et Kensuke Fukuyama. 1990. « An Active Suspension Employing an Electrohydraulic Pressure Control System ». In *IEEE the 29th conference on Decision md Control*. (Honolulu. Hawail). p. 2226-2231.

Seo, Jaho, R. Venugopal, Jean-Pierre Kenne. 2007. « Feedback linearization based control of a rotational hydraulic drive ». *ELSEVIER/ Control engineering practice*, vol. control engineering practice 15, nº 2007, p. 12.

Shaer, Basel, Jean-Pierre Kenné, C. Kaddissi et C. Fallaga. 2016. « Achattering free fuzzy hybrid sliding mode control of an electrohydraulic active suspension ». *SAGE Transactions of the Institute of Measurement and Control* . vol. 40, p. 222–238.

Smith, Malcolm C., et Fu-Cheng Wang. 2002. « Controller Parameterization for Disturbance Response Decoupling: Application to Vehicle Active Suspension Control ». *IEEE Transactions on control systems technology*, vol. 10, nº 3. p. 393-407.

Shirdel, A.H., E. Gatavi, Z. Hashemiyan. 2010. « Comparison of H-∞ and optimized-LQR controller in active suspension system ». In *Second International Conference on Computational Intelligence, Modelling and Simulation*. p. 213-216.

Slotine, Jean-Jacques, et Weiping Li. 1991. « *Applied Nonlinear Control* ». Prentice Hall, nº 1, p. 459.

Sun, Weichao, H. Pan, Y. Zhang, et H. Gao. 2014. « Multi-objective control for uncertain nonlinear active suspension systems ». *ELSEVIER/Mechatronics*, vol. 24, p. 318-327.

Talib, Mat Hussin, et Intan Z. Mat Darus. 2013. « *Self-Tuning PID Controller for Active Suspension System with Hydraulic Actuator* ».IEEE

Tandel, A., A. Deshmukhe, K. Jagtap. 2014. « Modeling, Analysis and PID Controller Implementation on Double Wishbone Suspension Using SimMechanics and Simulink ». *ELSEVIER/Procedia Engineering.* Vol. 97, p. 1274 – 1281.

Thompson, A. G. 1970. « DESIGN OF ACTIVE SUSPENSIONS ». Proceedings of the Institution of Mechanical Engineers, vol. 185, nº 36, p. 553-572.

Tran, D., M. Nguyen, K. Ahn. 2019. « RBF Neural Network Based Backstepping Control for an Electrohydraulic Elastic Manipulator ». *MDPI Applied Sciences,* vol. 9, p. 1-18.

Tseng, HE, JK Hedrick. 1994. « Semi-active suspension optimal and sub-opimal ». *Vehicle System Dynamics*, vol. 23, nº 1, p. 545-569.

Tuan, H.D., E. Ono, P. Apkarian et S. Hosoe. 2001. « Nonlinear H_∞ Control for an Integrated Suspension System via Parameterized Linear Matrix Inequality Characterizations ». *IEEE Transaction on control systems technology.* Vol. 9, nº 1, p. 175-185.

Wang, Gang. 2020. « Eso-based therminal sliding model control for uncertain full car active suspension systems ». *International Journal of Automotive Technology*, vol. 12, nº 3, p. 691-702.

Wang, H, Y Lu, Y Tian, N Christov. 2021. « Fuzzy sliding mode based active disturbance rejection control for active suspension system ». *Institution of mechanical engineers/ Journal of automobile engineering*, vol. 234 nº 2-3, p. 449–457.

Xing, Y., et Lv C. 2019. « Dynamic state estimation for the advance brake system of electric vehicle by using deep recurrent neural networks ». *IEEE Trans. Ind. Electron*, doi:10.1109/TIE.2019.2952807.

Yamashita, Masashi, Kazuo Fujmori, Kisaburo Hayakawa, et Hidenori Kimura. 1994. « Application of Control to Active Suspension Systems ». *Pergamon Automatica*, vol. 30, nº 11. p. 1717-1729.

Yang, G., J. Yao, G. Le et D. Ma. 2016. « Adaptive integral robust control of hydraulic systems with asymptotic tracking». *ELSEVIER Mechatronics.* Vol. 40, p. 78-86.

Yao, Bin, Fanping Bu, George Chiu. 1998. « Nonlinear Adaptive Robust Control of Electro-Hydraulic Servo Systems with discontinuous Projection ». In *the 37th IEEE Conference on Decision & Control*, Tampa, Florida USA. p. 2265-2270.

Yao, Z., J. Yao et W Sun, 2019. «Adaptive rise control of hydraulic systems with multilayer neural networks». *IEEE Transactions on industrial electronics*, vol. 66, p. 8638-8647.

Yatak, M, F Sahin. 2021. « Ride comfort-road holding trade-off improvement of full vehicle active suspension system by interval type-2 Fuzzy control ». *ELSEVIER/Journal of Engineering Science and Technology*, vol. 24, p. 259–270.

Yin, Xunyuan, Zhaojian Li, et Ilya Kolmanovsky. 2021. « Distributed state estimation for linear systems with application to full-car active suspension systems ». *IEEE Transactions on Industrial Electronics*, vol. 68, nº 2, p. 1615-1626.

Yue, Chinny. 1987. « Control law designs for active suspensions in automotive vehicles ». Massachusetts.

Yuvapriya, T., P. Lakshmi, et S. Rajendiran. 2020. « Vibration control and performance analysis of full car active suspension system using fractional order terminal sliding mode controller ». *PAN Archives of Control Sciences*, vol. 30, nº 2, p. 295–324.

Zheng, J. et J. Yao. 2019. « Robust adaptive tracking control of hydraulic actuators with unmodeled dynamics ». *SAGE Transactions of the Institute of Measurement and Control,* vol. 41, nº 14, p. 3887–3898.

Zhang, Y., Y. Lin et L. Liu. 2019. « Minimal learning parameters-based adaptive neural control for vehicle active suspensions with input saturation ». *ELSEVIER Neurocomputing*. p. 1-9.

Zheng, Z., Y. Zou. 2016. « Adaptive integral LOS path following for an unmanned airship with uncertainties based on robust RBFNN backstepping ». *ELSEVIER/ISA Transactions.* vol. 65, p. 210-219.